LUMINESCENT MATERIALS FOR ORGANIC LIGHT-EMITTING DIODES (OLEDS) AND BIOIMAGING

YAO JUN HONG

NATIONAL UNIVERSITY OF SINGAPORE

2007

LUMINESCENT MATERIALS FOR ORGANIC LIGHT-EMITTING DIODES (OLEDS) AND BIOIMAGING

YAO JUN HONG

A THESIS SUBMITTED FOR THE DEGREE OF DOCTOR OF SCIENCE

DEPARTMENT OF CHEMISTRY

NATIONAL UNIVERSITY OF SINGAPORE

2007

Acknowledgements

I would like to express my deepest sense of gratitude to my supervisor Dr. Chen Zhi Kuan for his valuable guidance, discussions, advice, continued encouragement and inspirations throughout my Ph. D. study. With sincere thanks, I want to thank my co-supervisor, Assoc. Professor Loh Kian Ping for his constant support and suggestion during the years. I gratefully appreciate his kind help and concern.

I wish to express my gratitude to our group members, Soon Yee, Huang Chun, Chang Gua, Richard, Meili, Ahmed, Mdm. Xiao Yang and Kok Haw. It is a big pleasure to have the opportunity to work together and learn from them. I feel lucky to work in such a harmonious lab.

I am also grateful to Dr. Li Xu and Dr. Khine Yi Mya who have devoted their valuable time to instruct me in micelle sample preparation and property measurements. I would also say thanks to Mr. Loh Xian Jun for GPC measurement and Ms. Shen Lu for patient AFM training.

Special thanks and appreciation are due to my good friends in China for their non-stop support all the time.

I would like to express my thanks to Institute of Materials Research and Engineering (IMRE) and National University of Singapore (NUS) for the award of the research scholarship.

Finally, I wish to pay my gratitude to my loving family members, my parents and my cousin Sun Lei for their encouragement and moral support throughout my studies.

Table of contents

List of Abbreviations and Symbols

acac	acetyl acetone
a. u.	arbitrary unit
AFM	atomic force microscopy
Alq_3	tris-(8-hydroxyquinoline)aluminum (III)
BCP	2,9-dimethyl-4,7-diphenyl-1,10-phenanthroline
BuL	butyl lithium
CAC	critical association concentration
CBP	4,4'-N, N'-dicarbazole-biphenyl
$CDCl_3$	deuterated chloroform
CIE	commission Internationale de l'Echairage
CV	cyclic voltammetry
DCM	dichloromethane
DSC	differential scanning calorimetry
DLS	dynamic light scattering
EBL	electron-blocking layer
EL	electroluminescence
EQE	external quantum efficiency
ETL	electron transport layer
GPC	gel permeation chromatography
HBL	hole-blocking layer
^{1}H-NMR	proton nuclear magnetic resonance spectroscopy

HOMO	highest occupied molecular orbital
HTL	hole transport layer
ITO	indium tin oxide
LS	light scattering
LUMO	lowest unoccupied molecular orbital
MLCT	metal-ligand charge transfer
MS	mass spectrometry
NPB	N, N'-diphenyl-N, N'-bis(1-naphthyl)–(1,1'-biphenyl)-4,4'-diamine
NBS	N-bromoosuccinimide
NMR	nuclear magnetic resonance
OLEDs	organic light emitting diodes
PBD	2-(4-biphenylyl)-5-(4-tert-butylphenyl)-1,3,4-oxadiazole
PDI	polydispersity index
$Pd(PPh_3)_4$	tetrakis(triphenylphosphine)palladium (0)
PE	power efficiency
PEDOT/PSS	poly(3,4-ethylenedioxythiophene)/polystyrene sulfonate
PEO	poly(ethylene oxide)
PEG	poly(ethylene glycol)
PF	polyfluorene
PL	photoluminescence
PPO	poly(propylene oxide)
PPP	poly (*para*-phenylene)

PPV	poly (phenylenevinylene)
PS	poly(styrene)
PT	polythiophene
PVK	poly (vinylcarbazole)
QD	quantum dots
RT	room temperature
SLS	static light scattering
TAZ	3-(4-biphenyl)-4-phenyl-5-tert-butylphenyl-1,2,4-triazole
$TBAPF_6$	tetrabutylammonium hexafluorophosphate
TCSPC	time-correlated single-photon counting
TCTA	4,4',4''-tris (N-carbazolyl)-triphenylamine
TEM	transmission electron microscopy
TGA	thermogravimetric analysis
THF	tetrahydrofuran
TPBI	2,2',2''-(1,3,5-phenylene)tris(1-phenyl-1*H*-benzimidazole)
TPD	N,N'-diphenyl-N, N'-bis(3-mehtylphenyl)-1,1'-biphenyl-4, 4'-diamine
UV-vis	ultraviolet-visible
δ	chemical shift
λ	wavelength
A_2	second virial coefficient
dn/dc	refractive index increment
eV	electron volt

E_{pa}	anodic peak potential [V]
E_{pc}	athodic peak potential [V]
fs	femtosecond
M_n	number averaged molecular weight
M_w	weight averaged molecular weight
$M_{w,agg}$	apparent molecular weight of aggregates
N_{agg}	aggregation number
ppm	parts per million
R_g	radius of gyration
R_h	hydrodynamic radius
τ	lifetime
T_g	glass transition temperature

List of Tables

Part I

Part II

List of Figures

Part I

Part II

Summary

Luminescent materials can find wide application in flat-panel-display and biolabeling technologies. The focuses of this project are the design and synthesis of phosphorescent small molecules and polymers for organic light-emitting diodes (OLEDs) and fluorescent amphiphilic graft copolymers for bioimaging.

The first topic is the design, synthesis and application of phosphorescent small molecular iridium complexes based on three dimensional spirobifluorene ligands. Yellow to red light emission of iridium complexes were obtained by modifying ligand structures. All the iridium complexes have been obtained in good yields with well-defined facial conformation structures. The device based on new guest materials and PVK host materials realized highest external quantum efficiency of 10%. The device performance can be improved further by optimizing device structure.

The second topic is related to the synthesis and characterization of phosphorescent polymers with fluorene-*co*-diphenylamine backbones and iridium complex pendant group. The feed ratio of iridium complexes was changed from 4% to 10%, 15% and 20 % in mole fractions to tune the energy levels of the polymers. The energy gap of the polymers decreased with the increase of iridium complex. All the resulting polymers demonstrated excellent thermal stability and film-forming ability.

The last section is referred to the synthesis, characterization and application of a series of fluorescent amphiphilic graft copolymers containing oligofluorene/polyfluorene backbones and poly(ethylene glycol) side chains. The copolymers self-assemble into nano-scaled micelles. The water solubility and micelle size were tuned in wide range by structure modification. Monodispersed fluorescent nanoparticles have been developed.

Their self-assembling behaviors and morphologies were studied by light scattering, TEM and AFM. Their optical properties were investigated by steady state and time-resolved fluorescence spectroscopy. Preliminary biocharacterization of the fluorescent micelles demonstrated excellent stability and non-cytotoxicity. Potential application of the micelles for bio-imaging has been substantiated by BV-2 cells.

Keywords: Phosphorescent materials, spirobifluorene, iridium complex, organic light-emitting diodes (OLEDs), polyfluorene, triphenylamine, Suzuki coupling, fluorescence, amphiphilic graft copolymer, PEG, self assembling, micelle, bioimaging.

1. Introduction

Electroluminescence (EL) is a non-thermal generation of light resulting from the application of an electric field to an active material by radiative decay of an excited state of the material.[1] The process responsible for electroluminescence requires injection of electrons from one electrode and holes from the other, the capture of oppositely charged carriers (recombination), and the radiative decay of the excited electron-hole state pairs (excitons) produced by this process.

Electroluminescence was first discovered by Destriau *et al* from inorganic materials (ZnS) in 1936,[1] while organic materials from anthracence until 1963.[2] However, at the beginning, organic materials didn't catch people's eyes due to the high operation voltage and low efficiency. Until 1987, Tang and Van Slyke fabricated an organic light-emitting diode (OLED) based on tris(8-hydroxyquinolinato)aluminum (Alq_3), together with N,N'-diphenyl-N, N'-bis(3-methylphenyl)-1,1'-biphenyl-4, 4'-diamine(TPD) to achieve very bright green emission at a low driving voltage of 10V. The brightness was higher than 1000 cd/m^2 and external quantum efficiency (EQE) reached around 1%.[3] Following this success, in 1990, Friend *et al*. fabricated polymer LEDs by spin-coating a precursor conjugated polymer poly (phenylenevinylene)(PPV) as emitter in a similar device structure(Figure 1.1).[1,4-6] These great progresses attracted extensive studies to OLEDs and contributed greatly to their rapid development. Owing to their thin-film, light-weight, fast-response, wide-viewing-angle, high-contrast, full color and low-power attributes, OLEDs showed their unlimited potential to be mainstream of flat-panel-display technologies and they will be able to compete with the now-dominant liquid-crystal displays (LCDs) in the future display market.

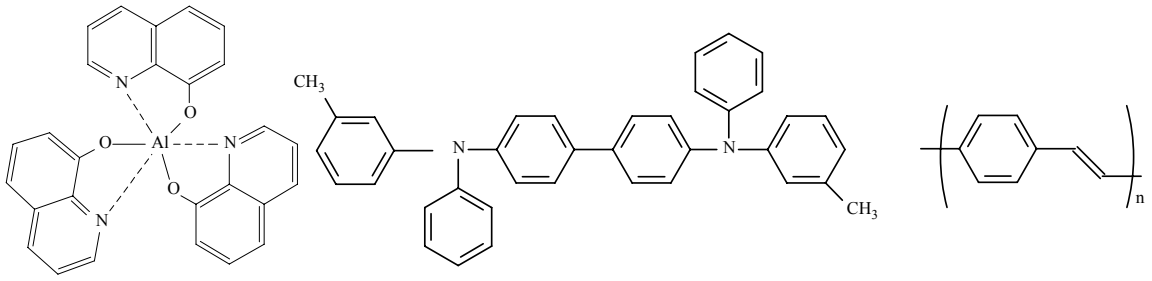

Alq$_3$ **TPD** **PPV**

Figure 1.1. Molecular structures of Alq_3, TPD and PPV.

1.1 Mechanism and structure of organic light-emitting diodes (OLEDs)

Electroluminescence is obtained from light-emitting diodes (LEDs) when incorporating the light-emitting layer between the anode and cathode. Single layer OLED device includes anode, light-emitting layer and cathode, which is the basic and simplest OLED structure. However, due to different mobility between holes and electrons, the combining areas tend to close to one electrode, causing charge consumed on the electrode surface and thus affecting the device efficiency. Improved device performance was achieved when a more complicated multilayer device configuration was adopted (Figure 1.2).[7] Hole injection/transport layer (HTL) and electron injection/transport layer (ETL) were inserted to balance the charge injection and transport and control the recombination. In order to confine charges in active layer, hole-blocking layer (HBL) and electron-blocking layer (EBL) were added to prevent holes and electrons leakage. Multilayer structures permit improvement in charge injection, transport and recombination. When a voltage is applied onto the device, holes are injected from the anode and electrons from the cathode, then they migrate through the hole transport layer and electron transport layer, respectively. Finally they recombine in the organic light-emitting layer to form

excitons. The relaxation of the excitons from excited state to ground state will produce light emission and the color of light depends on the energy difference between the excited states and the ground states. In short, the fundamental physical process of the OLEDs can be divided into four steps: charge injection, transport, recombination and radiative exciton decay.

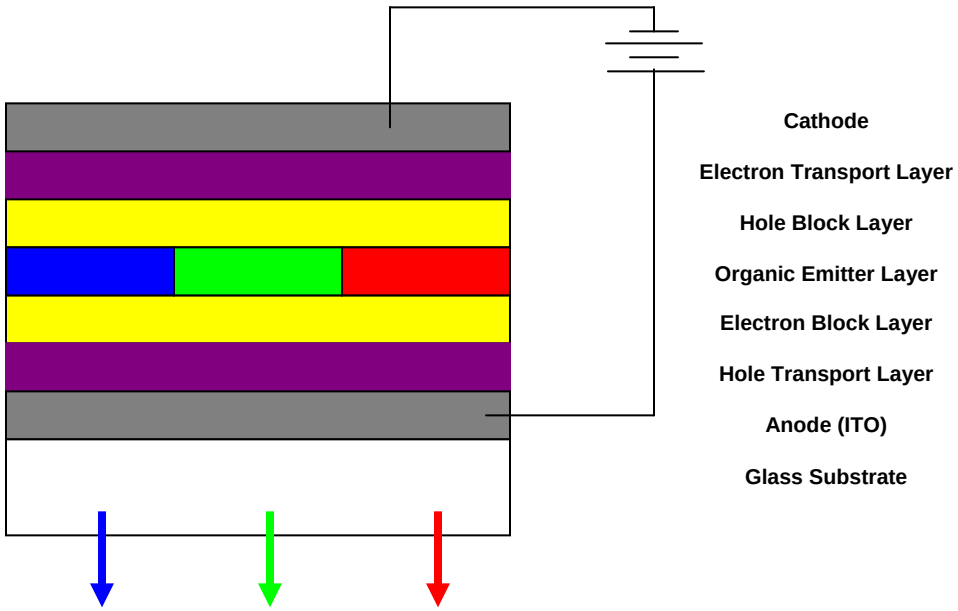

Figure 1.2. Sandwich structure of OLEDs.

For OLEDs, indium-tin-oxide (ITO)-coated glass substrate is a universal choice for their anode. Up to now, other non-ITO anodes are seldom used. ITO is composed of indium oxide (In_2O_3) and a small amount of tin oxide (SnO_2). Its high work function, high transparency (90%) to visible light, wide band gap (E_g=3.5 - 4.3 eV), conductive and good adhesion ability with organic layer are the main considerations. Before using, ITO must be cleaned ultrasonically in detergent solution and rinsed in deionized water in sequence. After cleaning, further surface treatment, such as, using plasma or UV-ozone to

enhance its work function further to 5 eV and facilitate its hole injection. The sequent ITO treatment is very important, which will improve the efficiency and stability of OLED.[8-10]

However, the work function of treated ITO is still lower than the highest occupied molecular orbital (HOMO) of most hole transport materials. For further improved device performance, a hole-injection layer is inserted between ITO and hole transporting layer. This layer will enhance hole injection at interface. Copper phthalocyanine (CuPc)[11,12] and poly(3,4-ethylene dioxythiophene)–poly(styrene sulfonic acid) (PEDOT/PSS)[13,14] are popular choices, especially the latter, PEDOT/PSS can smooth the surface of ITO, decrease device turn-on voltage, reduce the probability of electrical short circuits. The structures of PEDOT/PSS and CuPc are shown in Figure 1.3.

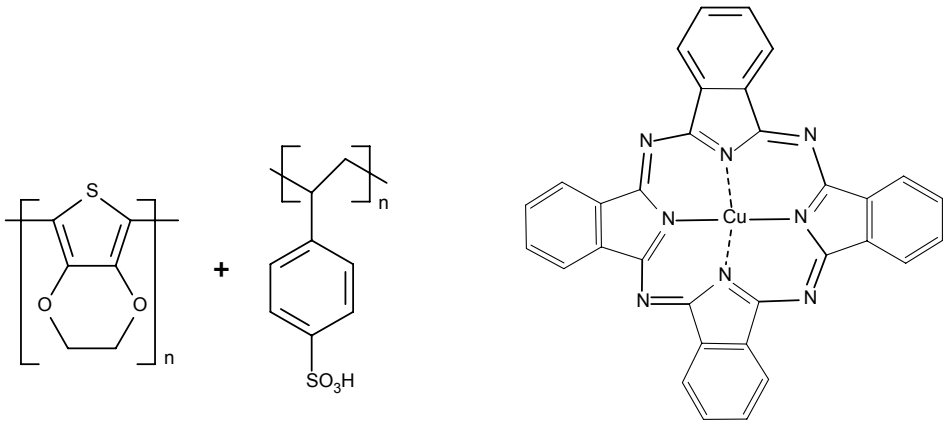

Figure 1.3. Structures of PEDOT/PSS and CuPc.

For the cathode, usually electropositive and low work function metals are used, because they minimize the energy barrier for electron injection from cathode to the organic materials and offer high current density.[15,16] The attempt to use Ca, K and Li for

effective cathode materials revealed that they exhibit poor corrosion resistance and high chemical reactivity with the organic layer. One solution is to use low-work function metal alloys such as Mg-Ag and Al-Li, which have better stability. Currently, bilayer cathode, such as LiF/Al was adopted and exhibited pronounced boost in device performances, thus it has been widely used in OLEDs.

In OLEDs, electron and hole transport layers are used to guarantee balanced charges, which will improve the device efficiency. Because most organic materials prefer to transport only one kind of charges, i.e., electrons or holes, with the mobility ranging from 10^{-8} to 10^{-2} $cm^2/(V{\cdot}s)$.[1] Hole-transporting materials account for the majority of organic materials due to their intrinsic low electron affinity. Numerous hole-transporting materials have been developed. Among them, triarylamine and carbazole derivatives are prevalent, such as, N,N'-diphenyl-N,N'-bis(1-naphthyl)–(1,1'-biphenyl)-4,4'-diamine (NPB),[17] 4,4′-N,N′-dicarbazol-biphenyl (CBP),[18] and TPD[19] (Figure 1.4). To date, the most widely used electron transport materials are some metal chelates (Alq_3, Be and Zn chelates).[20] PBD,[20] 2,2',2''-(1,3,5-phenylene)tris(1-phenyl-1*H*-benzimidazole) (TPBI),[18,21,22] 3-(4-biphenyl)-4-phenyl-5-tert-butylphenyl-1,2,4-triazole (TAZ) (Figure 1.5),[23,24] and oxadiazole derivatives have also been widely used in preparing organic EL devices as an electron transporting material.[25,26]

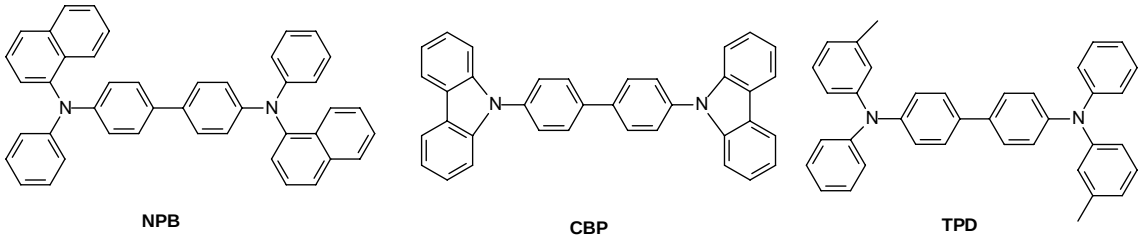

Figure 1.4. Hole-transporting materials for OLEDs.

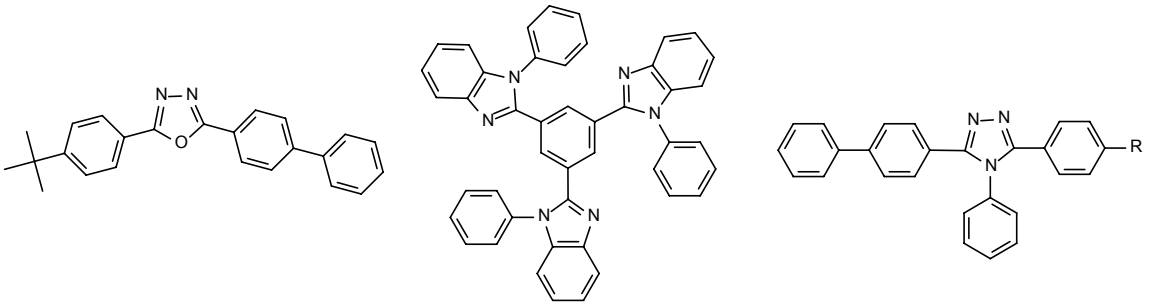

Figure 1.5. Electron-transporting materials for OLEDs.

The energy diagram of single layer OLEDs and multilayer OLEDs are shown in Figure 1.6.[27,28] It can be seen that the introduction of hole and electron injection layers helps to effectively reduce the barrier for charge injection. Matched energy levels will greatly enhance the device efficiency.

According to the mechanism and structure of OLEDs, the performance of an OLED depends on two key factors: device configuration and light-emitting material. In this project, we mainly focus on luminescent material research.

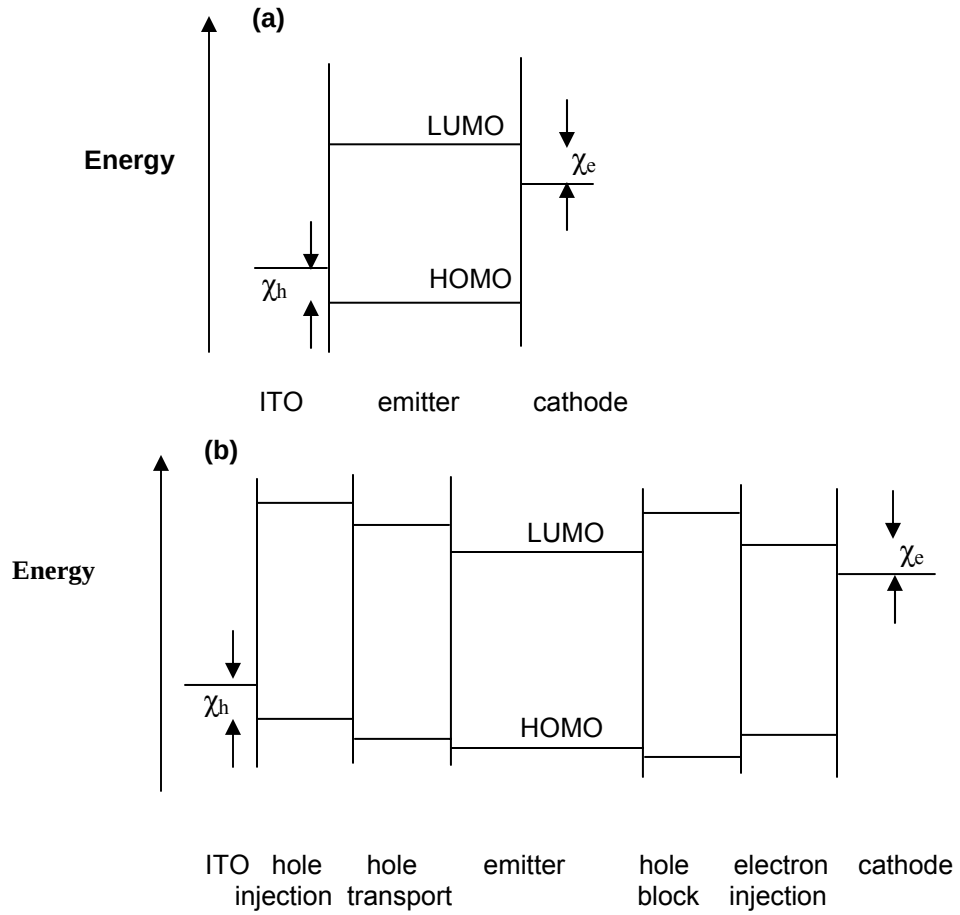

Notes: LUMO represents lowest unoccupied molecular orbital. The energy barriers for the injection of holes and electrons are denoted as χ_h and χ_e, respectively.

Figure 1.6. Schematic energy level diagram of an (a) single-layer OLED and (b) OLED with additional hole-injection/hole transport/hole-blocking /electron injection layers.

1.2 Light-emitting materials for OLEDs

For OLEDs, luminescence comes from radiatively decay of excitons. There are two kinds of excitons, singlet and triplet. Approximately one singlet exciton is created for every three triplet excitons. Singlet excitons can decay radiatively at room temperature, producing luminescence known as fluorescence, while radiative decay of triplet excitons is forbidden at room temperature. The process can be illustrated by Jablonski diagram (Figure 1.7).[29] The ground, first and second electronic states are depicted by S_0, S_1 and S_2,

respectively. Absorption of energy excites molecules from ground state S_0 to excited state S_1 or S_2. With a few rare exceptions, molecules in higher excited state S_2 rapidly relax to lower excited state S_1 by internal conversion. Molecules in the S_1 state can decay directly to produce fluorescence. Molecules in the S_1 state can also undergo an intersystem crossing to the first triplet state, T_1. Emission from T_1 is termed phosphorescence and is generally shifted to longer wavelengths (lower energy) relative to fluorescence.

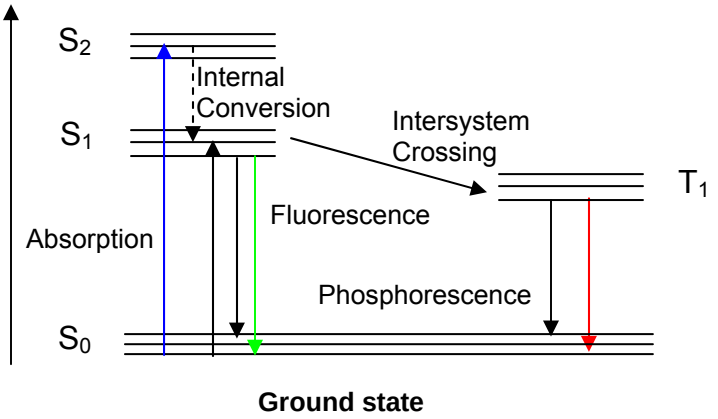

Figure 1.7. Simplified Jablonski diagram.

The lifetimes of singlet and triplet excitons are different; fluorescence lifetime is fast and is on the order of subnanoseconds,[30] while the triplet exciton has a considerably longer lifetime as compared to the singlet, with typical lifetimes on the order of 10 - 100 μs.[31] Due to the long lifetime of triplet excitons, they tend to undergo deactivated process, decay nonradiatively or quench emission. Since the radiative decay of triplet excitons is forbidden at room temperature, the early organic light-emitting material research mainly concentrated on fluorescent materials. The inclusion of transition heavy metal atoms in the molecular structure can give strong spin-orbit coupling which leads to singlet-triplet state mixing, realizing phosphorescence at room temperature.

According to the nature of excitons and the mechanism of luminescence, organic luminescent materials can be divided into two main categories: fluorescent and phosphorescent materials.

1.2.1 Fluorescent materials

There are two branches for fluorescent materials, small molecules and polymers based on the molecular weight. Besides Alq_3, coumarin and rubrene, some metal chelates, such as zinc and beryllium, copper and barium chelates[32] and conjugated small molecules have been widely used as small molecular emitters in OLEDs (Figure 1.8).

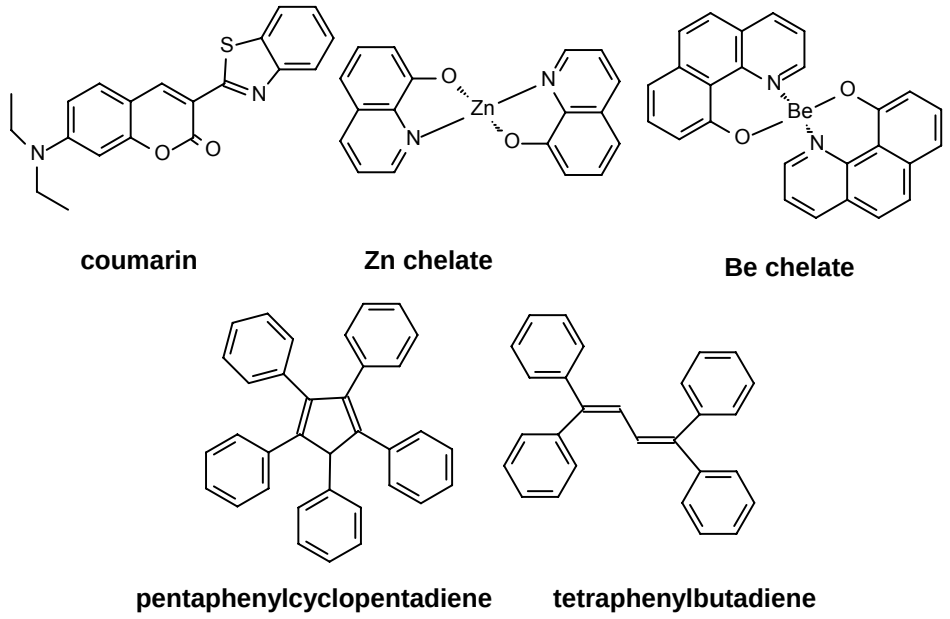

Figure 1.8. Structures of small molecular fluorescent materials for OELDs.

Fluorescent small molecules can be easily synthesized and purified. Up to now, the three primary colors, red, green and blue (RGB) light emission, all can be obtained from small molecular materials with high brightness and efficiency in multilayer devices. For example, in the device that rubrene and coumarin were used as dopants, the current

efficiency reached 6.4 cd/A and 9.0 cd/A at 100 mA/cm^2 respectively.[33] Currently, green fluorescent OLEDs with small molecules as dopants have achieved EQE of nearly 10% with CIE coordinates of (0.24, 0.62).[34] However, the poor solubility of small molecules will not allow them to be solution processed. Thus, their thin films were prepared by vacuum vapor deposition and caused high cost. Furthermore, small molecules tend to crystallize readily and hence they usually exist as crystals below their melting points, which will shorten the lifetime of devices. Thus one effort for small molecules is to improve their solubility by introducing some substituents to render them solution processibility and at the same time suppress their crystallization in solid state by designing three dimensional structural molecules.

The development of fluorescent polymers almost paralleled to small molecules. The semi-conducting properties of conjugated polymers result from their extensively delocalized *p*-orbitals along the polymer chains. The first green light-emitting polymer, PPV,[4,35] initially was prepared from precursor route. However, its insoluble, intractable and infusible properties make it uneasily processed. Its derivative poly[2-methoxy-5-(2-ethylhexyloxy)-p-phenylenevinylene] (MEH-PPV)[36,37] enhanced the solubility by introducing dialkoxy side chains and also shifted the light emission to red region. It was found that the introduction of substituents not only has a favorable effect on solubility of the polymer, but also allows the modification of the electronic properties, e.g. bandgap, electron affinity and ionization potential. Ever since they were synthesized, PPV and its derivatives have been extensively studied and blue, green and red emissions have been achieved.[38] Polythiophene (PT) and its derivatives provided a new series of materials from red to blue light emission.[39-43] As for red emitters, the most widely known polymers

were MEH-PPV and regioregular poly (3-hexylthiophene) (P3HT) and they found wide application in optoelectronic devices due to their well ordered thin film, high charge carrier mobility.[44-48] Although blue emission from PPV and PT derivatives has been reported, their device performances cannot meet the requirement for commercial display application. For blue fluorescent polymers, they need large HOMO-LUMO energy gap and thus short conjugated segments. Poly(*para*-phenylene) (PPP),[1,5,48,49] polyfluorene (PF), and their derivatives[6,37,50-52] are the most widely used blue emitters which realized bright and high efficient blue light emission (Figure 1.9). However, compared with other color light emission, the efficiency of blue EL materials are still low. Thus, highly efficient blue light-emitting polymers are the main challenge for fluorescent polymers and a variety of blue fluorescent polymers have been designed and synthesized aiming to improve their brightness, efficiency and color purity. Except the above conjugated homopolymers, conjugated copolymers were also developed to optimize properties of materials and tune their bandgap further, such as fluorene-thiophene and fluorene-carbazole based copolymers. Fluorene based copolymers have received a lot of attention due to their excellent solubility, excellent charge mobility, convenient color tunability and high regioselectivity in coupling reactions.[53-59]

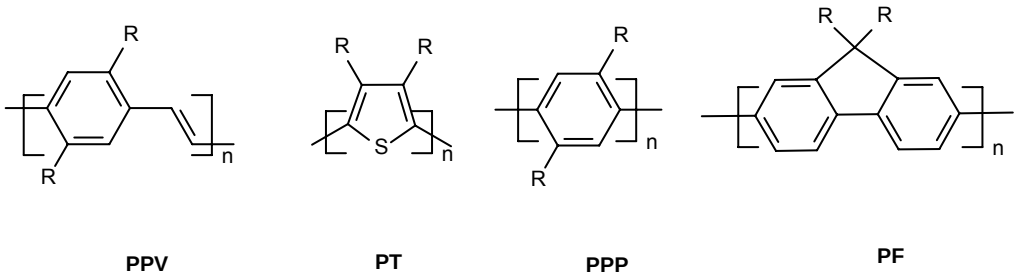

Figure 1.9. Structures of conjugated polymers.

For the above conjugated polymers, their emission wavelength and solubility considerably depend on the nature and regularity of their side chains. Alternation of substituents and regioregularity has a crucial effect on properties of polymers, which offers a flexible and versatile approach to achieve the desired properties for polymers.

Polymers are advantageous in processibility over small molecules and the efficiency of materials is mainly determined by the polymer structures. However, the purity of polymers normally is poorer than that of small molecules, which results in relatively low device efficiencies and lifetime. The device performance is also affected by two other factors, one is the excimer and the other is quenching center in the materials. Excimers may be formed when the backbones of neighboring chains are closely packed, resulting in red shifted and broaden spectrum.[56,60-62] The quenching sites are the defects in polymers. For example, there are some fluorenone defects in polyfluorenes, and these ketones will act as charge carrier traps.[63] Thus, improving the purity, and reducing defects in polymers, suppressing their close packing are the effective ways to enhance the efficiency of PLEDs.

1.2.2 Phosphorescent materials

Different from singlet excitions, radiative decay of triplet excitons is spin-forbidden and often very inefficient at room temperature. The presence of transition heavy metal atoms in cyclometalated complexes provides a strong spin-orbit interaction that allows for efficient intersystem crossing between singlet and triplet excited states, which results in triplet excitons radiatively decay.[64] Transition heavy metal (Pt, Ru, Ir, Re, Os) complexes and rare-earth metal complexes (Eu, Tb) containing suitable ligands have

realized highly efficient phosphorescence at room temperature. The photophysics of these cyclometalated complexes have been extensively investigated. Their luminescence originates from the lowest triplet metal to ligand charge transfer excited state (^{3}MLCT). In the process of MLCT, an electron located in a metal-based *d*-orbital is transferred to the ligands. Phosphorescent materials can harvest both singlet and triplet excitons and triplet harvesting allows all the excited states to contribute to light emission. Thus, in theory, the internal quantum efficiency of phosphorescent materials can reach 100%. Comparing with the lifetime of singlet excitons, the lifetime of triplet excitons is in microsecond. In the last decade, much attention in OLEDs has been directed to phosphorescent materials and they have demonstrated much higher external quantum efficiency (EQE). As a matter of fact, phosphorescent materials have broken through the EQE upper limit for fluorescent materials, which is around 5%. EQEs of phosphorescent materials can be as high as 20%. Three primary color polymer electrophosphorescent light-emitting diodes have already been demonstrated and the efficiencies of the devices are improving steadily.

1.2.2.1 Transitional metal complexes

A prior reported phosphorescent material was an Eu complex, tris(1,3-diphenyl-1,3-propanediono)(monophenanthroline)Eu [Eu(DBM)$_3$(phen)] in 1994, which showed sharp red emission with EQE of 1.4%.[65] Five years later, a much better deep red light-emitting platinum porphyrin complex, PtOEP was developed. It was found that PtOEP based device EQE was improved from 4 to 5.6% with different host, Alq_3 and CBP, respectively. The Commission Internationale de l'Echairage (CIE) coordinates are (0.70,

0.30).[66,67] After that, several kinds of transitional metal complexes have been used in phosphorescent materials, Ir complexes, Ru complexes,[68,69] and Os complex[70,71] are well-known cyclometallated complexes for OLEDs, examples are listed in Figure 1.10.

In these phosphorescent materials, metals act as light transfer centers and ligands (organic part) tune light emission color, solubility of complexes, exciton lifetime and thus device efficiency.

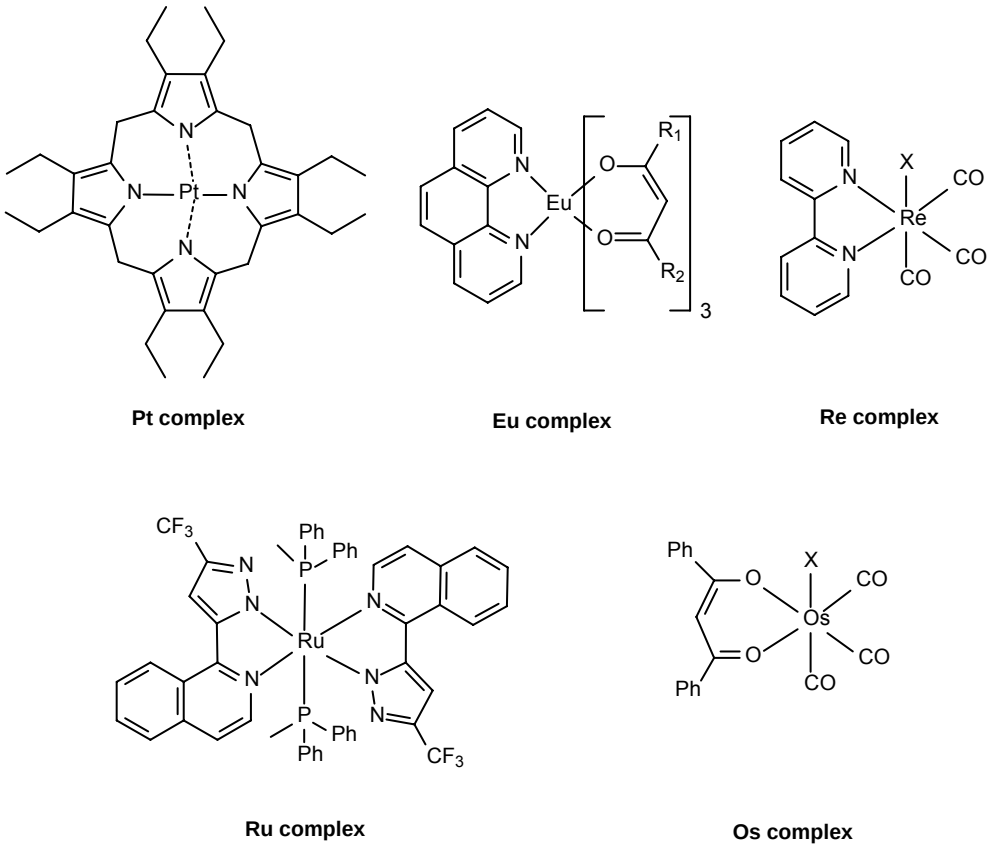

Figure 1.10. Phosphorescent cyclometalated complexes for OLEDs.

It was found that most of the phosphorescent complexes except Ir complexes can only realize orange or red light emission, the emission color of complexes is not sensitive to their ligand structures.

1.2.2.2 Iridium complexes and their advantages

Among Pt, Eu, Os, Re, Ru, Ir based transitional organometallic complexes that have employed as phosphorescent emitters, Ir complexes have attracted much more attention due to their higher efficiency and flexible color tunability, reversible electrochemistry, synthetic versatility, and robust nature. Ir complexes represent the most efficient and versatile class of phosphorescent emitters produced to date. Ir complexes for OLEDs are octahedral with a 3+ oxidation state and the observed luminescence is the emission primarily from a triplet MLCT state or a ligand-based (π-π^*) excited state.[72] The key ligands in the Ir complex are generally derivatives of *o*-pyridylarene or *o*-pyridylheterocycle that coordinate to the metal center via formation of an Ir-N and Ir-C bond. Light emission of Ir complexes is sensitive to their ligand structures and the cyclometalating and ancillary ligands can be independently modified. Thus it is possible to endow a complex with specific photophysical and electrochemical traits. It is also an advantage over other metal complexes to achieve tunable light emission over the whole visible range through modification of the ligand structures. The high efficiency of Ir complexes comes from their shorter exciton lifetimes, which were within the range of 1 to14 μs,[73] and effectively alleviated triplet-triplet annihilation at high currents.

According to the ligand structures, the existing Ir complexes can be divided into three subareas: small molecules, dendrimers, and polymers. The ease of synthesis and color tuning has attracted a lot of efforts in developing new small molecular ligands to improve the efficiency of Ir complexes. Facial tris(2-phenylpyridine) iridium complex [$Ir(ppy)_3$], bis[2-[2'-benzo(4,5-a)thienyl]pyridinato-N,C3'] iridium(acetylacetonate) [$(btp)_2Ir(acac)$] and bis[(4,6-difluorophenyl)-pyridinato-N,C2'] (picolinate)iridium (FIrpic) are the most well-known representatives for small molecular Ir complexes owing to their simple

structure and high efficiency, which emit green, red and blue light, respectively. Their structures are shown in Figure 1.11.

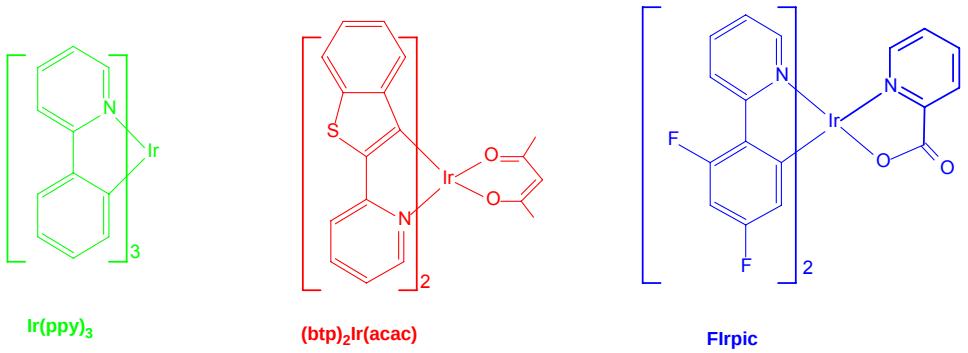

Figure 1.11. Structure of green, red and blue light-emitting Ir complexes.

Hitherto, homoleptic Ir complex *fac*-Ir(ppy)$_3$ is the most widely investigated green light-emitting material since it was reported in 1999.[74] The phosphorescent decay time of Ir(ppy)$_3$ is shorter than 1μs, which greatly reduces saturation of phosphors at high current density. Thus, a variety of devices employed Ir(ppy)$_3$ as phosphorescent dopant materials have been reported and the device efficiency was improved continuously.[17,75] So far, the peak external quantum efficiency and power efficiencies had reached 19.3% and 77 lm/W, respectively.[76] The device employed a double emission layers that TAZ acted as electron-transporting host and TCTA as hole-transporting host. Due to the advantage of simple structure and easy synthesis, a large number of Ir(ppy)$_3$ derivatives were synthesized and fabricated into devices. For example, attaching electron-withdrawing groups, such as fluorine onto the ligand can result in blue light emission complexes.[77]

The first red light emitting Ir complex (btp)$_2$Ir(acac) was developed by Thompson and Forrest in 2001.[67,78] EQE of 7.0%, with CIE coordinates of (0.67, 0.33) has been achieved with a device configuration of ITO/NPD(50 nm)/BCP:7%(btp)$_2$Ir(acac) (20 nm)/BCP(10

nm)/Alq_3(65 nm)/Mg:Ag/Ag. The color is very close to the standard red light, which CIE is (0.65, 0.35). Recently, Tsuboyama et al synthesized another red Ir complexes tris(1-phenylisoquinoline) iridium [$Ir(piq)_3$]. The corresponding device realized pure color and long lifetime with CIE (0.68, 0.32) and EQE of 10.3%.[79]

The first blue Ir complex FIrpic was also reported by Thompson and Forrest in the same year of 2001.[67] The EQE of FIrpic reached 5.7% with CIE of (0.16, 0.29) based on the device configuration of ITO/CuPc(10 nm)/NPB(30 nm)/CBP:6 wt% FIrpic (30 nm)/BAlq (30 nm)/LiF (1 nm)/Al (100 nm). Two years later, the EQE of FIrpic was further enhanced to 7.5% in 2003 by using N,N'-dicarbazolyl-3,5-benzene (mCP) as host.[80] In the same year, the deep blue light emission device employed bis(4',6'-difluorophenylpyridinato)tetrakis(1-pyrazolyl)borate (FIr6) as guest and silane based wide energy gap materials as host, the device realized 11.6% EQE with the CIE coordinates of (0.16, 0.26).[81]

In comparison with small molecular complexes, dendrimeric complexes are macromolecules consist of cores, dendrons and surface groups. The cores can be designed to determine the key electronic properties, such as light emission wavelength. The dendrons can offer steric hindrance and surface groups can ensure essential solubility. Dendrimers have two main advantages over small molecules. First, they can be produced via modular synthesis giving a greater flexibility over controlling the properties. Second, the processing and electronic properties can be optimized independently. However, their synthesis and purification are not as easy as small molecules.

So far, Ir dendrimeric complexes were mainly developed by Paul L. Burn's group. The red, green and blue light emission dendrimer structures are shown in Figure 1.12. In

2002, a green phosphorescent dendrimer, IrppyD was reported by his group,[82] achieving a maximum efficiency of 55 cd/A (40 lm W^{-1}) at 400 cd m^{-2} based on device structure of ITO/13 wt% IrppyD:TCTA/TPBI/LiF/Al. In 2004, two red dendrimers were synthesized and fabricated into devices, realizing EQE of 5.7% based on the device structure of Al (50 nm)/Ca (12 nm)/LiF (0.4 nm)/TPBI(50 nm) /dendrimer: CBP(20:80 wt %)(50 nm)/ITO.[83] At the end of 2005, a light-blue light emission dendrimer was reported by the same group,[84] which achieved EQE of 10.4% with 30 wt % blending of dendrimer in 2,3-bis(N-carbazolyl)benzene (mCP).

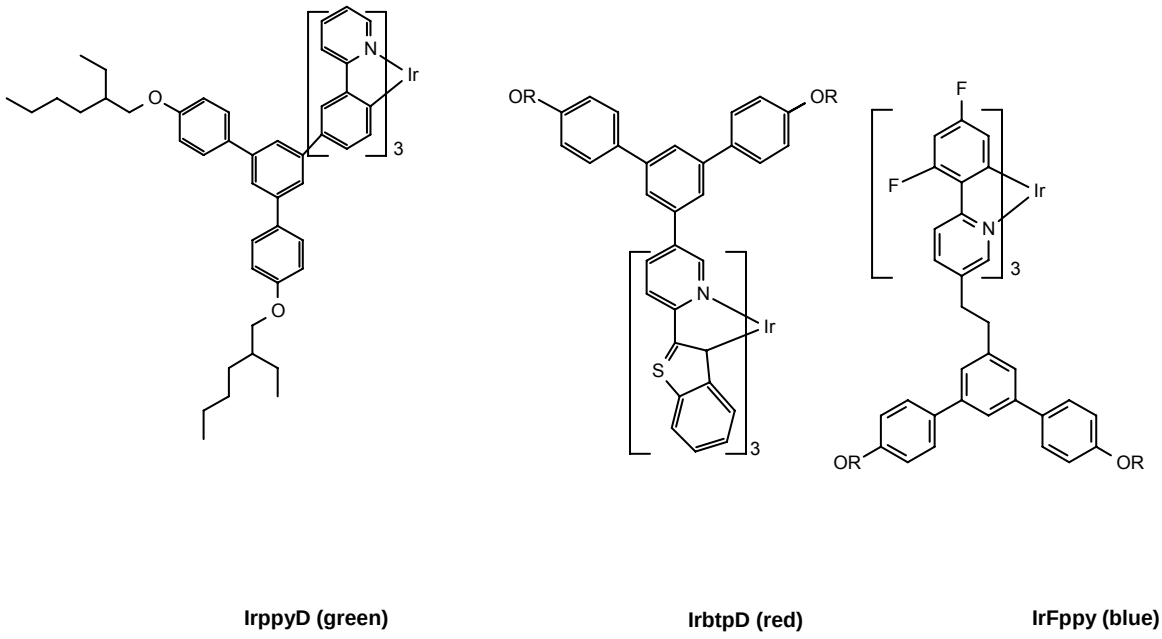

Figure 1.12. Structures of RGB Ir dendrimeric complexes.

For phosphorescent OLEDs, one of the main issues is triplet-triplet (T_1-T_1) annihilation at high currents due to the relatively long phosphorescence lifetimes, which cause saturation of emission sites and quench the light emission. Long emission lifetimes also cause a longer range of exciton diffusion, which may be more easily quenched by

trap sites in the materials. Consequently, significant electroluminescent energy loss occurs. To solve this problem, novel ligands were synthesized to achieve complexes with short exciton lifetime. It was found that a relatively short phosphorescence lifetime can suppress significantly T_1-T_1 annihilation and improve the performance of a phosphorescent material, especially with respect to its maximum brightness and efficiency at high current density. Another issue for phosphorescent OLEDs is the concentration quench due to the aggregation of phosphors. Hence organic phosphorescent materials are often adopted as dopants dispersed in host materials with good carrier transport property and processibility, which can help to suppress concentration quenching. In the doping system, energy transfers from host to guest following Forster-type.[85] Their relative energy level will also affect the device efficiency.

Usually, the host and guest combine to form thin film by co-evaporation or co-spin casting. The basic requirement for an effective guest and host system is that the energy gap of the guest molecule must be smaller than that of the host molecules and at least one of HOMO or LUMO level of guest should be located within HOMO-LUMO levels of the host. Only the matched energy levels between host and guest can guarantee effective energy transfer from host to guest. The schematic energy levels between host and guest is shown in Figure 1.13. The energy difference between the triplet energies of host and guest materials is very important in the confinement of triplet energy on the guest molecules.[86-88] Besides the matched energy levels, the doping concentration of guest must be well controlled. The blending concentration must be higher than a critical concentration to suppress the light emission from host, and also need to be lower than another critical concentration to prevent self-quenching (concentration quenching) among

the guest emitters owing to aggregation of dye molecules. If the dopants possess large steric hindrance, concentration quenching weakens.

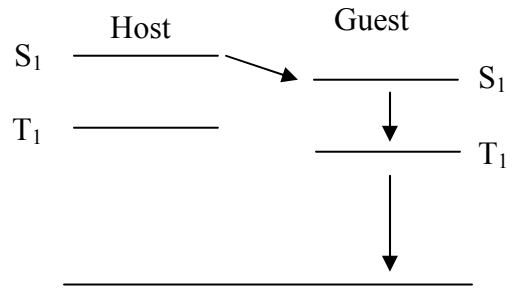

Figure 1.13. Energy levels of an efficient host and guest system.

Usually most of the hosts are good at hole transport due to the low electron affinity of organic materials. Arylamino-containing organic substances are the most popular host material candidates.[89] Good host materials at least meet the following basic requirements. First, they should be semi-conducting and the photoluminescence (PL) wavelength must be within the range of visional light; second, good hole or electron transporting ability is necessary; third, they should form uncrystallized uniform film, which means that nonplanar molecular configuration is preferred; the last, they must have good thermal stability, i.e., high glass transition temperature (T_g). Small molecules, such as, 4,4'-N,N'-dicarbazole-biphenyl (CBP),[90] and 4,4',4"-tri(N-carbazolyl)triphenylammine (TCTA),[91] polymer poly(vinylcarbazole) (PVK)[92-94] have excellent hole transport ability and high triplet energy levels. Thus they were widely used as host materials for phosphorescent emitters. Their structures are shown in Figure 1.14. In order to balance the charge transport, electron transporting materials were also necessary. To date, the most widely used electron-transporting host material is still Alq_3 due to its excellent electron transport

ability, thermal and morphology stability.[1,95] Thus it cannot only be used as green emitter, but also as host materials for red or orange phosphors due to its relatively low energy gap. Along with Alq_3 and its derivatives, other metal chelates, lanthanide and boron complexes have been used as electron-transporting host in OLEDs.[96]

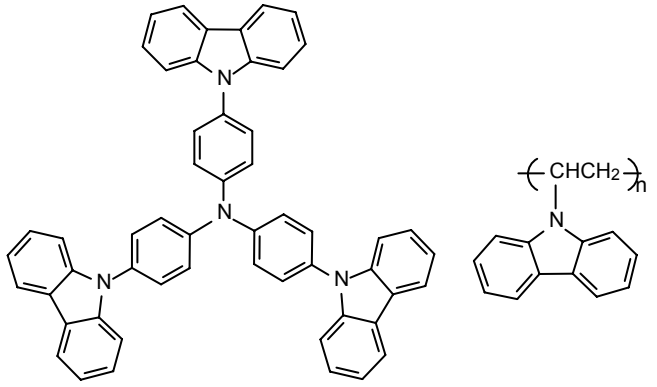

Figure 1.14. Host materials of TCTA and PVK.

Up to now, most of the works on electrophosphorescence devices using transition metal complexes have adopted doping systems in either organic molecules or polymer, which realized solution processibility and uniform thin film. However, the blending system for small molecules and dendrimers may intrinsically suffer from the limitation of efficiency and stability due to the possible energy loss by transfer from host to low-lying triplet states aggregation of dopants even at low-doping concentrations, and potential phase separation which results in fast decay of efficiency with the increasing of current density.[97] An approach to circumvent the problem of phase separation is to attach low molecular weight phosphorescence dye to the polymer by covalent bonds.

Extensive investigation has been done in small molecular and dendrimeric complexes. The development of polymeric complexes was however sluggish and mostly based on Ir

complexes. In 2002, an Ir complex based copolymer, poly((Ir(ppy)$_2$(2-(4-vinylphenyl)pyridine))-co-vinylcarbazole)), containing both carbazole and Ir complex as side groups, had been developed. The device showed EQE of 4.4%.[98] Another attempt was made to obtain polymeric Ir complexes by attaching the phosphorescent groups to the side chain of polymers in 2003 by Chen's group.[99] Polyfluorene was chosen as backbone, the cyclometalated Ir complexes and carbazole were grafted to the side chains (Figure 1.15). The Ir complexes act as phosphorescent dopants and carbazole offer excellent charge transport ability, while the polyfluorene act as polymer host. The device based on the above polymeric Ir complex realized red light emission with EQE of 1.59%.

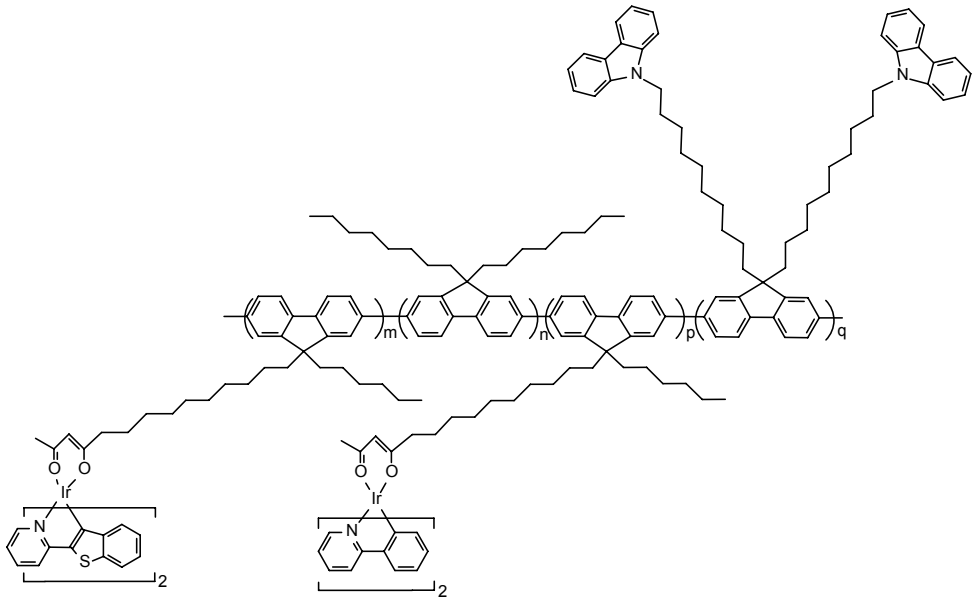

Figure 1.15. Structure of PF-Cz-Ir complexes.

In 2006, phosphorescent polymers with Ir complexes bound to the polymer backbone were reported.[100] Fluorene, pyridine, thiophene were chosen as the monomers to form copolymer backbones. The fluorene-pyridyl blocks also acted as ancillary ligands of Ir complexes and were linked to the polymer backbones; the main ligands were 2-

phenylpyridine. The polymer structures were shown in Figure 1.16. Through changing the molar fraction of the Ir complexes in polymers, the energy levels of copolymers were tuned to reduce triplet quenching. However, the energy transfer from the polymer backbone to the Ir complex was not effective, which resulted in low efficiency. The highest EQE was only 1.29% from the thiophene-fluorene based copolymer.

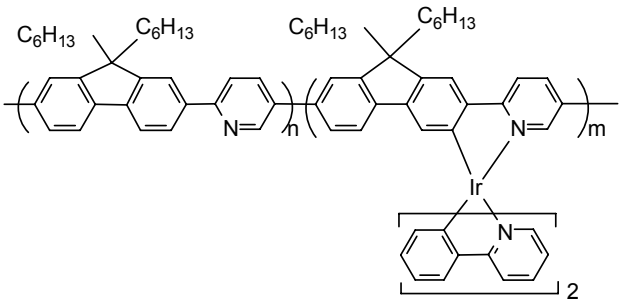

PFPyIr

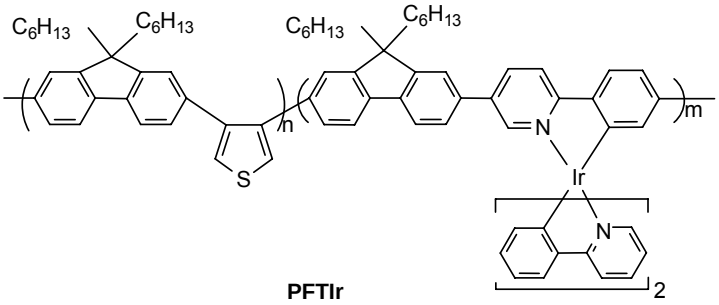

PFTIr

Figure 1.16. Structures of PF-Py-Ir and PF-T-Ir complexes.

Hitherto, the efficiency of polymeric phosphorescent light emission materials is far below small molecules. The main reason is supposed to be inefficient energy transfer from the polymer backbone to cyclometalated complexes.

1.3 Challenges for the phosphorescent OLEDs research

Although great progress has been made in development of phosphorescent OLEDs, much effort is still needed to improve device efficiency by developing higher efficiency materials or optimizing device structures. For Ir complexes, there are still three main issues need to be addressed before it can be successfully commercialization for display application. The first and also the major one is triplet-triplet (T_1-T_1) annihilation. The long lifetime of excitons will tend to cause saturation of the emission sites and results in T_1-T_1 annihilation at high current density. Thus development of phosphors with shorter triplet exciton lifetime is one of the effective remedies.

Efficient OLEDs also require materials that are highly luminescent in solid state. Most light-emitting materials are strongly luminescent in dilute solution. However interactions between the molecules at high concentrations presented in solid state lead to excimer or aggregate formation, which will quench the luminescence. To address the second issue of concentration quenching, which appears when emitting centers are closely packed in the solid state (thin film), development of metal complexes incorporated with bulky ligands is an effective solution. 3-D structural ligands are preferable and they will effectively suppress both concentration and T_1-T_1 quenching.

The third issue that need be considered is the processibility of phosphorescent emitters. Materials with poor solubility can only be fabricated into device by vacuum deposition, which increase the cost. Good processibility can realize versatile low cost processing techniques, i.e., printing, spin-coating, solution-injecting. Usually phenyl rings are the most popular moieties presented in ligands for Ir complexes due to their conjugation properties. The main side effect is the poor solubility especially when the

structure is bulky. Thus designing ligands and complexes with good solubility is much desired.

For polymeric phosphors, the efficiency of reported polymeric Ir complexes was much lower than small molecular Ir complexes due to the unmatched energy levels between polymer backbone and phosphors. There are two ways to improve the energy transfer between host and guest. One way is to enhance the energy gap of the polymer, another method is to decrease the energy level of Ir complexes. Low molecular weight of the phosphorescent polymers is another issue, which is attributed to achieve uniform thin film. The reason lies in the bulky Ir complexes and their poor solubility.

1.4 Objectives and significance

To address the issues of OLEDs based on phosphorescent small molecular materials, the first purpose of this research is to minimize T-T annihilation in device operation. Thus design and synthesis of novel ligands for Ir complexes to shorten the lifetime of triplet excitons is the best choice. The second purpose of this research is to suppress concentration quenching effectively by designing a series of ligands based on spirobifluorene structures. Reported results indicated that aryl substituents at C9 of fluorene will not affect the absorption and emission maxima but have a pronounced effect on the solid-state photoluminescence efficiencies. Introduction of aryl substituents to fluorene based materials is significantly beneficial in improving the morphological stability and resistance to thermal decomposition.[101] Spiro-annulated molecules utilize the spiro-bridge to connect two fluorene units and the resulting three dimensional structures have large steric hindrance to prevent molecules to be closely packed.[102] Their three

dimensional structural feature minimizes the close packing of molecules in the solid state. Thus concentration quenching will be decreased by incorporating spirobifluorene based ligands. Weak concentration quenching also allows higher guest doping concentration, which will result in higher efficiency of devices. The third aim of this research is to improve the processibility of Ir complexes. OLEDs prefer to be fabricated by using glassy and amorphous organic thin films, which will provide significant advantages in cost reduction and device performances. In this project, introduction of a spirolinkage into low molecular weight organic compounds is expected to improve the morphological stability as well as the processability.

In addition to address the above mentioned issues that Ir complexes faced, color tuning can also be realized by changing the effective conjugation length of the ligands because color of the emitting light depends on the chemical structures of ligands. Therefore, the additional aim of this research is to synthesize a series of high efficient, multiple color emission Ir complexes by modifying conjugation length of the spirobifluorene-based ligands.

The novel series of small molecular Ir complexes based on spirobifluorene ligands that were designed and synthesized in this project could overcome the problems that impair the efficiency and lifetime of OLEDs and realize highly efficient and stable OLEDs. The Ir complexes obtained here should offer a useful reference for researchers who focus on phosphorescent light emitting materials for OLEDs.

For phosphorescent polymers, an appealing strategy is the covalent attachment of the desired metal complex to a polymer backbone or side chain to guarantee efficient energy transfer from polymer backbone to Ir complex. Thus, the Ir complexes should have a

lower energy gap than that of the polymer. In addition, inclusion of electron-transport or hole transport moieties will help to improve the device performance further. Processiblity is the last consideration. Solution processibilty is one of the advantages of polymers and uniform thin film is necessary to guarantee the device efficiency. Thus the molecular weight of the phosphorescent polymers needs to be increased further. Since polyfluorene has excellent solubility and film-forming ability, it was chosen as polymer backbones. Diphenylamine based materials is well-known for their outstanding hole transporting ability, thus diphenylamine based ancillary ligand can be copolymerized with fluorene units and form the backbones of the polymers to improve the hole transport. For Ir complexes, 2-phenylpyridine is a simple and commercial available ligand, thus, it was chosen as the main ligands of the Ir complex. It was expected that the light emission of the Ir complex will be in the region of yellow to orange or to red. The polymer backbone is blue light-emitting and the Ir complex is yellow to orange light-emitting. Therefore, efficient energy transfer was expected to be realized from polymer backbones to Ir complexes.

References

1. U. Mitschke, P. Bauerle, *J. Mater. Chem*. **2000**, *10*, 1471.
2. M. Pope, H. Kallmann, P. Magnante, *J. Chem. Phys.* **1963**, *38*, 2042.
3. C. W. Tang, S. A. VanSlyke, *Appl. Phys. Lett*. **1987**, *51*, 913.
4. J. H. Burroghes, D. D. C. Bradley, A. R. Brown, R. N. Marks, K. Mackay, R. H. Friend, P. L. Burns, A. B. Holmes, *Nature* **1990**, *347*, 539.
5. A. Kraft, A. C. Grimsdale, A. B. Holmes, *Angew. Chem. Int. Ed.* **1998**, *37*, 402.
6. F. Cacialli, *Phil. Trans. R. Sco. Lond. A* **2000**, *358*, 173.
7. E. Holder, B. M. W. Langeveld, U. S. Schubert, *Adv. Mater.* **2005**, *17*, 1109.
8. S. Jung, N. G. Park, M. Y. Kwak, B. O. Kim, K. H. Choi, Y. J. Cho, Y. K. Kim, Y. S. Kim, *Opt. Mater*. **2003**, *21*, 235.
9. N. G. Park, M. Y. Kwak, B. O. Kim, O. K. Kwon, Y. K. Kim, B. You, T. W. Kim, Y. S. Kim, *Jpn. J. Appl. Phys*. **2002**, *41*, 1523.
10. Z. Y. Zhong, Y. D. Jiang, *Eur. Phys. J. Appl. Phys*. **2006**, *34*, 173.
11. W.-L. Yu, J. Pei, Y. Cao, W. Huang, *J. Appl. Phys*. **2001**, *89*, 2343.
12. F.-Ch. Chen, L.-J. Kung, T.-H. Chen, Y.-Sh. Lin, *Appl. Phys. Lett*. **2007**, *90*, 073504.
13. P. K. H. Ho, J. S. Kim, J. H. Burroughes, H. Becker, S. F. Y. Li, T. M. Brown, F. Cacialli, R. H. Friend, *Nature* **2000**, *404*, 481.
14. M. M. de Kok, M. Buechel, S. I. E. Vulto, P. van de Weijer, E. A. Meulenkamp, S. H. P. M. de Winter, A. J. G. Mank, H. J. M. Vorstenbosch, C. H. L. Weijtens, V. van Elsbergen, *Phys. Stat. Sol. A* **2004**, *201*, 1342.
15. B. S. Bettington, I. D. W. Samuel, Z. Wang, *J. Mater. Chem*. **2003**, *13*, 80.
16. B. Choudhury, Dissertaion, Iowa State University, Ames, Iowa, **2005.**

17. M. A. Baldo S. Lamansky, P. E. Burrows, M. E. Thompson, S. R. Forrest, *Appl. Phys. Lett.* **1999**, *75*, 4.

18. J.-P. Duan, P.-P. Sun, C. H. Cheng, *Adv. Mater*. **2003**, *15*, 224.

19. C. Qiu, H. Chen, M. Wong, H. S. Kwok, *IEEE Trans. Electron Devices* **2002**, *49*, 1540.

20. Y. Kim, W. B. Im, *Phys. Stat. Sol. A* **200**4, *201*, 2148.

21. X.-M. Yu, H.-S. Kwok, W.-Y. Wong, G.-J. Zhou, *Chem. Mater.* **2006**, *18*, 5097.

22. R. Ragni, E. A, Plummer, K. Brunner, J. W. Hofstraat, F. Babudri, G. M. Farinola, F. Naso, L. D. Cola, *J. Mater. Chem*. **2006**, *16*, 1161.

23. F.-I. Wu, P.-I. Shih, Y.-H. Tseng, G.-Y. Chen, C.-H. Chien, C.-F. Shu, Y.-L. Tung, Y. Chi, A. K.-Y. Jen, *J. Phys. Chem. B* **2005**, *109*, 14000.

24. B. J. Chang, J. H. Park, K. H. Lee, Y. C. Kim, J.-W. Yu, J. K. Kim, *Curr. Appl. Phys*. **2006**, *6*, 658.

25. A. P. Kulkarni, C. J. Tonzola, A. Babel, S. A. Jenekhe, *Chem. Mater*. **2004**, *16*, 4556.

26. J. Bettenhausen, P. Strohriegl, W. Brütting, H. Tokuhisa, T. Tsutsui, *J. Appl. Phys*. **1997**, *82*, 4957.

27. H.-T. Shih, C.-H. Lin, H.-H. Shih, C.-H. Cheng, *Adv. Mater*. **2002**, *14*, 1409.

28. M.-H. Tsai, H.-W. Lin, H.-C. Su, T.-H. Ke, C.-C. Wu, F.-C. Fang, Y.-L. Liao, K.-T. Wong, C.-I. Wu, *Adv. Mater*. **2006**, *18*, 1216.

29. K. Fleming, *Technique in Biophysics 250.690*. **2005** Handout No.8.

30. M. A. Baldo, M. E. Thompson, S. R. Forrest, *Pure Appl. Chem*. **1999**, *71*, 2095.

31. K. Haskins-Glusac, M. R. Pinto, C. Tan, K. S. Schanze, *J. Am. Chem. Soc*. **2004**, *126*, 14964.

32. C. H. Chen, J. Shi, *Coord. Chem. Rev*. **1998**, *171*, 161.

33. B. Wei, K. Furukawa, M. Ichikawa, T. Koyama, Y. Taniguchi, *Mol. Cryst. Liq. Cryst*. **2005**, *426*, 295.

34. K. Okumoto, H. Kanno, Y. Hamaa, H. Takahashi, K. Shibata, *Appl. Phys. Lett*. **2006**, *89*, 063504.

35. D. Braun, A. J. Heeger, *Appl. Phys. Lett*. **1992**, *62*, 385.

36. D. Dini, *Chem. Mater*. **2005**, *17*, 1933.

37. I. D. Rees, K. L. Robinson, A. B. Holmes, C. R. Towns, R. O'Dell, *MRS Bull*. **2002**, *27*, 451.

38. J. A. Mikroyannidis, *J. Appl. Poly. Sci*. **2006**, *101*, 3842.

39. M. Berggren, G. Gustafsson, O. Inganas, M. R. Andersson, T. Hjertberg, O. Wennerstrom, *J. Appl. Phys*. **1994**, *76*, 7530.

40. M. Mazzeo, D. Pisignano, L. Favaretto, G. Barbarella, R. Cingolani, G. Gigli, *Synth. Met*. **2003**, *139*, 671.

41. K. R. Radke, K. Ogawa, S. C. Rasmussen, *Org. Lett*. **2005**, *7*, 5253.

42. I. F. Perepichka, D. F. Perepichka, H. Meng, F. Wudl, *Adv. Mater*. **2005**, *17*, 2281.

43. E. Bundgaard, F. C. Krebs, *Macromolecules* **2006**, *39*, 2823.

44. F.-C. Chen, Q. Xu, Y. Yang, *Appl. Phys. Lett*. **2004**, *84*, 3181.

45. R. P. Barber, Jr. R. D. Gomez, W. N. Herman D. B. Romero, *Org. Electron*. **2006**, *7*, 508.

46. H. Sirringhaus, P. J. Brown, R. H. Friend, M. M. Nielsen, K. Bechgaard, B. M. W. Langeveld-Voss, A. J. H. Spiering ,R. A. J. Janssen, E. W. Meijer, P. Herwig, D. M. de Leeuw, *Nature* **1999**, *401*, 685.

47. J. H. Schon, A. Dodabalapur, Z. Bao, C. Kloc, O. Schenker, B. Batlogg, *Nature* **2001**, *410*, 189.

48. W.-X. Jing, A. Karft, S. C. Moratti, J. Gruner, F. Cacialli, P. J. Hamer, A. B. Holmes, R. H. Friend, *Synth. Met*. **1994**, *67*, 161.

49. Y. Yang, Q. Pei, A. J. Heeger, *J. Appl. Phys*. **1996**, *79*, 934.

50. D. Y. Kim, H. N. Cho, C. Y. Kim, *Prog. Polym. Sci*. **2000**, *25*, 1089.

51. B. Liu, W.-L. Yu, Y.-H. Lai, W. Huang, *Macromolecules* **2002**, *35*, 4975.

52. M. T. Bernius, M. Inbasekaran, J. O'Brien, W. Wu, *Adv. Mater*. **2000**, *12*, 1737.

53. G. Klarner, M. H. Davey, W.-D. Chen, J. G. Scott, R. D. Miller, *Adv. Mater*. **1998**, *10*, 993.

54. Y. He, S. Gong, R. Hattori, J. Kanicki, *Appl. Phys. Lett*. **1999**, *74*, 2265.

55. B. Liu, W.-L. Yu, Y.-H. Lai, W. Huang, *Macromolecules* **2000**, *33*, 8945.

56. S. Setayesh, A. C. Grimsdale, T. Weil, V. Enkelmann, K. Mullen, F. Meghdadi, E. J. W. List, G. Leising, *J. Am. Chem. Soc*. **2001**, *123*, 946.

57. C. D. Muller, A. Falcou, N. Reckefuss, M. Rojahn, V. Wiederhirn, P. Rudati, H. Frohne, O. Nuyken, H. Becker, K. Meerholz, *Nature* **2003**, *421*, 829.

58. J.-H. Lee, D.-H. Hwang, *Chem. Commun*. **2003**, 2836.

59. H. P. Rathnayake, A. Cirpan, Z. Delen, P. M. Lahti, F. E. Karasz, *Adv. Funct. Mater.* **2007**, *17*, 115.

60. S. A. Jenekhe, J. A. Osaheni, *Science* **1994**, *265*, 765.

61. I. D. W. Samuel, G. Rumbles, C. J. Collison, *Phys. Rev. B* **1995**, *52*, 573.

62. I. D. W. Samuel, G. Rumbles, C. J. Collison, R. H. Friend, S. C. Moratti, A. B. Holmes, *Synth. Met*. **1997**, *84*, 497.

63. X.-H. Zhou, Y. Zhang, Y.-Q. Xie, Y. Cao, J. Pei, *Macromolecules* **2006**, *39*, 3830.

64. K.-C. Tang, K. L. Liu, I.-C. Chen, *Chem. Phys. Lett*. **2004**, *386*, 437.

65. J. Kido, H. Hayase, K. Hongawa, K. Nagai, *Appl. Phys. Lett.* **1994**, *65*, 2124.

66. D. F. O'Brien, M. A. Baldo, M. E. Thompson, S. Forrest, *Appl. Phys. Lett*. **1999**, *74*, 442.

67. C. Adachi, M. A. Baldo, S. R. Forrest, S. Lamansky, M. E. Thompson, R. C. Kwong, *J. Am. Chem. Soc*. **2001**, *123*, 1622.

68. H. Xia, C. Zhang, X. Liu, S. Qiu, P. Lu, F. Shen, J. Zhang, Y. Ma, *J. Phys. Chem. B* **2004**, *108*, 3185.

69. Y.-L. Tung, L.-S. Chen, Y. Chi, P.-T. Chou, Y.-M. Cheng, E. Y. Li, G.-H. Lee, C.-F. Shu, F.-I. Wu, A. J. Carty, *Adv. Funct. Mater*. **2006**, *16*, 1615.

70. Y.-L. Tung, P.-C. Wu, C.-S. Liu, Y. Chi, J.-K. Yu,Y.-H. Hu, P.-T. Chou, S.-M. Peng, G.-H. Lee, Y. Tao, A. J. Carty, C.-F. Shu, F.-I. Wu, *Organometallics* **2004**, *23*, 3745.

71. T.-H. Liu, C. H. Chen, *Appl. Phys. Lett*. **2006**, *100*, 094508.

72. Y. Wang, N. Herron, V. V. Grushin, D. LeCloux, V. Petrov, *Appl. Phys. Lett*. **2001**, *79*, 449.

73. F.-C. Chen, Y. Yang, M. E. Thompson, J. Kido, *Appl. Phys. Lett*. **2002**, *80*, 2308.

74. T. Tsutsui, M.-J. Yang, M. Yahiro, K. Nakamura, T. Watanabe, T. Tsuji, Y. Fukuda, T. Wakimoto, S. Miyaguchi, *Jpn, J. App. Phys*. **1999**, *38*, 1502.

75. M. Ikai, S. Tokito, Y. Sakamoto, T. Suzuki, Y. Taga, *Appl. Phys. Lett*. **2001**, *79*, 156.

76. G. He, M. Pfeiffer, K. Leo, M. Hofmann, J. Birnstock, R. Pudzich, J. Sadbeck, *Appl. Phys. Lett*. **2004**, *85*, 3911.

77. R. Ragni, E. A. Plummer, K. Brunner, J. W. Hofstraat, F. Babudri, G. M. Farinola, F. Naso, L. D. Cola, *J. Mater. Chem*. **2006**, *16*, 1161.

78. S. Lamansky, P.Djurovich, D. Murphy, R. A. Razzaq, R. Kwong, I. Tsyba, M. Bortz, B. Mui, R. Bau, M. E. Thompson, *Inorg. Chem*. **2001**, *40*, 1704.

79. A. Tsuboyama, H. Iwawaki, M. Furugori, T. Mukaide, J. Kamatani, S. Igawa, T. Moriyama, S. Miura, T. Takiguchi, S. Okada, M. Hoshino, K. Ueno, *J. Am. Chem. Soc.* **2003**, *125*, 12971.

80. R. J. Holmes, S. R. Forrest, Y.-J. Tung, R. C. Kwong, J. J. Brown, S. Garon, M. E. Thompson, *Appl. Phys. Lett*. **2003**, *82*, 2422.

81. R. J. Holmes, B. W. D'Andrade, S. R. Forrest, X. Ren, J. Li, M. E. Thompson, *Appl. Phys. Lett.* **2003**, *83*, 3818.

82. S.-C. Lo, N. A. Male, J. P. J. Markhan, S. W. Magennis, P. L. Burn, O. V. Salata, I. D. W. Samuel, *Adv. Mater*. **2002**, *14*, 975.

83. T. D. Anthopoulos, M. J. Frampton, E. B. Namdas, P. L. Burn, I. D. W. Samuel, *Adv. Mater*. **2004**, *16*, 557.

84. G. J. Richards, J. P. J. Markham, S.-C. Lo, E. B. Namdas, S. Sharma, P. L. Burn, I. D. W. Samuel, *Adv. Funct. Mater*. **2005**, *15*, 1.

85. T. Tsuboi, N. Aljaroudi, *J. Lumin.* **2007**, *122-123*, 597.

86. S. Tokito, *Appl. Phys. Lett*. **2003**, *83*, 569.

87. X. H. Yang, D. Neher, *Appl. Phys. Lett*. **2004**, *84*, 2476.

88. S. A. Choulis, V.-E. Choong, M. K. Mathai, F. So, *Appl. Phys. Lett*. **2005**, *87*, 113503.

89. S.-J. Yeh, M.-F. Wu, C.-T. Chen, Y.-H. Song, Y. Chi, M.-H. Ho, S.-F. Hsu, C. H. Chen, *Adv. Mater*. **2005**, *17*, 285.

90. X. Zhang, J. Gao, C. Yang, L. Zhu, Z. Li, K. Zhang, J. Qin, H, You, D. Ma, *J. Organometallic Chem*. **2006**, *691*, 4312.

91. G. Schwartz, K. Fehse, M. Pfeiffer, K. Walzer, K. Leo, *Appl. Phys. Lett*. **2006**, *89*, 083509.

92. T.-H. Kim, D.-Y. Yoo, J. H. Park, O. O. Park, J.-W. Yu, J. K. Kim, *Appl. Phys. Lett.* **2005**, *86*, 171108.

93. X. H. Yang, F. Jaiser, S. Klinger, D. Neher, *Appl. Phys. Lett*. **2006**, *88*, 021107.

94. X.-Y. Wang, A. Kimyonok, M. Weck, *Chem. Commun*. **2006**, 3933.

95. L. S. Hung, C. H. Chen, *Mater. Sci. Eng. R* **2002**, *39*, 143.

96. T. Sano, Y. Nishio, Y. Hamada, H. Takahashi, T. Usuki, K. Shibata, *J. Mater. Chem*. **2000**, *10*, 157.

97. K. Zhang, Z. Chen, C. Tang, S. Gong, J. Qin, Y. Cao, *Macromol. Rapid Commun*. **2006**, *27*, 1926.

98. C.-L. Lee, N.-G. Kang, Y.-S. Cho, J.-S. K. Lee, J.-J. Kim, *Opt. Mater*. **2003**, *21*, 119.

99. X. Chen, J.-L. Liao, Y. Liang, M. O. Ahmed, H.-E. Tseng, S.-A. Chen, *J. Am. Chem. Soc*. **2003**, *125*,636.

100. G. L. Schulz, X. Chen, S. Holdcroft, *Macromolecules* **2006**, *39,* 915.

101. K.-T. Wong, Y.-Y. Chien, R.-T. Chen, C.-F. Wang, Y.-T. Lin, H.-H. Chiang, P.-Y. Hsieh, C.-C. Wu, C. H. Chou, Y. O. Su, G.-H. Lee, S.-M. Peng, *J. Am. Chem. Soc*. **2000**, *124*, 11576.

102. Y.-H. Kim, D.-C. Shin, S.-H. Kim, C.-H. Ko, H.-S. Yu, Y.-S. Chae, S.-K. Kwon, *Adv. Mater*. **2001**, *13*, 1690.

2 Development of highly efficient small molecular iridium complex for OLEDs

2.1 Molecular design

For OLEDs that based on small molecules, crystallization of the thin films may lead to formation of excimer and exciplex, which will decrease device efficiency. To address this issue, amorphous small molecules are well suited. Concentration quenching is another issue that decreases device efficiency at high current density. Reports showed that bulky molecules can prevent the close packing of molecules and thus suppress concentration quenching.[1,2] To address the above issues, amorphous spiro linkage structure is one of the good choices. Spiro-type structures offer good film-forming ability and their three dimensional conformation weaken close packing of molecules and thus enhance the luminescence efficiency in solid state.[3-6] In addition, their excellent solubility allows for procession in solution, which will be an advantage over other small molecules that need to be thermally deposited into films. Furthermore, color tuning will be realized by modifying conjugation length of the ligands (Figure 2.1). Thus, a series of small molecular Ir complexes based on spirobifluorene ligands was designed to improve the efficiency and tuning light emission by structure modification.

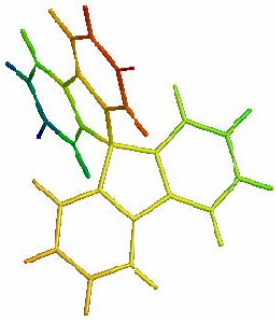

Figure 2.1. 3D structure of spirobifluorene.

The ligand structures that based on spirobifluorene are shown in Figure 2.2 and their corresponding bis-cyclometalated Ir complexes are shown in Figure 2.3. Heteroleptic Ir complexes have two cyclometalated ligands and a single bidentate, monoanionic ancillary ligand. Here, the spirobifluorene based structural ligands were the main ligands, and acetyl acetonate (acac) was chosen to be the ancillary ligand. Acac group together with its derivatives are common choices as ancillary ligands for Ir complexes. For bis-cyclometalated and tricyclometalated structural Ir complexes, normally there are two kinds of isomers, i.e., meridional (mer-) and facial (fac-) co-exisiting in complexes. The meridional isomers display red-shifted emission and decreased QE relative to their facial isomers.[7,8] The meridional isomers could be converted to facial isomers at high temperature, which is a thermodynamic process. Complexes with bulky ligands will prefer to be meridional conformation due to lower steric hindrance. Thus, small ancillary ligand acac was chosen as the ancillary ligand, which will help to reduce the steric hindrance and increase the yield of product and the ratio of facial bis-cyclometalated isomers in the complexes. The stereochemistry of final products depends on the nature of ligand and the reaction temperature. For heteroleptic bis-cyclometalated Ir complexes, the emission wavelength can be tuned through variation of the structure of phenylpyridine C^N, while changing the ancillary ligand leads only to a relatively minor shift.[9]

Ligand **L1** is the parent ligand. From **L1** to **L2**, tert-butyl group was introduced to further enhance the bulk of ligand, and also increased the solubility. From **L2** to **L4**, the conjugation length was increased to tune the emission to longer wavelength. **L5**, **L6**, **L7** is another way to tune the emission color by incorporating naphthyl and quinolyl groups.

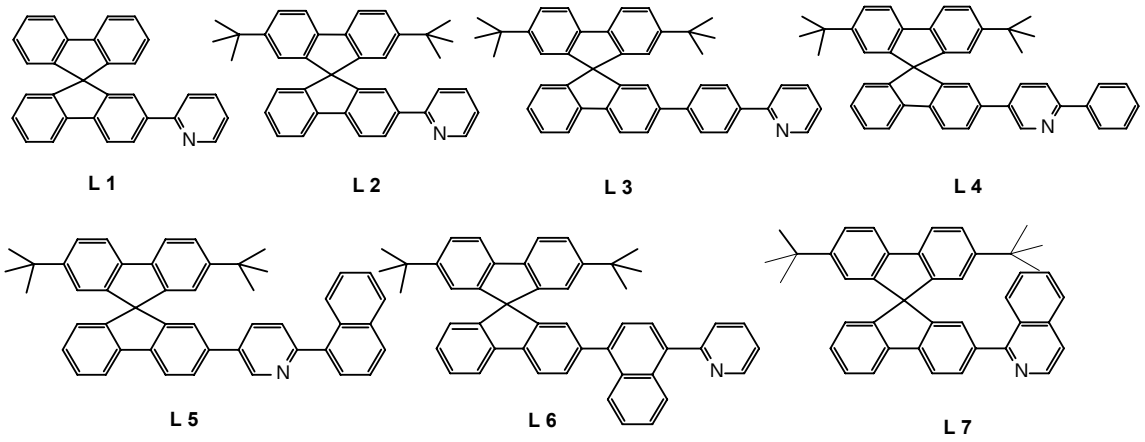

Figure 2.2. Structures of spirobifluorene based ligands.

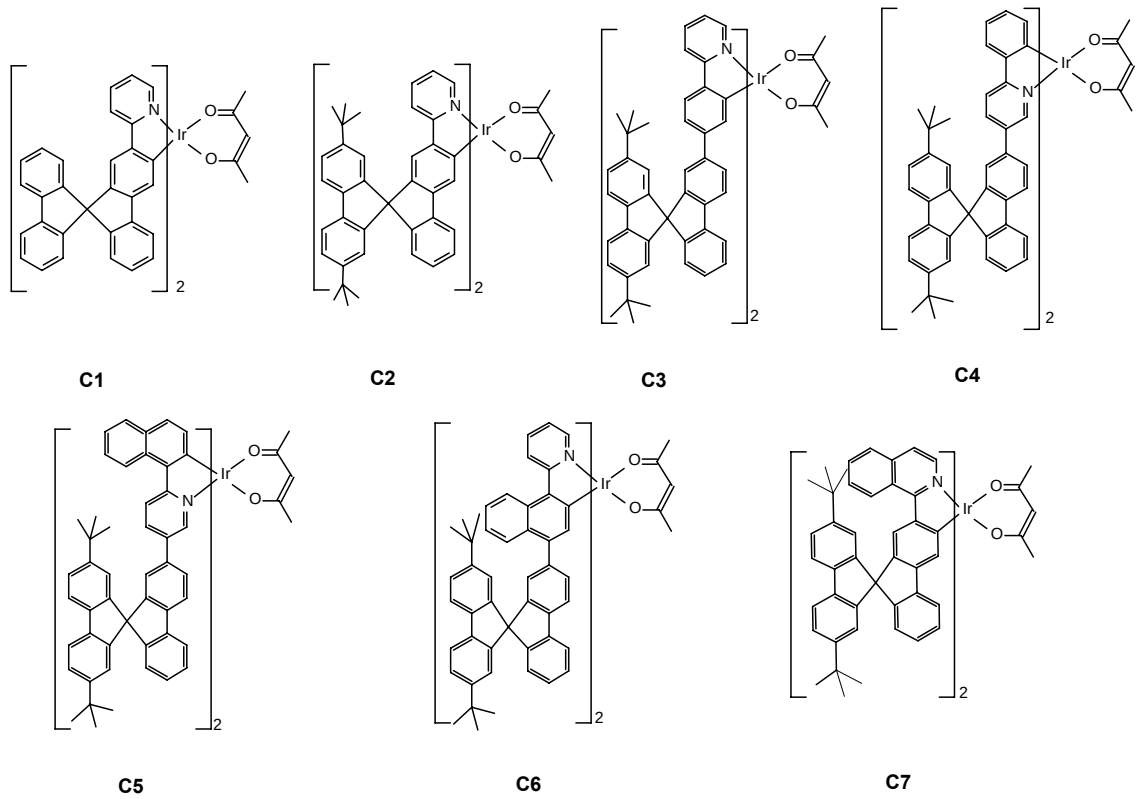

Figure 2.3. Structures of bis-cyclometalated Ir complexes.

2.2 Synthesis and characterization

All the starting materials were purchased from Aldrich, Lancaster, TCI, and Acros. Catalyst tetrakis(triphenylphosphine)palladium(0) [$Pd(PPh_3)_4$] was purchased from Strem and Aldrich, iridium chloride trihydrate ($IrCl_3 \cdot 3H_2O$) was purchased from Grikin Advanced Materials. All the above chemicals were used without further purification. Anhydrous tetrahydrofuran (THF) was distilled from sodium-benzophenone immediately prior to use.

^1H NMR and ^{13}C NMR spectra were measured in $CDCl_3$ solution on a Bruker DPX (400 MHz) NMR spectrometer with tetramethylsilane (TMS) as the internal standard. Mass spectra (MS) were recorded on a Bruker Autoflex TOF/TOF (MALDI-TOF) instrument using dithranol as a matrix.

The general synthetic routes towards the ligands are outlined in Scheme 2.1. First, 4,4'-di-*t*-butylbiphenyl **1** was synthesized from biphenyl, which reacted with tert-butyl chloride in dichloromethane in the presence of catalytic amount of anhydrous ferric chloride with a 100% yield. 2-Bromo-4,4'-di-*t*-butylbiphenyl **2** was obtained from 4,4'-di-*t*-butylbiphenyl through bromination reaction catalyzed by anhydrous ferric chloride in chloroform with a yield of 50%. Then, 2-bromo-9-fluorenone reacted with 4,4'-di-*t*-butylbiphenyl-2-lithium in anhydrous THF solution at -78 ºC, followed by cyclization reaction, producing spirobifluorene **3** with a yield of 54%. Following standard butyl lithium reaction, 2-bis(4,4,5,5-tetramethyl-1,3,2-dioxaborolan-2-yl)-2',7'-di-tert-butyl)-9,9'-spirofluorene **4** was synthesized with a yield of 64% from compound **3**. Ligands **L3** to **L7** were synthesized by following standard Suzuki coupling reactions between compound **4** with **5**, **6**, **7**, **8** and 2-chloroquinoline, respectively, with yields ranging from 74% to 100%.[10]

Due to the steric hindrance and the abnormal reactivity of 2-bromopyridine, ligands **L1** and **L2** cannot be obtained from coupling reaction between spirobifluorene boronic ester and 2-brompyridine. Thus, ligand **L1** and **L2** were synthesized by different routes with other ligands. First, 2-pyridylfluorenone **9** was synthesized by oxidizing 2-fluorenepyridine in pyridine solution by oxygen with a yield of 97%. Following the cyclization procedure, compound **2** and 2-bromobiphenyl reacted with compound **9** to form spiro structures **L1** and **L2** with the yield of 69% and 48%, respectively.

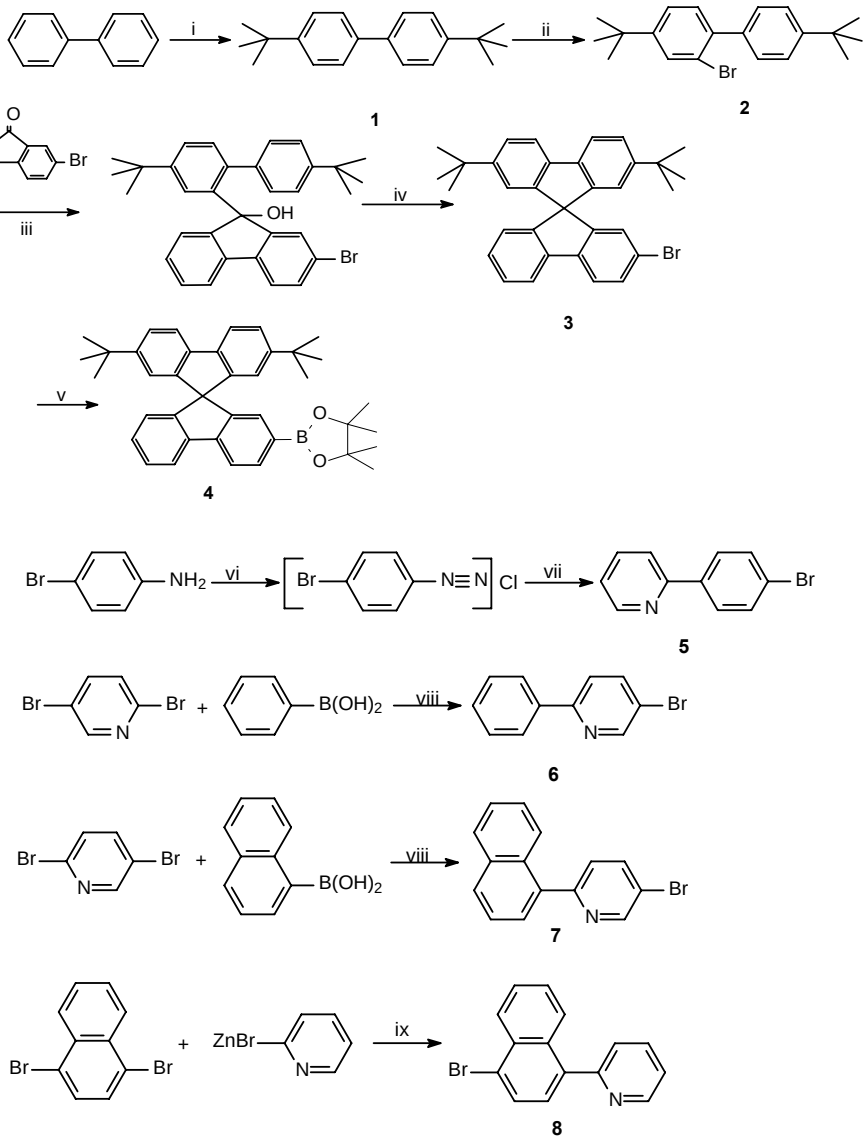

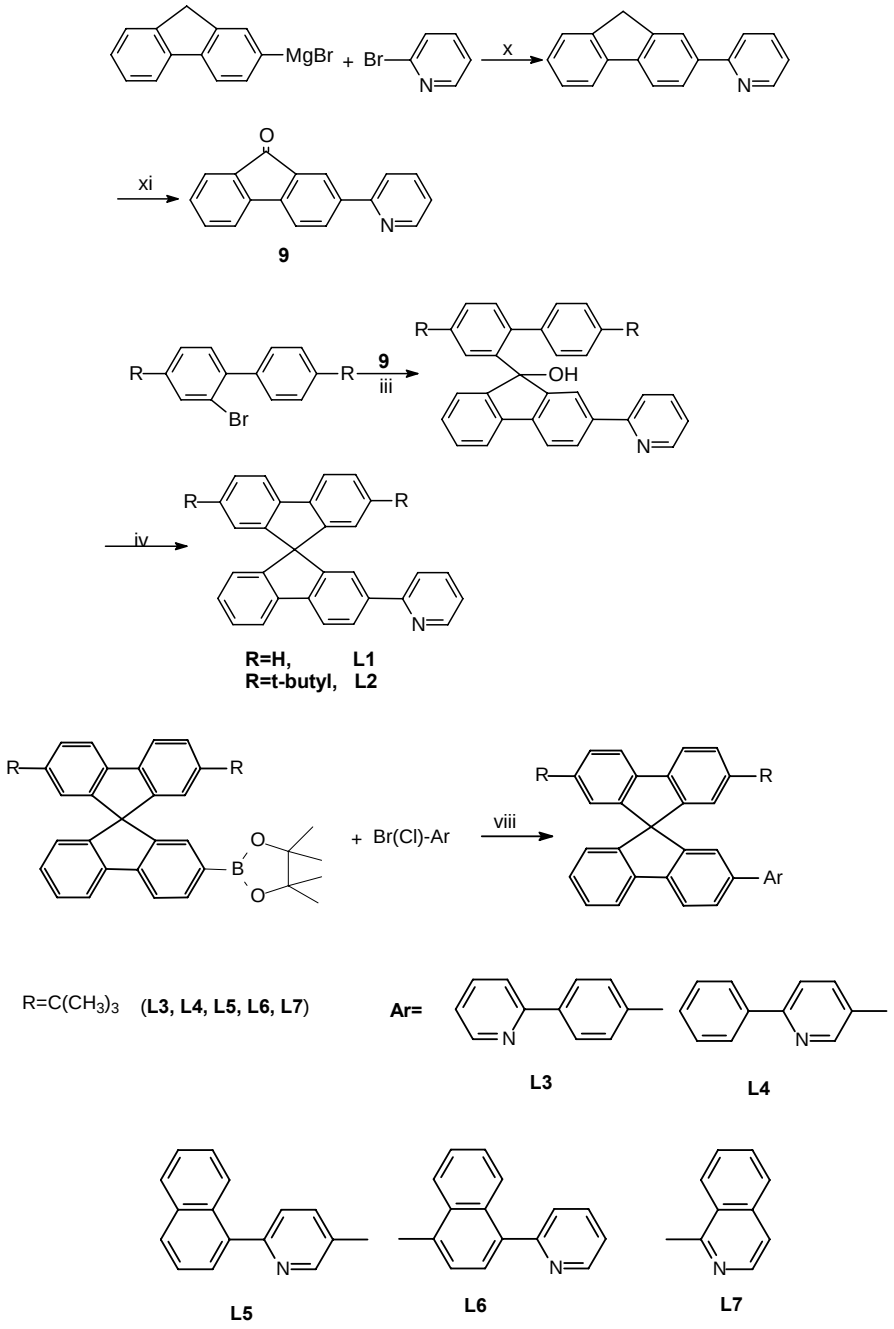

Scheme 2.1. Synthetic routes for the ligands.
Reagents and conditions: i. t-butyl chloride, anhydrous $FeCl_3$, DCM; ii. Br_2, $CHCl_3$, anhydrous $FeCl_3$, 0 ºC; iii. n-BuLi, THF, -78 ºC; iv. HCl, acetic acid, reflux; v. n-BuLi, THF, -78 ºC, 2-isopropoxy-4, 4, 5, 5-tetramethyl-1, 3, 2-dioxaborolane; vi. HCl, H_2O, $NaNO_2$, 0 ºC; vii. pyridine, 40 ºC, Na_2CO_3; viii. Na_2CO_3, toluene, $Pd(PPh_3)_4$, reflux, 24 h; ix. THF, $Pd(PPh_3)_4$, reflux, 24 h; x. THF, $Pd(PPh_3)_4$, reflux, 24 h; xi. pyridine, O_2, overnight.

A standard two-step procedure was followed to synthesize the final heteroleptic Ir complex from the ligand. First, ligands reacted with iridium chloride trihydrate in refluxing 2-ethoxyethanol and water mixture (3:1) overnight under nitrogen to give the intermediate chloride-bridged dimers in medium yields. The dimmer was converted to final Ir complexes after reacting with acac under reflux either in dicholormethane or in 2-ethoxyethanol in the presence of base. The procedure is depicted in Scheme 2.2.

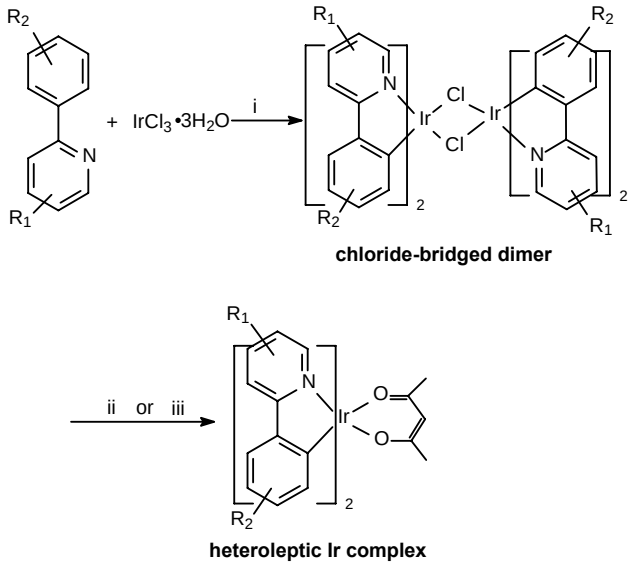

Scheme 2.2. Synthetic routes for the complexes.
Reagents and conditions: i. 2-ethoxyethanol: H_2O = 3:1, reflux, 24 h; ii, DCM, acac, tetrabutylammonium hydroxide, ethanol, reflux, 5 h; iii. 2-ethoxyethanol, acac, Na_2CO_3, reflux, 24 h.

For Ir complexes, there are two kinds of isomers in facial (*fac*) and meridional (*mer*) configuration. Meridional isomers are kinetically favored products. Their structures can be investigated by X-ray graphy and NMR spectroscopy.[8,11] Their stereochemical representation is shown in Figure 2.4.

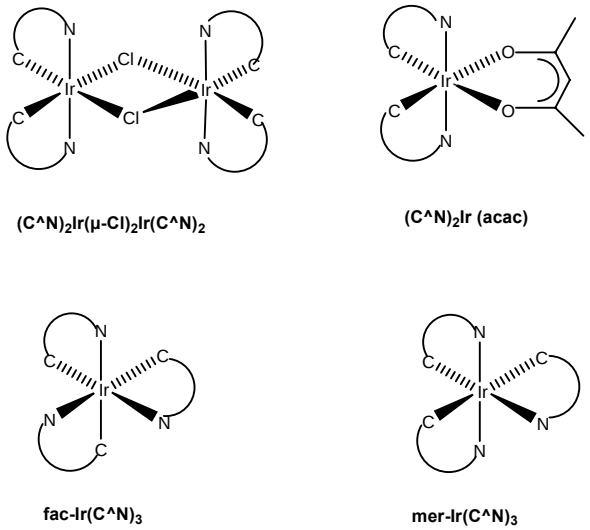

Figure 2.4. Stereochemical representations of chloride-bridged dimer, heteroleptic and homoleptic Ir complexes.

It can be seen that for facial isomers, phenylpyridine ligands are chemically equivalent, and thus their NMR spectra are simpler, while for meridional isomers, the NMR spectra are much more complicated because ligands are under different chemical environments.

2.3 Experimental details

4,4'-Di-tert-butylbiphenyl (1)[12]

To a stirred mixed solution of biphenyl (15.4 g, 100 mmol) and catalyst anhydrous ferric chloride (80 mg) in dichloromethane (100 mL) at room temperature was added slowly tert-butyl chloride (23.2 mL, 216 mmol). After stirring overnight, water was added to terminate the reaction. The organic phase was separated and the water phase was extracted with hexane (100 mL) 3 times. The combined organic phase was then washed with saturated brine, dried over anhydrous $MgSO_4$ and concentrated in vacuo and

gave 26.6 g product (100%). Compound **1** was used directly for next reaction without further purification.

^{1}H NMR ($CDCl_3$, 400 MHz): δ, 7.54 (d, 4H), 7.44 (d, 4H), 1.37(s, 18H).

2-Bromo-4,4'-di-tert-butylbiphenyl (2)

To a solution of 4,4'-di-tert-butylbiphenyl (3.99 g, 15 mmol) and catalyst anhydrous ferric chloride (20 mg) in chloroform (30 mL) at 0 ºC was added bromine (2.4 g, 15 mmol) solved in chloroform (10 mL) dropwisely. The reaction was stirred overnight. The resultant reaction mixture was quenched with sodium carbonate until the orange color disappeared. The organic layer was washed with water and extracted with hexane (50 mL) 3 times. The combined organic phase was washed with saturated brine, dried over anhydrous $MgSO_4$ and concentrated in vacuo to get a mixture of product and starting material. The yield was estimated from NMR spectrum to be about 50%. The product and the starting material have very similar polarity and cannot separate by silica gel column chromatography. The starting material will not affect the next step reaction. Thus product mixture was not purified and was used for next reaction directly.

2-Bromo-(2',7'-di-tert-butyl)-9,9'-spirobifluorene (3)[13]

To a solution of the mixture of 4,4'-di-tert-butylbiphenyl and 2-bromo-4,4'-di-tert-butylbiphenyl (3.06 g, 5 mmol) in anhydrous THF (50 mL) was added dropwise n-BuLi (5 mL, 6 mmol) in hexane at -78 °C, After stirring for 1 h, the mixture was transferred to a solution of 2-bromofluorenone (1.3 g, 5 mmol) in THF (20 mL) at -78 °C and stirred overnight. Then the reaction was quenched with water and extracted with ethyl acetate

(50 mL) 3 times. The organic layer was combined and washed with saturated brine and dried over anhydrous $MgSO_4$ and concentrated in vacuo.

The residue was dissolved in glacial acetic acid (15 mL) and one drop of concentrated HCl was added. The mixture was heated to gentle reflux for 1 h. After the mixture was cooled down to room temperature, the precipitate was filtered and washed with water. The mixture of 2-bromo-(2',7'-di-tert-butyl)-9,9'-spirobifluorene and 4,4'-di-tert-butylbiphenyl was separated by silica gel column chromatography eluted with hexane to provide a white solid product 1.37 g (54%).

^{1}H NMR ($CDCl_3$, 400 MHz): δ, 7.84 (d, 1H), 7.74 (d, 3H), 7.50 (d, 1H), 7.42 (m, 3H), 7.14 (t, 1H), 6.87 (s, 1H), 6.75 (d, 1H), 6.65 (s, 2H), 1.18 (s, 18H).

^{13}C NMR ($CDCl_3$, 100 MHz): δ, 152.1, 151.3, 149.8, 148.5, 141.1, 141.0, 139.601, 131.0, 128.5, 128.0, 127.7, 125.4, 124.7, 121.5, 120.9, 120.2, 119.6, 35.2, 31.8.

2-(4,4,5,5-tetramethyl-1,3,2-dioxaborolan-2-yl)-2',7'-di-tert-butyl)-9,9'-spirobifluorene (4)[14]

To a solution of 2-bromo-(2',7'-di-tert-butyl)-9,9'-spirobifluorene (1.44 g, 2.8 mmol) in anhydrous THF (14 mL) was added dropwise n-BuLi (4.3 mL, 5.1 mmol) at -78 ºC. After stirring for 1 h, 2-isopropoxy-4,4,5,5-tetramethyl-1,3,2-dioxaborolane (1 mL, 4.8 mmol) was added. The mixture was stirred overnight. Then the reaction was quenched with water and extracted with dichloromethane (30 mL) 3 times. The organic layer was washed with saturated brine and dried over $MgSO_4$ and concentrated *in vacuo*. The residue was purified by column chromatography (silica gel, ethyl acetate:hexane=1:10) to give a white solid product 0.99 g (64%).

^{1}H NMR ($CDCl_3$, 400 MHz): δ, 7.86 (d, 3H), 7.71 (d, 2H), 7.37 (m, 3H), 7.19 (s, 1H), 7.08 (t, 1H), 6.67 (d, 1H), 6.62 (s, 2H).

2-(4'-Bromophenyl)pyridine (5)[15]

To a solution of 4-bromoaniline (2 g, 12 mmol) in concentrated HCl (4 mL) was added slowly a solution of $NaNO_2$ (1.66 g, 24 mmol) in H_2O (3 mL) at 0 ºC. The mixture was stirred at 0 ºC for 1 h and pyridine (50 mL) was added. The mixture was further stirred at 40 ºC for 4 h and then sodium carbonate (20 g) was added and the slurry was stirred overnight. After cooling to room temperature, water was added and the water phase was extracted with ethyl acetate. The organic layer was combined and washed with saturated brine and dried over anhydrous $MgSO_4$, and concentrated in vacuo. Pyridine was distilled off and the residue was purified by column chromatography (silica gel, ethyl acetate: hexane=1:10) to give white solid product 1.06 g (38%).

^{1}H NMR ($CDCl_3$, 400 MHz): δ, 8.69-8.68 (d, 1H), 7.89-7.87 (d, J=8.4 Hz, 2H), 7.8-7.74 (m, 2H), 7.71-7.69 (d, 2H), 7.61-7.59 (d, J=8.4 Hz, 2H).

5-Bromo-2-phenylpyridine (6)

Compound **6** was synthesized by following standard Suzuki coupling from 2,5-dibromopyridine and phenyl boronic acid in the presence of $Pd(PPh_3)_4$ with mixture of toluene and 2 M Na_2CO_3 aqueous solution. Due to the regioselectivity, position 2 in the 2,5-disubstituted pyridine ring is much more reactive than position 5 in the ring.[16] The coupling reaction will predominantly occur at position 2 to offer the title compound.

After purifying through column chromatography (silica gel, ethyl acetate: hexane=1:10), a white powder was obtained with a yield of 74%.

^{1}H NMR ($CDCl_3$, 400 MHz): δ, 8.74-8.74 (d, 1H), 7.974-7.954 (d, 2H), 7.89-7.86 (dd, J=2.4 Hz, 1H), 7.64-7.62 (d, 1H), 7.50-7.45 (m, 3H).

5-Bromo-2-(1-naphthyl)pyridine (7)

Compound **7** was synthesized from 1-naphthalene boronic acid and 2,5-dibromopyridine through Suzuki coupling reaction under the similar conditions for compound 6. The crude product was purified by column chromatography (silica gel, ethyl acetate: hexane = 1:20) and a white solid product was obtained with a yield of 72%.

^{1}H NMR ($CDCl_3$, 400 MHz): δ, 8.86 (d, 1H), 8.07 (d, 1H), 7.97-7.91 (m, 3H), 7.59-7.49 (m, 5H).

2-(4'-Bromonaphthyl)pyridine (8)

A mixture of 1,4-dibromonaphthalene (2.86 g, 10 mmol), 2-pyridylzinc bromide (0.5 M, 20 mL), $Pd(PPh_3)_4$ (0.35 g, 0.3 mmol) in anhydrous THF (40 mL) was deoxygenated and then heated to reflux under nitrogen, the mixture was stirred overnight. After cooling to room temperature, the mixture was washed with water and extracted with dichloromethane (50 mL) 3 times. The combined organic layers were then washed with saturated brine, dried over $MgSO_4$ and concentrated in vacuo. The residue was purified by column chromatography (silica gel, ethyl acetate: hexane=1:10) to give a white solid product 1.1 g (39%).

^{1}H NMR ($CDCl_3$, 400 MHz): δ, 8.80-8.79 (d, 1H), 8.35-8.33 (d, 1H), 8.08-8.05 (d, 1H), 7.88-7.81 (m, 2H), 7.64-7.50 (m, 3H), 7.45-7.43 (d, 1H), 7.37-7.34 (q, 1H).

2-Fluorenylpyridine

A solution of 2-fluorenylmagnesium bromide (20 mmol) in anhydrous THF (60 mL) was added dropwise to a stirred mixture of 2-bromopyridine (2.39 g, 15 mmol) and $Pd(PPh_3)_4$ (0.17 g, 0.15 mmol) in anhydrous THF (60 mL) at room temperature and stirred for 1 h. Then the mixture was heated to gentle reflux under nitrogen and stirred overnight. After cooling to room temperature, the mixture was washed with water and extracted with dichloromethane (50 mL) 3 times. The organic layer was then washed with saturated brine and dried over $MgSO_4$ and concentrated in vacuo. After purified by column chromatography (silica gel, ethyl acetate: hexane=1:20), 0.70 g (19.2%) of title compound was obtained.

2-(Fluorenon-2-yl)pyridine (9)

To a solution of 2-fluorenylpyridine (0.4 g, 1.6 mmol) in pyridine (10 mL), tetramethylammonium hydroxide (1 mL) was added at room temperature. Then air was filled into the system and the reaction was kept stirring overnight at room temperature. Then dilute H_2SO_4 solution was added into the resulting suspension in order to eliminate the volatile pyridine. The precipitate was filtered and purified by column chromatography (silica gel, ethyl acetate: hexane=1:5). 0.41 g of a yellow powder (97%) was obtained.

^{1}H NMR ($CDCl_3$, 400 MHz): δ, 8.71-8.70 (d, 1H), 8.27-8.26 (m, 2H), 7.79-7.78 (m, 2H), 7.71-7.69 (d, 1H), 7.65-7.63 (d, 1H), 7.59-7.57 (d, 1H), 7.54-7.50 (t, 1H), 7.35-7.26 (m, 2H).

^{13}C NMR ($CDCl_3$, 100 MHz): δ, 156.5, 150.2, 145.2, 144.5, 140.9, 137.3, 135.2, 133.8, 129.7, 124.8, 123.0, 121.1, 121.0, 120.7.

General synthetic procedure for L1 and L2 using L1 as an example

To a solution of 2-bromobiphenyl (0.58 g, 2.5 mmol) in anhydrous THF (6 mL) was added dropwise n-BuLi (2.8 mL, 2.3 mmol) in hexane at -78 °C. After stirring for 1 h, the mixture was transferred to a stirred solution of 2-(fluorenon-2-yl)pyridine (0.5 g, 2 mmol) in anhydrous THF (6 mL) at -78 °C. The reaction was kept stirring overnight and warmed to room temperature. Water was added to terminate the reaction. The organic layer was separated and water phase was extracted with ethyl acetate (20 mL) 3 times. The organic layer was combined and washed with saturated brine and dried over anhydrous $MgSO_4$ and concentrated in vacuo. The residue was dissolved in glacial acetic acid (6 mL) and added one drop of concentrated HCl, and the solution was heated to reflux for 1 h. After the reaction was cooled to room temperature, the precipitate was filtered and washed with water. The solution was neutralized with sodium hydroxide solution to PH = 7. Then, the mixed solution was extracted with ethyl acetate (20 mL) 3 times. The organic layer was combined and washed with saturated brine and dried over anhydrous $MgSO_4$ and concentrated in vacuo. The crude product was purified by column chromatography (silica gel, hexane first, then EA: hexane=1:10) to provide a light yellow solid product **L1**, 0.54 g (69%).

^{1}H NMR ($CDCl_3$, 400 MHz): δ, 8.57-8.56 (d, 1H), 8.08-8.06 (d, J=8 Hz, 1H), 7.96-7.94 (d, J=8 Hz, 1H), 7.89-7.85 (t, 3H), 7.63-7.53 (m, 2H), 7.40-7.35 (m, 4H), 7.13-7.09 (m, 4H), 6.78-6.71 (m, 3H).

^{13}C NMR ($CDCl_3$, 100 MHz): δ, 150.0, 149.1, 142.4, 141.7, 139.7, 136.97, 128.6, 128.4, 128.2, 127.4, 124.8, 124.5, 123.1, 122.3, 121.1, 120.7, 120.5.

MS (MALDI):393.138 (m/z), Calcd for $C_{30}H_{19}N$: 393.151.

L2 was synthesized by the same method with **L1**, with a yield of 48%.

^{1}H NMR ($CDCl_3$, 400 MHz): δ, 8.58 (d, 1H), 8.12-8.10 (d, 1H), 7.97-7.88 (dd, 2H), 7.73-7.71 (d, 2H), 7.63-7.52 (m, 2H), 7.39-7.36 (m, 3H), 7.31-7.26 (m, 1H), 7.14-7.09 (m, 1H), 6.72-6.68 (m, 2H), 1.14 (s, 18H).

^{13}C NMR ($CDCl_3$, 100 MHz): δ, 151.2, 150.8, 150.4, 149.7, 149.1, 143.3, 141.5, 139.7, 139.2, 7.0, 128.4, 127.8, 127.2, 125.3, 124.6, 123.0, 122.2, 121.1, 120.6, 120.5, 119.5, 35.2, 31.8.

MS (MALDI): 505.260 (m/z), Calcd for $C_{38}H_{35}N$: 505.276.

General procedure for synthesis of L3, L4, L5, L6 and L7 using L3 as an example

A mixture of 2-bis(4,4,5,5-tetramethyl-1,3,2-dioxaborolan-2-yl)-2',7'-di-tert-butyl)-9,9'-spirobifluorene (**3**) (0.554 g, 1 mmol), aryl bromide(chloride) (**5**, **6**, **7**, **8** and 2-chloroquinoline) (1 mmol), $Pd(PPh_3)_4$ (0.05 g, 0.043 mmol), aqueous sodium carbonate (2 M, 0.71 mL), toluene (2.9 mL) was deoxygenated and then heated to reflux under nitrogen with stirring overnight. After the reaction was cooled down to room temperature, the mixture was washed with water and extracted with ethyl acetate (20 mL) 3 times. The

organic layer was then washed with saturated brine and dried over $MgSO_4$ and concentrated in vacuo. The crude products were purified by column chromatography (silica gel, ethyl acetate:hexane=1:10) to give white solid products with the yields ranging from 74% to 98%.

L3 was synthesized with a yield of 100% as a white solid.

^{1}H NMR ($CDCl_3$, 400 MHz): δ, 8.70 (s, 1H), 7.97(t, 3H), 7.92 (d, 1H), 7.76 (m, 5H), 7.59 (d, 2H), 7.42 (d, 3H), 7.28 (d, 1H), 7.13 (t, 1H), 7.04 (s, 1H), 6.72 (d, 3H), 1.17 (s, 18H).

^{13}C NMR ($CDCl_3$, 100 MHz): δ, 157.3, 151.1, 150.6, 150.3, 149.9, 149.1, 141.9, 141.6, 141.5, 140.3, 139.5, 138.3, 136.8, 128.0, 127.6, 127.5, 127.3, 126.8, 125.0, 124.4, 122.9, 122.1, 120.9, 120.5, 120.3, 35.0, 31.6, 29.9.

MS (MALDI): 581.299 (m/z), Calcd for $C_{44}H_{39}N$: 581.308.

L4 was synthesized with a yield of 86.1% as a white solid.

^{1}H NMR ($CDCl_3$, 400 MHz): δ, 8.77 (d, 1H), 7.97-7.95 (m, 3H), 7.91-7.89 (d, 1H), 7.79-7.66 (m, 5H), 7.47-7.39 (m, 6H), 7.15-7.11 (t, 1H), 7.00 (s, 1H), 6.76-6.75(d, 1H), 6.70 (s, 2H), 1.15 (s, 18H).

^{13}C NMR ($CDCl_3$, 100 MHz): δ, 156.3, 151.3, 150.4, 149.1, 148.4, 142.2, 141.5, 139.7, 139.4, 137.5, 135.2, 129.2, 129.1, 128.4, 127.9, l27.1, 126.8, 125.3, 124.7, 123.0, 121.0, 120.8, 120.4, 119.5, 35.2, 31.8, 31.2.

MS (MALDI): 581.318 (m/z), Calcd for $C_{44}H_{39}N$: 581.308.

L5 was synthesized with a yield of 97.5% as white solid.

^{1}H NMR (400MHz, chloroform-*d*): δ, 8.87 (s, 1H), 8.01-8.00 (m, 2H), 7.92-7.83 (m, 4H), 7.75-7.72 (m, 3H), 7.58-7.39 (m, 8H), 7.16-7.12 (t, 1H), 7.03 (s, 1H), 6.78-6.72 (m, 3H).

^{13}C NMR ($CDCl_3$, 400 MHz): δ, 157.9, 151.1, 150.2, 148.9, 148.1, 142.2, 141.3, 139.5, 138.4, 137.3, 135.1, 134.7, 134.2, 131.5, 129.0, 128.5, 128.3, 127.8, 127.6, 126.8, 126.6, 126.0, 125.9, 125.4, 125.1, 124.8, 124.5, 122.9, 120.9, 120.7, 120.2, 119.4, 35.0, 31.6, 14.4.

MS (MALDI): 631.322 (m/z), Calcd for $C_{48}H_{41}N$: 631.323.

L6 was synthesized with a yield of 94% as white solid.

^{1}H NMR ($CDCl_3$, 400 MHz): δ, 8.78 (d, 1H), 8.04-7.99 (q, 2H),7.94-7.92 (d, 1H), 7.97 (t, 1H), 7.69-7.65 (m, 3H), 7.53-7.52 (m, 3H), 7.41-7.14 (m, 9H), 6.83 (s, 1H), 6.80-6.79 (m, 2H), 1.19 (s, 18H).

^{13}C NMR ($CDCl_3$, 100 MHz): δ, 159.4, 150.9, 145.0, 149.7, 149.0, 141.6, 141.2, 140.2, 139.4, 138.0, 136.5, 132.2, 131.6, 129.6, 128.0, 127.7, 127.0, 126.3, 126.2, 125.9, 125.9, 125.3, 124.9, 124.5, 122.1, 120.8, 120.1, 35.0, 31.6, 29.8.

MS (MALDI): 631.326 (m/z), Calcd for $C_{48}H_{41}N$: 631.323

L7 with synthesize with a yield of 74% as white needle crystal.

^{1}H NMR ($CDCl_3$, 400 MHz): δ, 8.35-8.33 (d, J=7.8 Hz, 1H), 8.10-8.02 (m, 3H), 7.93-7.91 (d, J=7.8 Hz, 1H), 7.76-7.74 (d, 3H), 7.69-7.64 (m, 2H), 7.48-7.38 (m, 5H), 7.14-7.11 (t, 1H), 6.74-6.71 (m, 3H), 1.14 (s, 18H).

^{13}C NMR ($CDCl_3$, 100 MHz): δ, 157.5, 151.0, 150.7, 150.2, 148.9, 148.3, 143.4, 141.3, 139.5, 139.5, 136.5, 129.8, 129.7, 128.3, 127.7, 127.7, 127.5, 127.2, 126.2, 125.1, 124.4, 123.4, 120.9, 120.5, 120.4, 119.4, 35.00, 31.6.

MS (MALDI): 555.295 (m/z), Calcd for $C_{42}H_{37}N$: 555.292.

General procedure for synthesis of complexes[7,17-19]

A mixture of a ligand (1.4 mmol), iridium chloride trihydrate (0.25 g, 0.7 mmol), water (7.5 mL) and 2-ethoxylethonal (22.5 mL) was deoxygenated and then heated to reflux under nitrogen for 24 h. After cooling to room temperature, the mixture was filtrated and washed with ethanol to give product chloride-bridged dimer. Then, a mixture of chloride-bridged dimer (0.56 g, 0.2 mmol), acetyl acetone (50 mg, 0.5 mmol), ethanol (0.3 mL), dichloromethane (15.6 mL) and tetrabutylammonium hydroxide (129 mg) was deoxygenated and heated to reflux under nitrogen for 2 h. After cooling to room temperature, the mixture was evaporated in vacuo. After column chromatography purification (silica gel, dichloromethane), final complex products were obtained with yields ranging from 32% to 52%.

C1 was synthesized from **L1** with a yield of 32% as yellow solid.

^{1}H NMR ($CDCl_3$, 400 MHz) δ, 8.59 (d, 2H), 7.84 (d, 4H), 7.63 (m, 4H), 7.34 (m, 6H), 7.14 (m, 8H), 7.08 (m, 4H), 6.97 (d, 2H), 6.77 (d, 4H), 6.70 (d, 2H), 5.23 (s, 1H), 1.81 (s, 6H).

MS (MALDI): 1075.309 (m/z), Calcd for $C_{65}H_{43}N_2IrO_2$: 1075.286.

C2 was synthesized from **L2** with the yield of 43% as a yellow solid.

^{1}H NMR ($CDCl_3$, 400 MHz) δ, 8.58 (d, 2H), 7.68 (m, 8H), 7.31 (m, 6H), 7.10 (m, 4H), 6.99 (s, 2H), 6.91 (t, 4H), 6.70 (d, 2H), 6.58 (d, 2H), 6.48 (s, 2H), 5.24 (s, 1H), 1.79 (s, 6H), 1.15 (s, 18H), 0.89 (s, 18H).

MS (MALDI): 1300.437 (m/z), Calcd for $C_{81}H_{75}N_2IrO_2$: 1300.546.

C3 was synthesized from **L3** with a yield of 37% as yellow solid.

^{1}H NMR ($CDCl_3$, 400 MHz) δ, 8.37 (d, 2H), 7.73 (m, 6H), 7.57 (d, 2H), 7.34 (m, 8H), 7.03 (t, 2H), 6.88 (m, 4H), 6.58 (m, 6H), 6.17 (s, 2H), 5.15 (s, 1H), 1.15-1.13 (d, 36H).

MS (MALDI)**:**1452.729 (m/z), Calcd for $C_{93}H_{83}N_2IrO_2$: 1452.609.

C4 was synthesized from **L4** with a yield of 52% as a yellow solid.

^{1}H NMR ($CDCl_3$, 400 MHz) δ, 8.59 (d, 2H), 7.96 (d, 2H), 7.89 (d, 2H), 7.79 (dd, 2H), 7.73 (t, 6H), 7.66 (dd, 2H), 7.42 (m, 8H), 7.12 (t, 2H), 6.97 (m, 2H), 6.71 (m, 8H), 6.58 (t, 2H), 6.24 (d, 2H), 4.89 (s,1H), 1.36 (s, 6H), 1.17 (d, 36H).

MS (MALDI): 1452.731 (m/z), Calcd for $C_{93}H_{83}N_2IrO_2$:1452.609.

C5 was synthesized from **L5** with a yield of 47% as a red solid.

^{1}H NMR ($CDCl_3$, 400 MHz) δ, 8.69 (d, 2H), 8.44 (m, 4H), 7.91 (m, 6H), 7.74 (m, 6H), 7.54 (d, 2H), 7.39 (m, 9H), 7.17 (m, 4H), 7.02 (m, 2H), 6.93 (d, 2H), 6.72 (m, 6H), 6.37 (d, 2H), 4.90 (s, 1H), 1.34 (s, 6H), 1.13 (d, 36H).

MS (MALDI): 1552.752 (m/z) Calcd for $C_{101}H_{87}N_2IrO_2$:1552.640.

C6 was synthesized from **L6** with a yield of 49% as a dark yellow solid.

^{1}H NMR ($CDCl_3$, 400 MHz) δ, 8.36 (d, 2H), 7.95 (d, 2H), 7.69 (m, 8H), 7.37 (m, 14H), 7.16 (m, 4H), 7.06 (t, 4H), 6.95 (t, 2H), 6.67 (m, 6H), 6.52 (m, 2H), 5.16 (s, 1H), 1.71 (s, 6H), 1.16 (d, 36H).

MS (MALDI**)**: 1552.740 (m/z) Calcd for $C_{101}H_{87}N_2IrO_2$:1552.640.

C7 was synthesized from **L7** with the yield of 32% as red solid.

^{1}H NMR ($CDCl_3$, 400 MHz) δ, 8.69 (d, 2H), 8.44 (m, 4H), 7.91 (m, 6H), 7.72 (m, 6H), 7.54 (d, 2H), 7.39 (m, 6H), 7.14 (m, 2H), 7.02 (d, 2H), 6.72 (m, 4H), 6.35 (d, 2H), 4.90 (s, 1H), 1.34 (s, 6H), 1.22 (d, 36H).

MS (MALDI): 1398.966 (m/z), Calcd for $C_{89}H_{79}N_2IrO_2$:1398.562.

The relative simplicity of ^{1}H NMR spectra suggests that all of the Ir complexes are formed exclusively as facial isomers, where the two ligands surrounding the iridium atom are chemically equivalent.[7,11] The small ancillary ligands effectively reduced the steric hindrance brought by bulky main ligands. The facial isomers are expected to have higher efficiency and better device performance comparing with the meridional isomers.

2.4 Results and discussion

2.4.1 Optical analysis

The UV-visible absorption spectra of the series of Ir complexes **C1**-**C7** in anhydrous dichloromethane solution are shown in Figure 2.5. They were measured at room temperature on UV-vis-NIR spectrophotometer (UV-3101, SHIMADZU). All the complexes showed similar spectra, with three main absorption bands for each material.

As can be seen, there are two low-intensity metal to ligand charge transfer (MLCT) transitions from 370 nm to 550 nm. The MLCT transitions are not pronounced enough to be assigned individually. The band at longer wavelength is assigned to triplet ^{3}MLCT *d*-π* excitations, while the band at shorter wavelength is attributed to singlet state ^{1}MLCT excitation. The high-intensity peaks which start from 330 nm to 380 nm belong to the π→π* transitions localized on the phenylpyridine-based ligands. The figures also showed that increasing the conjugation length of the cyclometalating ligand caused a red shift both in the π→π* peaks and d→π* of the complex, which is consistent with the reported results.[17-19]

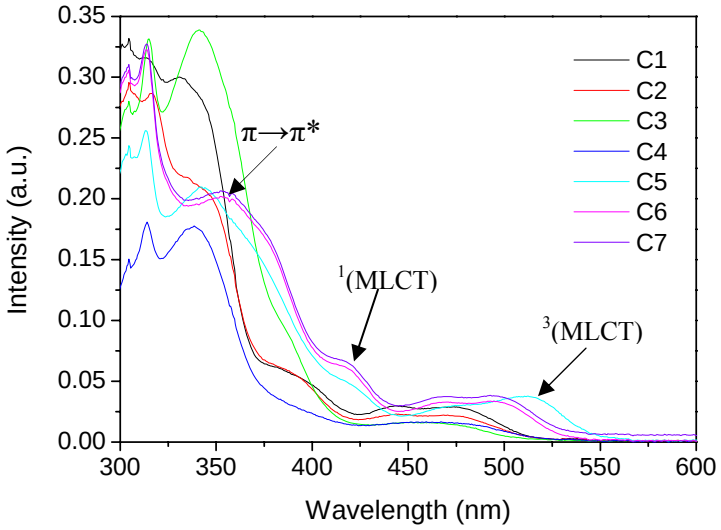

Figure 2.5. UV-vis absorption spectra of Ir complexes in anhydrous DCM.

The photoluminescence (PL) of the complexes was measured at room temperature in anhydrous dichloromethane (DCM) solution on Luminescence Spectrometer LS50B (Perkin Elmer). The emission spectra of all the complexes are shown in Figure 2.6. These

complexes emitted yellow to red light. The PL spectra can be divided into two main groups. Group 1 included complex **C1**-**C4**, whose peak wavelengths fall into the range of 545-560 nm and they all emitted yellow light; while another group includes complexes **C5**-**C7**, whose peak wavelengths range from 610 to 635 nm and their emission light is red. The color change in light emission complies with the theory that the light emission of Ir complexes can be tuned by changing the structures of the ligands. According to the theory that longer conjugation length will decrease energy gap and result in longer wavelength light emission, ligands **L5**, **L6**, and **L7** have longer conjugation length. Thus their energy gaps are decreased and obvious red shifts (longer wavelength) in PL spectra are observed compared with the shorter conjugation length ligands **L1**-**L4**.

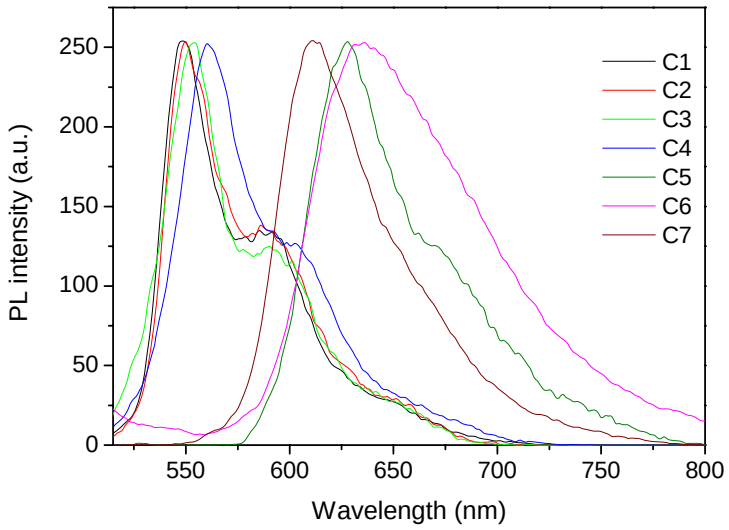

Figure 2.6. PL Spectra of complex **C1**-**C7** in anhydrous DCM.

Among the red light emission complexes, it can be seen that complex **C5** realized the longest wavelength emission and complex **C7** showed narrowest red light emission. Narrow light emission is favored due to its better color purity. The optical properties of spirobifluorene based Ir complexes in solution were summarized in Table 2.1.

Table 2.1. Photophysical properties of Ir complexes **C1**-**C7** in anhydrous DCM.

Complex	UV-vis				PL[a]
	λ_{onset}(nm)	λ_{max} (nm) $\pi\rightarrow\pi^*$	^{1}MLCT *d*-π^*	^{3}MLCT *d*-π^*	λ_{em} (nm)
C1	518.5	329.5	397.5	473.5	548.5 (591.5)
C2	535.3	340.5	390.5	468.5	550 (592)
C3	537.5	339.5	386.5	451.5	555.5 (592)
C4	535	336.5	390.5	467	561.5 (604)
C5	567.7	342	418	512	629
C6	543.8	355	417	492.5	637.5
C7	610	351.5	417.5	480	612.5

Note: The data in the parentheses are the wavelength of shoulders and sub-peaks

2.4.2 Thermal analysis (TGA and DSC)

The thermal stability of Ir complexes in nitrogen was evaluated by thermogravimetric analysis (TGA) using TGA Q500 instrument (heating rate of 10 °C·min^{-1}). The TGA traces of complex **C1** and **C3** are shown in Figure 2.7 and Figure 2.8 as examples.

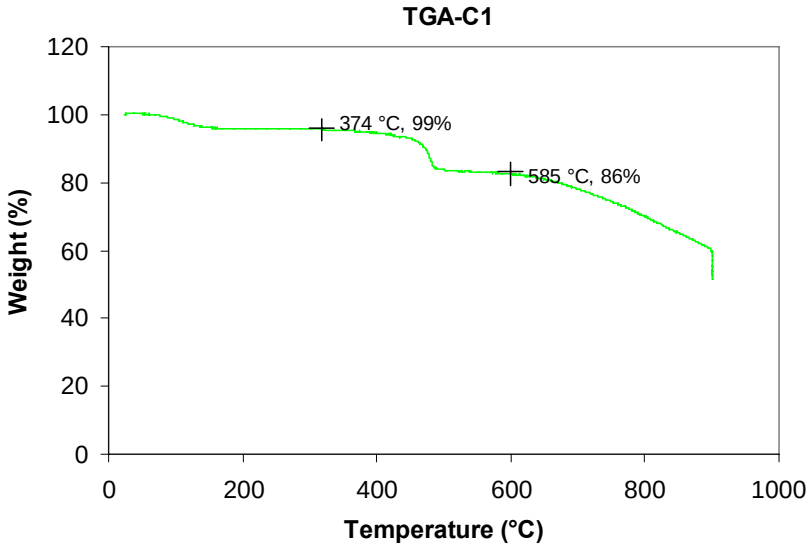

Figure 2.7. Thermogravimetric analysis of Ir complex **C1** in nitrogen atomosphere.

As can be seen from the TGA data, complex **C1** exhibited excellent thermal stability. The onset temperature of weight loss is 373 °C, and temperature for 5% weight loss is 460 °C. The first as well as the only one weight loss is due to the decomposition of ancillary ligand (acac group). Its theoretical weight percentage in **C1** is 9.21% and the actual weight loss percentage was 12.51%.

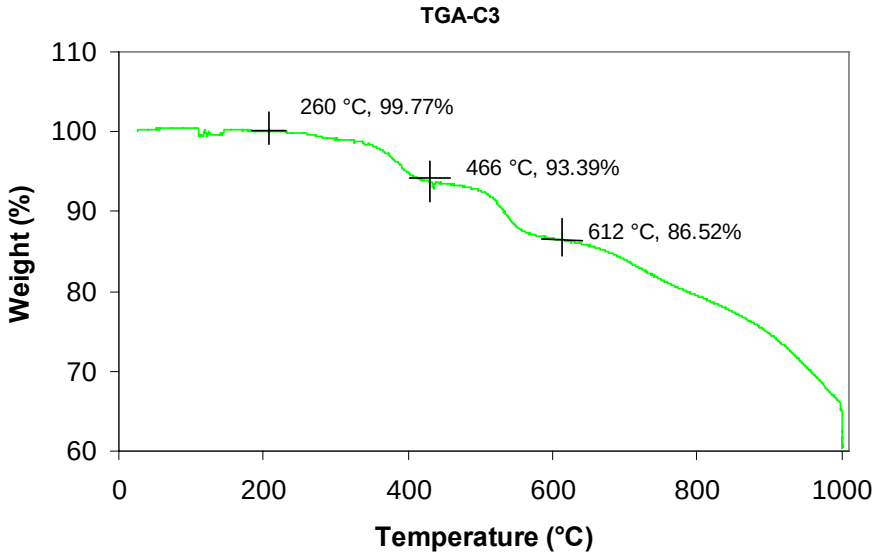

Figure 2.8. Thermogravimetric analysis of Ir complex **C3** in a nitrogen atmosphere.

Complex **C3** showed lower decomposition temperature than complex **C1**. The onset decomposition temperature is 260 °C. There were two stages of decomposition, which corresponded to loss of ancillary ligand (acac group) (actual weight loss 6.41% vs theoretical weight loss 6.75%) and loss of the tert-butyl groups that included in the cyclometalated ligands continuously.

Thermally induced phase transition behavior of Ir complexes was investigated by differential scanning calorimeter (DSC) under nitrogen atmosphere on a DSC Q100 instrument (scanning rate of 10 °C·min^{-1}). Figure 2.9 shows the DSC curve of **C1**. DSC curve revealed that the Ir complex is amorphous. On heating to 320 °C, no crystallization and melting were observed, which is matched with the prediction that the spirobifluorene structure is amorphous. Such amorphous materials are particularly favored for OLEDs because aggregation and crystallization will affect the device stability and lifetime

significantly[20]. The amorphous materials also exhibit excellent processibility, homogeneity and isotropic properties, which is favorable to OLEDs.[21]

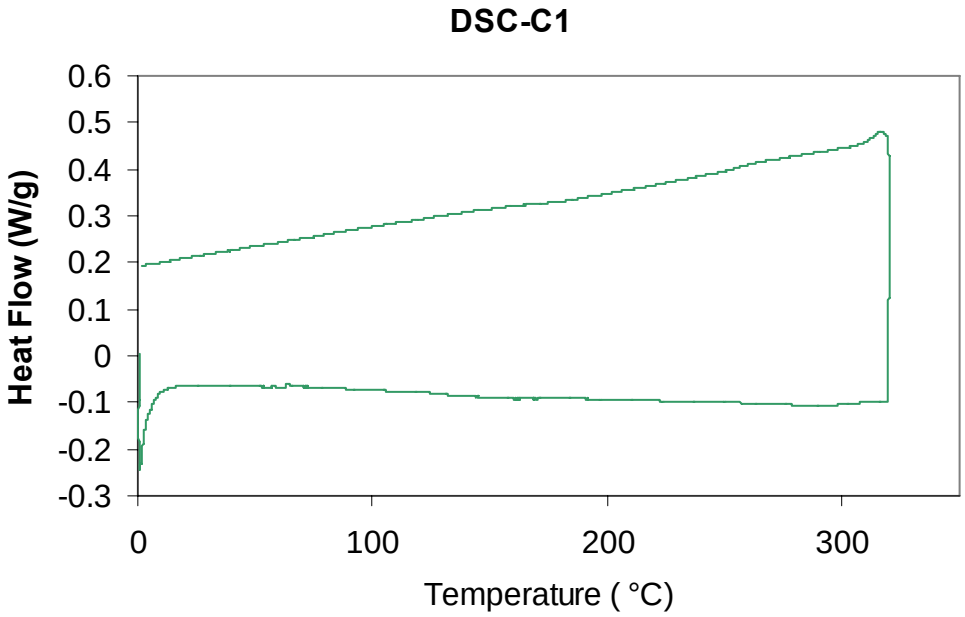

Figure 2.9. DSC trace of **C1** under nitrogen atmosphere.

2.4.3 Electrochemical properties

The electrochemical behavior of the materials was investigated by the cyclic voltammetry (CV). CV is commonly employed to measure the oxidation and reduction processes of the materials, which can be used to estimate the electron affinity (EA) and ionization potential (IP) of materials.

HOMO and LUMO can be estimated from the onset potential of oxidation and reduction, respectively. The difference between HOMO and LUMO is the energy gap (E_g) of the material, which can also be obtained from the lowest-energy absorption edge of the UV-vis absorption spectrum.

Cyclic voltammetry experiments were performed using an Autolab potentiostat (model PGSTAT30) by Echochimie. The CV measurements were carried out in anhydrous dichloromethane with 0.1 M tetrabutylammonium hexafluorophosphate ($TBAPF_6$) as the supporting electrolyte at a scan rate of 0.1 V/s at room temperature under the protection of nitrogen. A platinum plate was used as working electrode, a gold stick was used as counting electrode and Al/AgCl (3 M KCl solution) was used as reference electrode. The energy level was calculated by following equation 1, 2 and 3.

$$E_{g\,(uv)} = 1240.842/\lambda \quad (1)$$

$$HOMO = IP = -(E_{ox}+4.4) \quad (2)$$

$$E_{g(echem)} = HOMO-LUMO \quad (3)$$

Notes: E_{ox} represents the onset potential of oxidation; λ is the wavelength of lowest-energy absorption edge in UV absorption spectrum

All the Ir complexes showed obvious oxidation peaks and underwent a reversible one-electron oxidation process, demonstrating excellent electrochemical stability of their cations. However, there is no reduction peak was observed.[22] Thus, their energy band gaps were estimated from the long-wavelength absorption edge data collected from spectroscopic method (equation 1). From the oxidation potential data (equation 2) and the energy band gap, HOMO and LUMO values were calculated (equation 3).[23-25] For illustration purpose, a typical CV of **C1** is shown in Figure 2.10.

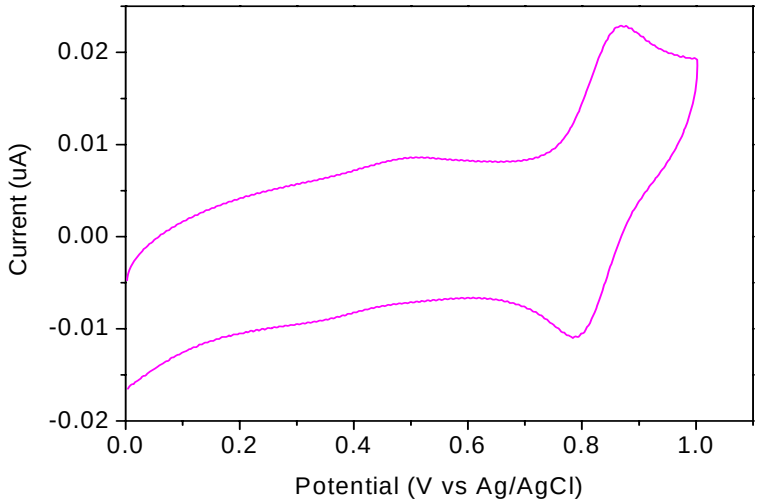

Figure 2.10. Cyclic voltammogram of Ir complex **C1** in anhydrous DCM containing $TBAPF_6$ as supporting electrolyte.

The electrochemical data and energy levels of all the Ir complexes are calculated and summarized in Table 2.2.

Table 2.2. Electrochemical properties of Ir complexes **C1-C7** in anhydrous DCM.

Complexes	E_{onset} (eV)	E_{pa} (eV)	E_{pc} (eV)	HOMO (eV)	LUMO (eV)	E_g (eV)
C1	0.76	0.86	0.79	-5.16	-2.77	2.39
C2	0.69	0.83	0.73	-5.09	-2.77	2.32
C3	0.81	0.90	0.84	-5.21	-2.90	2.31
C4	0.79	0.90	0.81	-5.19	-2.87	2.32
C5	0.75	0.83	0.77	-5.15	-2.97	2.18
C6	0.77	0.84	0.74	-5.17	-2.89	2.28
C7	0.74	0.84	0.77	-5.14	-3.11	2.03

E_{pa}: anodic peak potential, E_{pc}: cathodic peak potential

It is known that the HOMO of Ir complexes is determined by the 5*d* orbital of Ir with substantial mixing with the π orbitals of the ligand and LUMO is related to the π^* orbitals of lignad.[7,26,27] The LUMO energy level is cyclometalating ligand dependent, which is not affected by the nature of ancillary ligands.[28] Comparing the energy levels of **C1** and **C2**, it was found that their LUMOs are the same and **C2** showed higher HOMO, indicating that the introduction of tert-butyl groups decrease the energy band gap of the Ir complex due to strong electron-donating abilities.[29]

2.4.4 Device structure and performance

All the devices were fabricated through combination of high vacuum thermal deposition and spin-coating on pre-cleaned ITO glass substrates employing the synthesized Ir complexes as guest materials and PVK as host material. The device configuration is ITO/PEDOT/PSS (50 nm)/PVK (50%):PBD (40%):Ir complex (10%) (45 nm)/TPBI (40 nm)/LiF (0.5 nm)/Ca (20 nm)/Ag (150 nm). Figure 2.11 shows the device configuration.

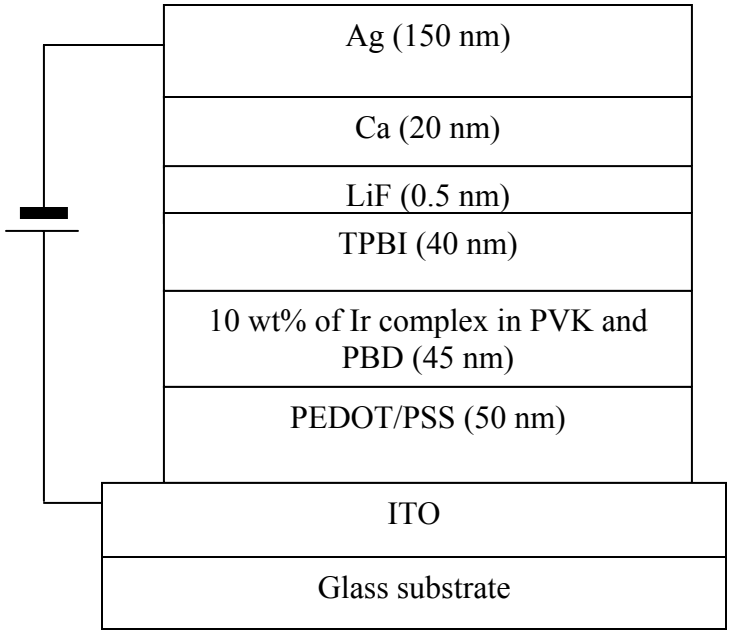

Figure 2.11. Device configuration for Ir complexes.

A first layer of poly(3,4-ethylenedioxythiophene) doped with poly(styrenesulfonic acid) (PEDOT/PSS) was spin-coated on a glass substrate with patterned ITO to form a hole injection layer with a thickness of about 50 nm. After drying in an oven at 120 ºC for 5 min, solution containing 4 ml ethyl benzoate, 25 mg PVK, 20 mg PBD, and 5 mg Ir complex was spin-coated onto the first layer to form an emitting layer with a thickness of about 45 nm. Prior to film casting, the polymer solution was filtered through a Teflon filter (0.45 μm). The TPBI layer, which was used as an electron-transporting layer and also used to block holes and confine excitons, was grown through thermal sublimation in vacuum (3 $x10^{-6}$ Torr). Subsequently, the cathode LiF (0.5 nm) and Ca (20 nm) were deposited through evaporation onto the TPBI layer in sequence; this process was followed by placing an additional layer of Ag (150 nm) onto the Ca as a protection layer.

In this configuration, The PEDOT/PSS layer serves to planarize the ITO anode and to enable a better and more reproducible injection of holes, while LiF is applied to buffer the cathode to improve electron injection, to reduce threshold voltage and to increase device efficiency.

The emissive Ir complexes were doped into a host polymer matrix of PVK and blended with the electron transport molecule, 2-(4-biphenylyl)-5-(4-tert-butylphenyl)-1,3,4-oxadiazole (PBD). The doping concentration of guest Ir complexes was fixed at 10 wt%. It is important to note that doping concentrations of guest is higher than 5 wt % are typically required to efficiently quench the host luminescence and achieve good carrier transport in phosphorescent OLEDs.[30]

The host materials also play an important role to determine the device efficiency as well as the guest materials. The most crucial parameter for host materials is their energy levels. Mismatch of the energy levels between the host materials and guest materials will affect the energy transfer from the host materials to guest materials. In order to guarantee effective energy transfer from host material to guest material and achieve good device performance, the triplet energy of the host should be higher than that of triplet emitters. The ideal host material will possess a HOMO level close to the work function of the hole injection layer and a LUMO level higher than that of electron injection layer. Usually, materials with a large HOMO-LUMO energy gap will posses a high triplet energy.[31] PVK is generally selected as the host in phosphorescent OLEDs for its relatively high triplet energy, good film formation and moderate hole transport ability.[32,33] PVK also provides an electron-blocking effect.[34] Therefore, PVK can confine the triplet excitons in the guest molecules and thus prevent luminescence quenching.[35,36] When PVK was used

as the host material, the electron transport will be weak. In order to enhance the electron transport, normally electron transporting material PBD was added, which can largely improve the balance of charge transport.

The EL of complex **C1-C7** with 10 wt% doping concentration is shown in Figure 2.12. Their CIE coordinate demonstration figure is shown in Figure 2.13. The EL peak values and CIE coordinates are summarized in Table 2.3.

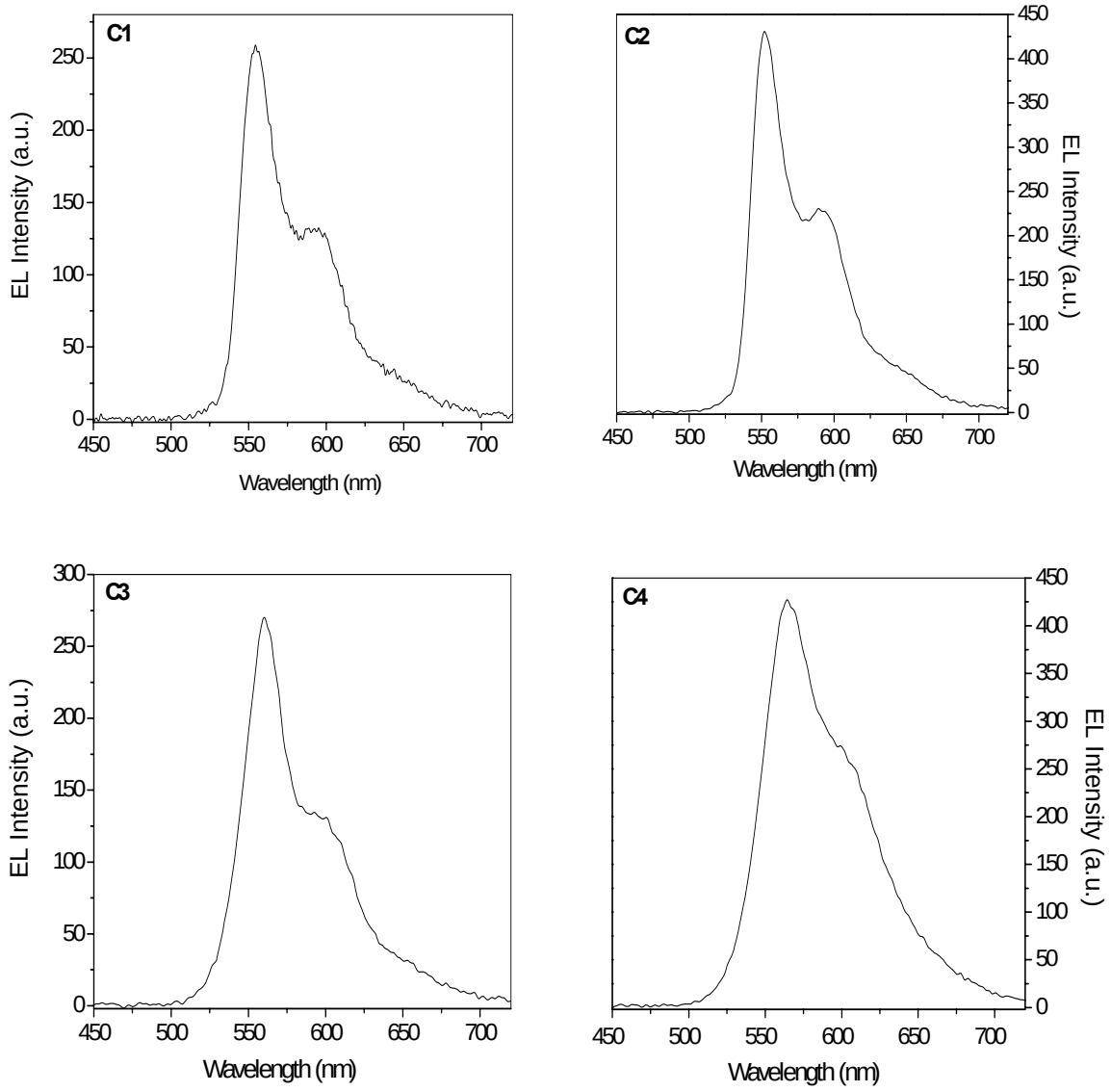

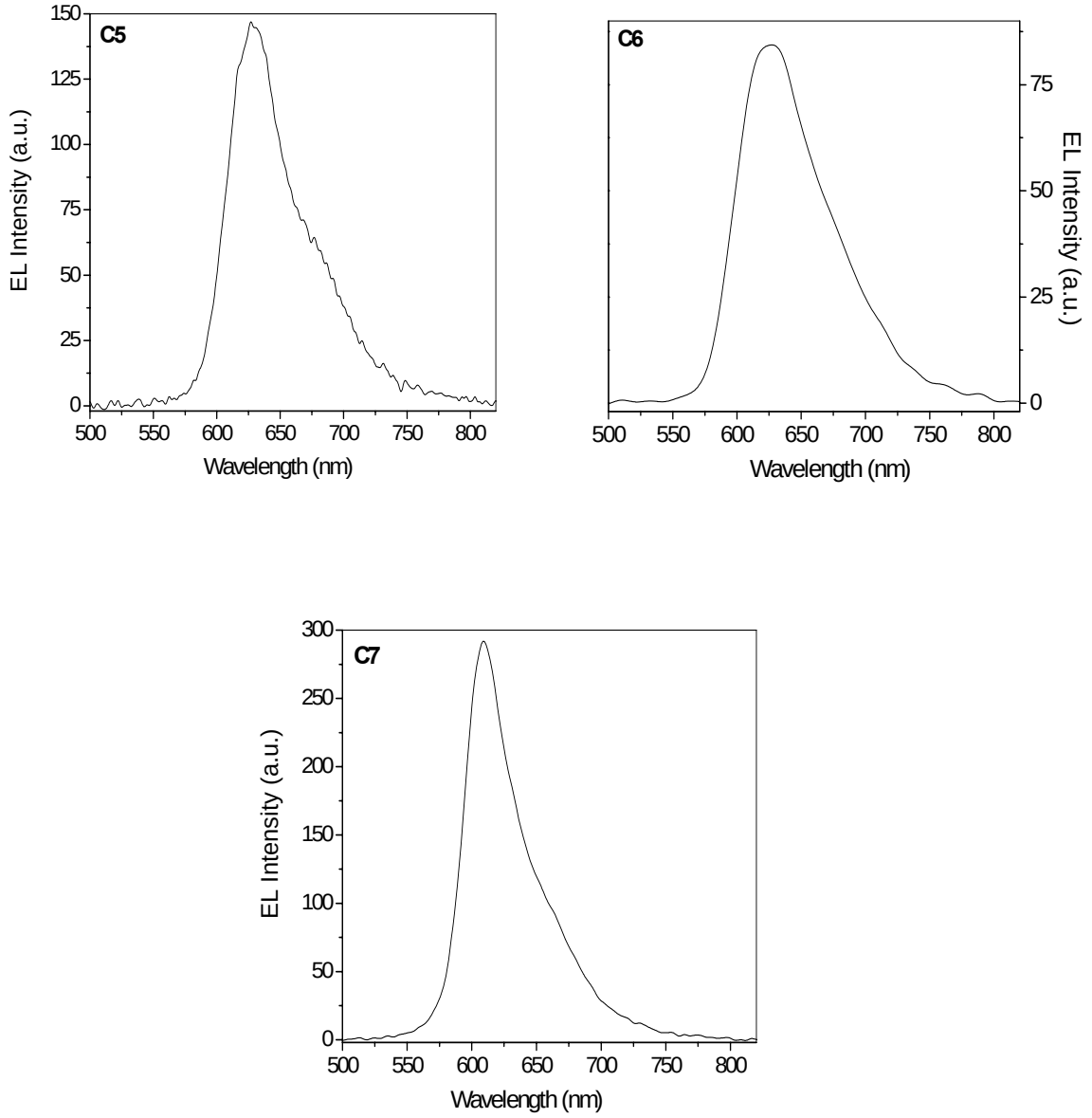

Figure 2.12. EL spectra of complex **C1-C7**.

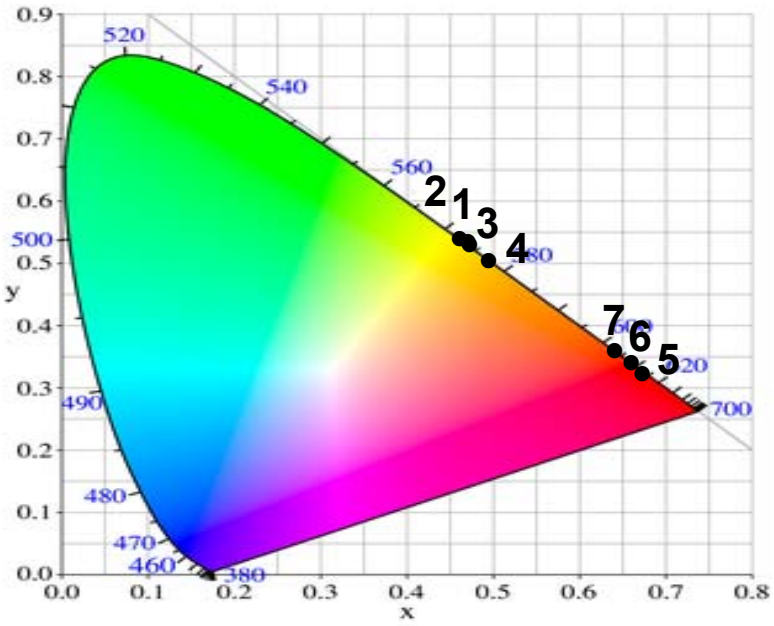

Figure 2.13. CIE coordinates of all the Ir complexes **C1-C7**.

Table 2.3. Summary of electroluminescence (EL).

Samples	EL	CIE coordinates		PL
	λ_{peak}(nm)	x	y	$\lambda_{peak(}$nm)
C1	554.5 (592)	0.469	0.528	548.5 (591.5)
C2	552 (589)	0.463	0.532	550 (586)
C3	560 (599.5)	0.470	0.522	554.5 (592)
C4	564.5 (606)	0.493	0.500	560.5 (602.5)
C5	627	0.671	0.324	628
C6	626.5	0.664	0.343	635.5
C7	609.5	0.644	0.356	611

Note: The data in the parentheses are the wavelength of shoulders and sub-peaks

It can be seen from the EL spectra showed in Figure 2.14, all the devices display yellow or red emission in the range of 548-560 nm and 611-635 nm, which resembled to those of the PL spectra of Ir complexes in DCM solution. There is no emission from PVK was observed, indicating that efficient energy transfer from the host materials to guest materials occurred and the EL emission of the device originated from the triplet excited states of the phosphors. For the peak wavelength, there was no big difference between the EL and their PL in solution.

In electrophosphorescent OLEDs, there are two kinds of possible emission mechanism. Electrons and holes are initially injected into polymer host materials and form excitons, and then exciton energy is transferred to phosphorescent emitters, which is called Forster and/or Dexter energy transfer mechanism.[37,38] There are three possible excitation processes that need to be considered: (1) energy transfer from polymer singlet exciton (Forster energy transfer), (2) energy transfer from polymer triplet exciton (Dexter energy transfer), and (3) sequential electron and hole capture by phosphorescent emitters.[39-41] Forster energy transfer has been widely used to explain energy transfer phenomena in molecular blending system, photosynthetic aggregates, polymer-polymer systems, and more recently in the polymer-organometallic emitter systems. The dominant mechanism in polymer-phosphorescent emitter systems, i.e., this PVK-Ir complex system are Forster energy transfer and/or charge trapping.[42]

The Voltage-Current-Luminescence (V-I-L) curves of complex **C1-C7** are shown in Figure 2.14. It can be seen from the figures that the turn-on voltage (defined as the voltage required to give a luminance of 1 cd/m^2) of the devices ranged from 5.8 V to 8.4 V. The relatively higher turn-on voltage is because that PVK has a low–lying HOMO

level at about -5.9 eV, and consequently, a large barrier for injection of holes from PEDOT/PSS, which translates into a high onset voltage.[31] The current density and luminescence increased with the increasing of voltages.

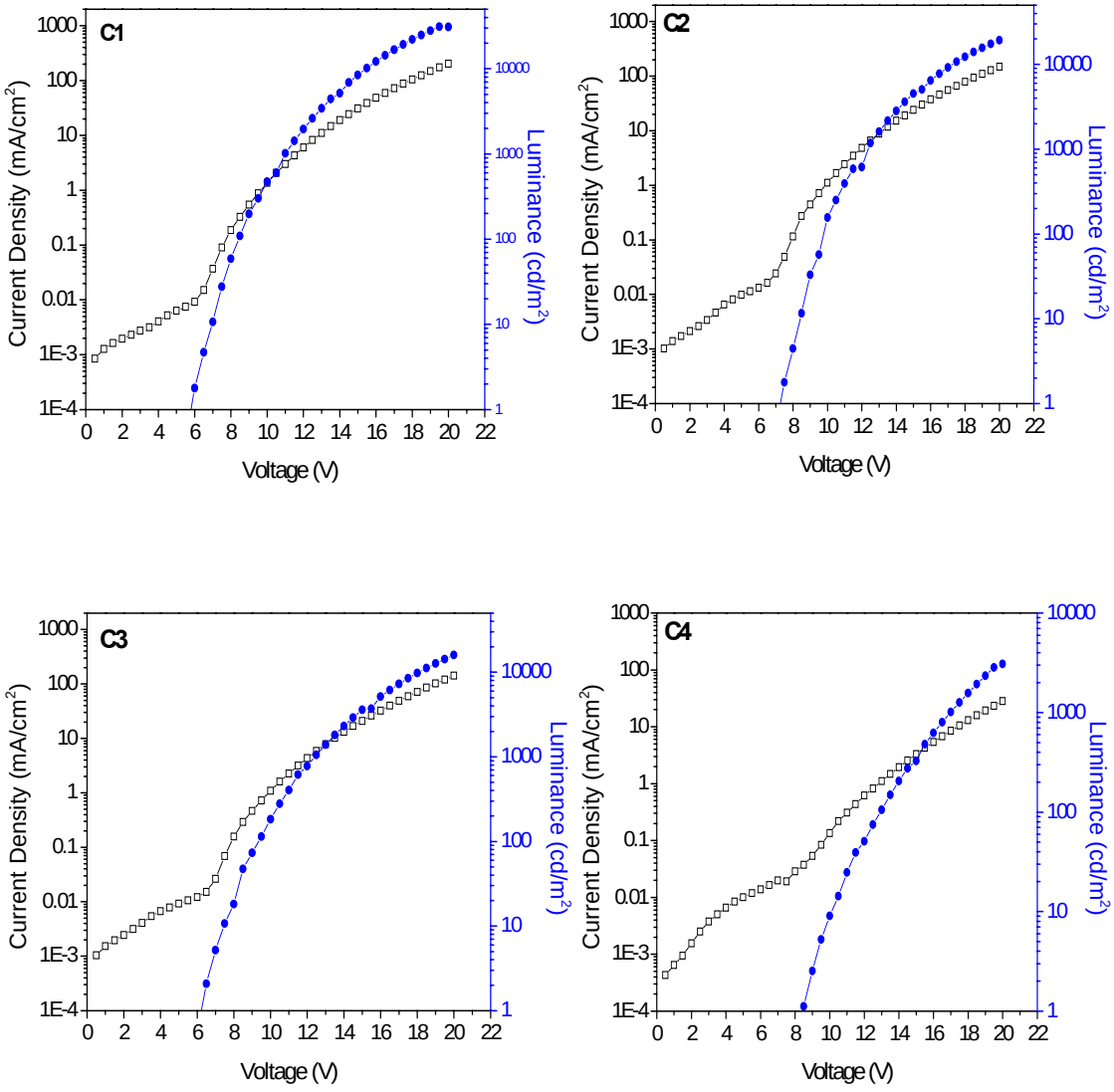

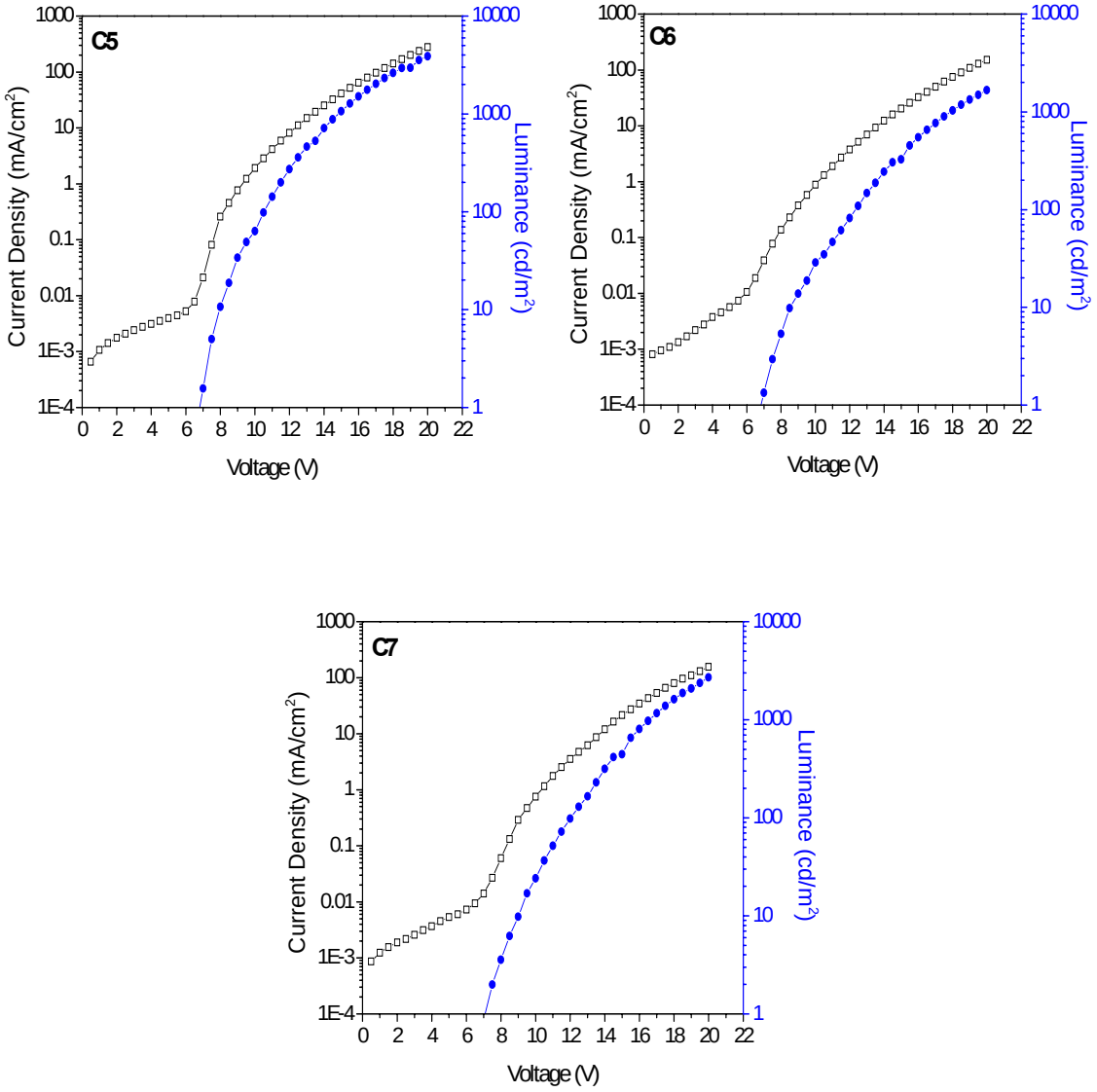

Figure 2.14. V-I-L curves of device based on Ir complexes **C1-C7**.

The external quantum efficiency (EQE_{ext}, or η_{ext}) and luminance efficiency (LE) of complex **C1-C7** are shown in Figure 2.15. Device with 10 wt% of **C1** exhibited the highest efficiency with η_{curr} = 36.4 cd/A and EQE_{ext} = 10.1% at 198 cd/m^2. All the devices showed gradual decrease of EQE with increasing current density, attributed to

increasing triplet-triplet annihilation of phosphor-bound excitions.[42] Combination of triplet-triplet annihilation and field-induced quenching effects, which are common and key issue for phosphorescent devices. However, the drop of efficiency is not severe, especially for **C1** to **C4**, when compared with other reported Ir complex devices. This result revealed that the T-T annihilation can be suppressed effectively by the introduction of bulky three-dimensional ligands. The device characteristics based on all the Ir complexes are summarized in Table 2.4.

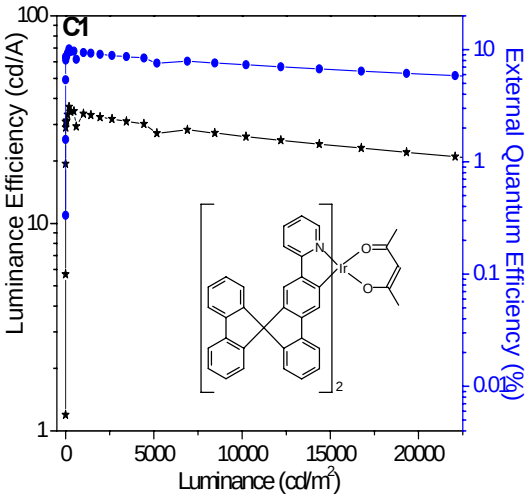

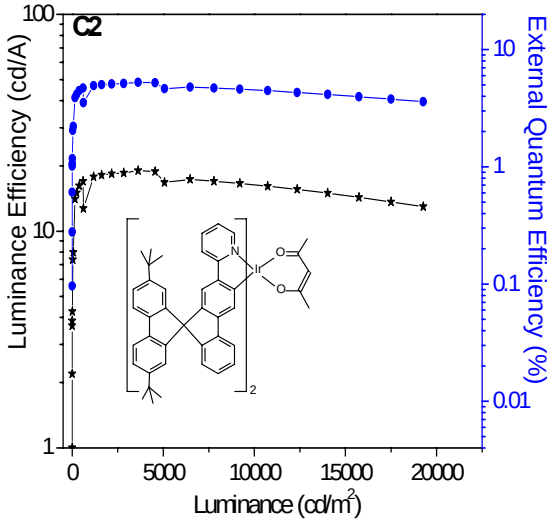

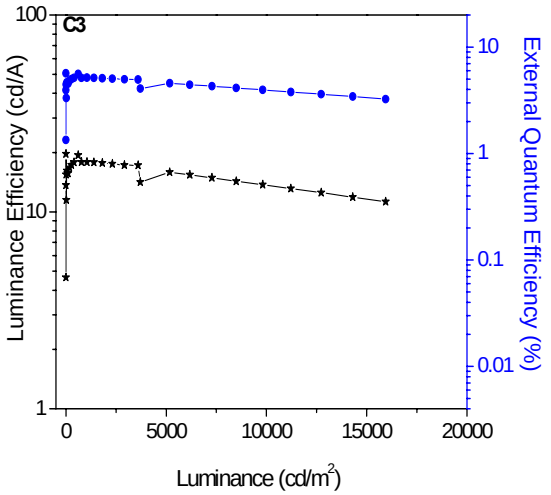
C3
Luminance Efficiency (cd/A)
External Quantum Efficiency (%)
Luminance (cd/m2)
100
10
1
0
5000
10000
15000
20000
10
1
0.1
0.01

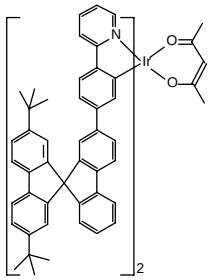
N
Ir
O
O
2

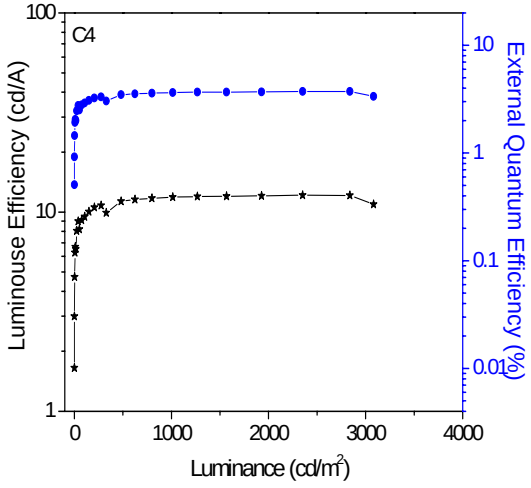
C4
Luminouse Efficiency (cd/A)
External Quantum Efficiency (%)
Luminance (cd/m2)
100
10
1
0
1000
2000
3000
4000
10
1
0.1
0.01

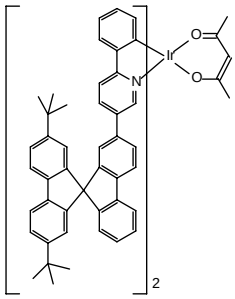
Ir
O
O
N
2

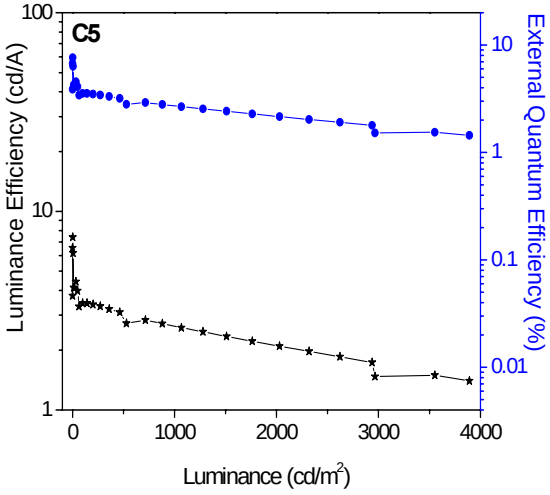
C5
Luminance Efficiency (cd/A)
External Quantum Efficiency (%)
Luminance (cd/m2)
100
10
1
0
1000
2000
3000
4000
10
1
0.1
0.01

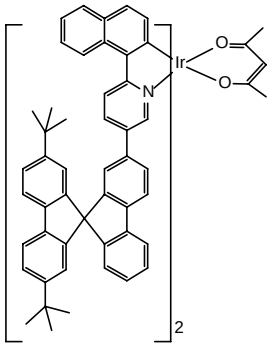
Ir
O
O
N
2

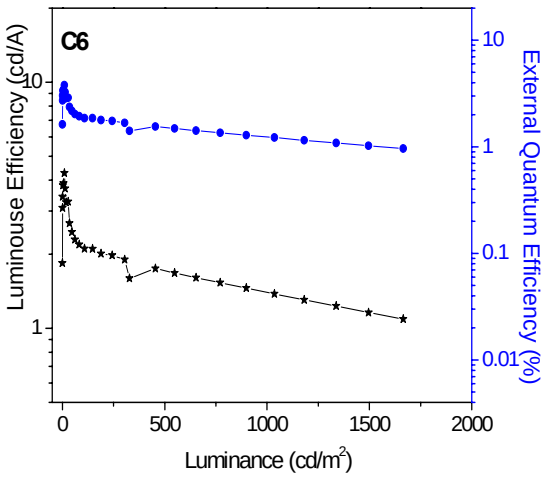
C6
Luminouse Efficiency (cd/A)
External Quantum Efficiency (%)
Luminance (cd/m2)
10
1
0
500
1000
1500
2000
10
1
0.1
0.01

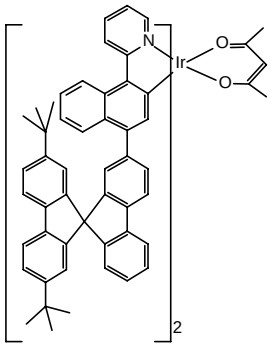
N
Ir
O
O
2

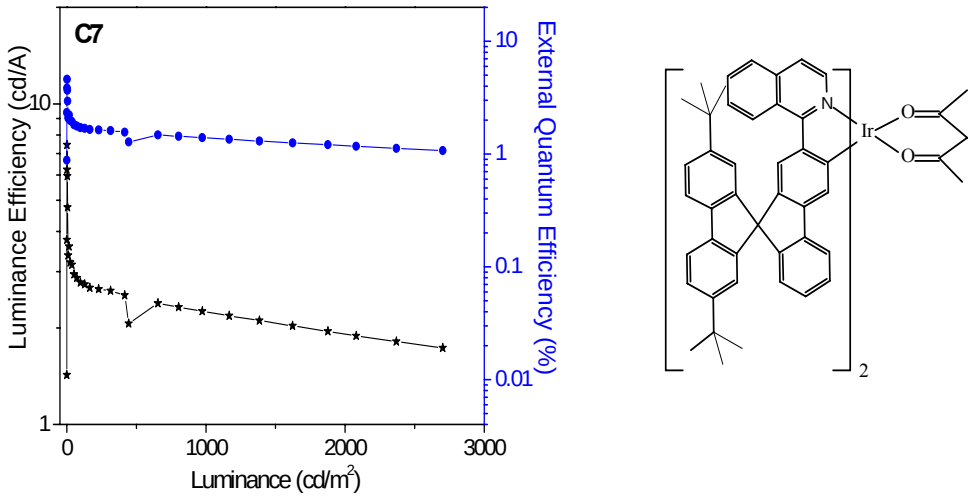

Figure 2.15. Luminance efficiency and external quantum efficiency of the devices based on Ir complex **C1**-**C7**.

Table 2.4. Device characteristics of Ir complexes **C1**-**C7**.

Complexes	η_{ext} (%)	Turn-on voltage (V)	λ (nm)	η_{curr} (cd/A)	L (cd/m^2) @ 20 V
C1	10.1	5.8	550, 598	36.4	30956
C2	5.3	7.2	552, 593.5	19.0	19271
C3	5.3	6.2	560.5, 600.5	19.4	15943
C4	3.7	8.4	564.5, 606	12.2	3081
C5	4.6	6.8	629	4.42	3893
C6	3.8	6.8	624	4.27	1666
C7	4.6	7.0	609	7.44	2702

From Table 2.4, it was found that among the yellow light-emitting materials, **C1** showed lowest turn-on voltage of 5.8 V and highest external quantum efficiency of 10.1%, while **C7** demonstrated highest efficiency among the red light emission materials.

PVK as the host material has the chemical compatibility with phosphorescent dyes and its photoluminescence spectrum is coincident with the absorption band of

phosphorescent materials. However, PVK/phosphorescence system had relatively low brightness and quantum efficiency because the barrier for hole injection is high.[43] Furthermore, PVK is a unipolar conductor that transports holes only. As a result, an electron conductor has to be admixed to PVK in order to balance charge transport. But the driving voltage of the devices was still very high because charge trapping of the iridium complex is the dominant mechanism in these LEDs.

To further improve the device performance, suitable host material other than PVK should be used. A small molecular host CBP could be a good alternative because it has a triplet energy gap of 2.56 eV.[31] It is a bipolar host material that can transport both holes and electrons. It also demonstrated good solubility and allows being solution processed. Besides CBP, TCTA is also the alternatives for PVK due to its amorphous states, excellent hole transporting ability and moderate solubility.[44,45]

2.5 Conclusions

In order to enhance performance of phosphorescent OLEDs, the key challenges that including T-T annihilation, concentration quenching and solution processability must be well addressed. This project aimed at designing novel ligands that were used to form light emitting Ir complexes, which can help to solve the above issues in phosphorescent OLEDs.

Seven novel ligands based on spirobifluorene have been synthesized. Most of the ligands were synthesized by palladium catalyzed Suzuki coupling reaction between spriobifluorene and arylpyrine derivatives. The ligands were obtained in good yields with well-defined structures. The ligands were converted to chloride-bridged dimmers first,

and then reacted with acac group to form heteroleptic Ir complex structures. All the Ir complexes were synthesized and characterized by NMR and MALDI-TOF. Their optical properties were measured by UV-vis and PL spectrometer. They realized yellow and red light emission. The thermal properties of all the Ir complexes were evaluated by TGA and DSC, indicating their good thermal stability at the temperature above 260 °C and amorphous state. HOMO, LUMO and energy band gaps of all the complexes were calculated combination of UV-vis absorption spectra and cyclic voltammogram analysis.

Devices were fabricated by doping the complexes at the concentration of 10 wt % into polymeric host materials PVK and PBD, showing satisfactory results. Based on the device configuration of ITO/PEDOT (50 nm)/PVK (50%): PBD (40%): Ir complex (10%) (45 nm)/TPBI (40 nm)/LiF (0.5nm)/Ca (20 nm)/Ag (150 nm), complex **C1** to **C4** realized yellow light emission and complex **C**5-**C7** red light emission. Most of them showed relatively high efficiency. For example, Complex **C1** achieved efficiency of 36.4 cd/A (10.1%) at 198 cd/m^2 and complex **C7** reached external quantum efficiency of 4.6%. The external quantum efficiency did not decrease much at high current density, which means that the T_1-T_1 annihilation was largely suppressed by the new designed complexes. The efficiencies of the seven complexes could be further enhanced by modifying the device structure and doping concentration because only one kind of device structure was tried so far. For example, to replace PVK with a new host materials to reduce the barrier for hole injection/transport by using CBP, TCTA or other host materials could largely improve the device performance.

2.6 Outlook

The seven synthesized Ir complexes can be used as guest materials for phosphorescent OLEDs. However, the efficiency can be improved further in later research.

The series of Ir complexes did not realize blue light emission because this is not the focus of this research. As we know, blue light emission is indispensably for full color display. However, only a few blue phosphorescent complexes were developed. So far, to realize blue light emission, one approach is to incorporate electron-withdrawing groups to spirobifluorene ligand, which will cause a blue shift for the light emission. Development of other novel ligand based complexes could be an alternative to realize blue light emission.

Besides light-emitting materials, development of suitable host materials can also help to improve device performance. There are some basic requirements for host materials. To prevent reverse energy transfer from the guest back to the host and effectively confine triplet excitons on guest molecules, the triplet energy level of the host must be larger than that of the triplet emitter. Correspondingly, the host materials must have rather large energy gaps. To have a large energy gap, the extent of conjugation in the molecule must be confined, which usually require the molecules to be bulky and steric. Such a standard in turn will be helpful to form a uniform amorphous thin film. Materials based on three-dimensional and interrupted conjugated carbazoles or triphenylamines should be a good choice.

In order to prevent phase separation of the thin film in the host-guest system, polymeric Ir complexes should be considered. Polymeric Ir complexes that containing both hole and electron transport moieties can have uniformly distributed emitting centers

over the thin film. In addition, OLEDs device based on the polymeric phosphorescent materials will have much simpler device structure, which reduces the cost for device fabrication.

References

1. J. S. Yang, T. M. Swager, *J. Am. Chem. Soc*. **1998**, *120*, 5321.
2. J. S. Yang, T. M. Swager, *J. Am. Chem. Soc*. **1998**, *120*, 11864.
3. N. Johansson, D. A. dos Santos, S. Guo, J. Cornil. M. Fahlman, J. Salbeck, H. Schenk, H. Arwin, J. L. Bredas, W. R. Salanek, *J. Phys. Chem*. **1997**, *107*, 2542.
4. N. Johansson, J. Salbeck, J. Bauer, F. Weissortel, P. Broms, A. Andersson, W. R. Salaneck, *Adv. Mater*. **1998**, *10*, 1136.
5. F. Steuber, J. Staudigel, M. Stossel, J. Simmerer, A. Winnacker, H. Speritzer, F. Weissortel, J. Salbeck, *Adv. Mater*. **1999**, *12*, 130.
6. J. Kim, *Pure Appl. Chem*. **2002**, *74*, 2031.
7. A. B. Tamayo, B. D. Alleyne, P. I. Djurovich, S. Lamansky, I. Tsyba, N. N. Ho, R. Bau, M. E. Thompson, *J. Am. Chem. Soc.* **2003**, *125*, 7377.
8. R. Ragni, E. A. Plummer, K. Brunner, J. W. Hofstraat, F. Babudri, G. M. Farinola, F. Naso, L. D. Cola, *J. Mater. Chem*. **2006**, *16,* 1161.
9. Y. You, S. Y. Park, *J. Am. Chem. Soc*. **2005**, *127*, 12438.
10. P. L. Burn, I.D. W. Samuel, *Macromolecules* **2003**, *36*, 9721.
11. C. S. K. Mak, A. Hayer, S. I. Pascu, S. E. Watkins, A. B. Holmes, A. Kohler, R. H Friend, *Chem. Commun*. **2005**, 4708.
12. R. Rathore, C. L. Burns, *J. Org. Chem*. **2003**, *68*, 4071.
13. W.-L. Yu, J. Pei, W. Huang, A. J. Heeger, *Adv. Mater*. **2000**, *12*, 828.
14. S.-C. Lo, E. B. Namdas, P. L. Burn, I. D. W. Samuel, *Macromolecules* **2003**, *36*, 9721.

15. A. J. Sandee, C. K. Williams, N. R. Evans, J. E. Davies, C. E. Boothby, A. Kohler, R. H. Friend, A. B. Holmes, *J. Am. Chem. Soc*. **2004**, *126*, 7041.

16. J. W. Tilley, S. Zawoiski, *J. Org. Chem*. **1998**, *53*, 386.

17. S. Lamansky, P. Djurovich, D. Murphy, F. Abdel-Razzaq, H.-E. Lee, C. Adachi, P. E. Burrows, S. R. Forrest, M. E. Thompson, *J. Am. Chem. Soc*. **2001**, *123*, 4304.

18. X. Chen, J.-L. Liao, Y. Liang, M. O. Ahmed, H.-E. Tseng, S.-A. Chen, *J. Am. Chem. Soc*. **2003**, *125*, 636.

19. J.-P. Duan, P.-P. Sun, C.-H. Cheng, *Adv. Mater*. **2003**, *15*, 224.

20. Y.-H. Sun, X.-H. Zhu, Z. Chen, Y. Zhang, Y. Cao, *J. Org. Chem*. **2006**, *71*, 6281.

21. S. Jung, Y. Kang, H. S. Kim, Y. H. Kim, C. L. Lee, J. J. Kim, S. K. Lee, S. K. Kwon, Eur. *J. Inorg. Chem*. **2004**, *17*, 3415.

22. A. Higuchi, K. Ohnishi, S. Nomura, H. Inada, Y. Shirota, *J. Mater. Chem*. **1992**, *2*, 1109.

23. P. E. Burrows, Z. Shen, V. Bulvic, D. M. McCarty, S. R. Forrest, *J. Appl. Phys*. **1996**, *79*, 7991.

24. C.-H. Yang, K.-H. Fang, W.-L. Su, S.-P. Wang, S.-K. Su, I-W. Sun, *J. Organometallic Chem*. **2006**, *691*, 2767.

25. K.-H. Fagn, L.-L. Wu, Y.-T. Huang, C.-H. Yang, I-W. Sun, *Inorg. Chimica Acta* **2006**, *359*, 441.

26. P. J. Hay, *J. Phys. Chem. A* **2002**, *106*, 1634.

27. J. Ding, J. Gao, Q. Fu, Y. Cheng, D. Ma, L. Wang, *Synth. Met*. **2005**, *155*, 539.

28. L. Chen, C. Yang, J. Qin, J. Gao, H. You, D. Ma, *J. Organometallic Chem*. **2006**, *691*, 3519.

29. K. Ono, M. Joho, K. Saito, M. Tomura, Y. Matsushita, S. Naka, H. Okada, H. Onnagawa, *Eur. J. Inorg. Chem*. **2006**, 3676.

30. V. Adamovich, J. Brooks, A. Tamayo, A. M. Alexander, P. I. Djurovich, B. W. D' Andrade, C. Adachi, S. R. Forrest, M. E. Thompson, *New J. Chem*. **2002**, *26*, 1171.

31. A. van. Dijken, J. J. A. M. Bastiannsen, N. M. M. Kiggen, B. M. W. Langeveld, C. Rothe, A. Monkman, I. Bach, P. Stossel, K. Brunner, *J. Am. Chem. Soc*. **2004**, *126*, 7718.

32. C.-L. Lee, K. B. Lee, J.-J. Kim, *Appl. Phys. Lett.* **2000**, *77*, 2280.

33. S. Lamansky, R. C. Kwong, M. Nugent, P. I. Djurovich, M. E. Thompson, *Org. Electron*. **2001**, *2*, 53.

34. C.-I. Chao, S.-A Chen, *Appl. Phys. Lett*. **1998**, *73*, 426.

35. X. H. Yang, F. Jaiser, S. Klinger, D. Neher, *Appl. Phys. Lett*. **2006**, *88*, 021107.

36. S. A. Choulis, M. K. Mathai, V.-E. Choong, F. So, *Appl. Phys. Lett*. **2006**, *88*, 203502.

37. F.-I. Wu, P.-I. Shih, Y.-H. Tseng, G.-Y. Chen, C.-H. Chien, C.-F. Shu, Y.-L. Tung, Y. Chi, A. K.-Y. Jen, *J. Phys. Chem. B* **2005**, *109*, 14000.

38. I. Tanaka, S. Tokito, *J. Appl. Phys*. **2006**, *99*, 073501.

39. X. Gong, J. C. Ostrowski, D. Moses, G. C. Bazan, A. J. Heeger, *Adv. Funct. Mater.* **2003**, *13*, 439.

40. B. J. Chang, J. H. Park, K. H. Lee, Y. C. Kim, J.-W. Yu, J. K. Kim, *Curr. App. Phys*. **2006**, *6*, 658.

41. X. Zhang, J. Gao, C. Yang, L. Zhu, Z. Li, K. Zhang, J. Qin, H. You, D. Ma, *J. Organometallic Chem*. **2006**, *691*, 4312.

42. X. Gong, S. H. Lim, J. C. Ostrowski, D. Moses, G. C. Bazan, A. J. Heeger, *J. Appl. Phys*. **2004**, *95*, 948.

43. M. A. Baldo, C. Adachi, S. R. Forrest, *Phys. Rev. B* **2000**, *62*, 10967.

44. T.-H. Kim, D.-Y. Yoo, J. H. Park, O. O. Park, J.-W. Yu, J. K. Kim, *Appl. Phys. Lett*. **2005**, *86*, 171108.

45. S.-C. Loh, N. A. H. A. Male, J. P. J. Marham, S. W. Magennis, P. L. Burn, O. V. Salata, I. D. W. Samuel, *Adv. Mater*. **2002**, *14*, 975.

46. B. W. D'Andrade, R. J. Holmes, S. R. Forrest, *Adv. Mater*. **2004**, *16*, 624.

3. Development of highly efficient polymeric Ir complexes for OLEDs

3.1 Molecular design

The general strategy for OLEDs based on small molecular Ir complexes is to dope the Ir complexes into polymeric or small molecular hosts, which have excellent charge transport ability. The device can be fabricated by vacuum deposition or spin-coating depend on the solubility of host. However, such devices faced some performance issues, such as phase separation, aggregation of phosphors, phosphorescent quenching and inefficient energy transfer. Another consideration is their high cost due to complicated device structures. The ideal situation is to combine triplet emitter and polymer host into one material, which not only overcome the above shortcomings, but also allow for solution process and simple device structures. That is the reason why polymeric Ir complexes were developed. However, their current progress is not satisfactory because of their low efficiency. Thus, the target for OLEDs based polymeric Ir complexes is to achieve high efficiency and long lifetime operation. The main obstacle is the inefficient energy transfer from polymer to Ir complex due to the unmatched energy levels. To guarantee efficient energy transfer, controlling the energy levels of the polymer and iridium complex play key role.

It is well-known that arylamino-containning materials as well as carbazole-based materials have excellent hole transport ability and large energy gaps. Electron donating character of the carbazole and triphenylamine moiety provides their photoconductive properties and the ability to form charge-transfer complexes. The structure of triphenylamine is shown in Figure 3.1. Its excellent hole-transporting ability and good film-forming properties made them good building blocks for blue-light emitters in

PLEDs.[1-4] Although the luminescence properties were found to be lower than those of the poly(2,7-fluorene)s, carbazole, triphenylamine and their derivatives are suitable candidates as host materials for triplet emitters, even for blue triplet emitters. Such as, poly(N-vinyl carbazole) (PVK),[5-7] CBP,[8] TCTA,[9,10] and 4,4'-bis(9-carbazolyl)-2,2'-dimethyl-biphenyl (CDBP) with high triplet energy level.[11]These carbazole and triphenylamine containning materials are widely used as host materials for phosphorescent OLEDs. It was found that the introduction of hole transporting materials can dramatically lower the driving voltage and greatly increase luminance and efficiency of the device.[12,13]

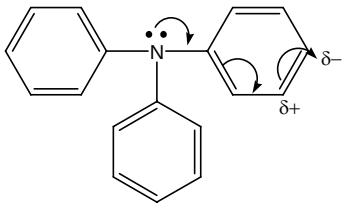

Figure 3.1. Chemical structure of triphenylamine.

For the polymeric Ir complexes, in order to guarantee effective energy transfer from polymer backbone to Ir complexes, large bandgap polymers i.e., blue light-emitting polymers are preferred. For the Ir complexes, low bandgap materials, such as green, orange or red light-emitting complexes will be desirable.

Polyfluorenes (PFs) that emit in the blue region are very promising candidates for light-emitting materials due to their high photoluminescence (PL), electroluminescence (EL) efficiencies and excellent thermal stabilities. They can also be used for host materials due to excellent processibility and good charge transport ability. In order to obtain high molecular weight and maintain good solubility for the phosphorescent

polymers, dihexylfluorene was selected to form the backbone of phosphorescent polymers.

For Ir complex monomers, their energy gaps must be smaller than the triplet energy level of the backbone, the green to red light-emitting Ir complexes are preferred. Among all the ligand for Ir complexes, the simplest and highly efficient Ir complex was green light emitting Ir complex that based on 2-phenylpyridine ligand. Thus, 2-phenylpyridine was selected as main ligands for Ir complex. In order to guarantee efficient energy transfer from polymer to Ir complexes, one of the ligands of the Ir complexes should be incorporated into the main chain of polymers. On the other hand, hole-transporting ability need to be considered, the diphenylamine moiety was included in the ancillary ligand for Ir complex. The three dimensional structure of the resulting complex can also suppress the intermolecular close packing. Thus diphenylamine will copolymerize with fluorene and form the backbone of polymers. The chemical structures of phosphorescent polymers are shown in Figure 3.2. In order to reduce triplet quenching and tune the energy levels of phosphors, the molar fraction of iridium complexes was varied from 4 - 20 mol%. The reported high-lying HOMO level of poly(9,9-dioctylfluorene-2,7-diyl-*co*-bis-N, N-(4-butylphenyl)-bis-N N'-phenyl-1,4-phenylene-diamine) (PFB)[4] was expected to be obtained from the fluorene and diphenylamine copolymer backbones.

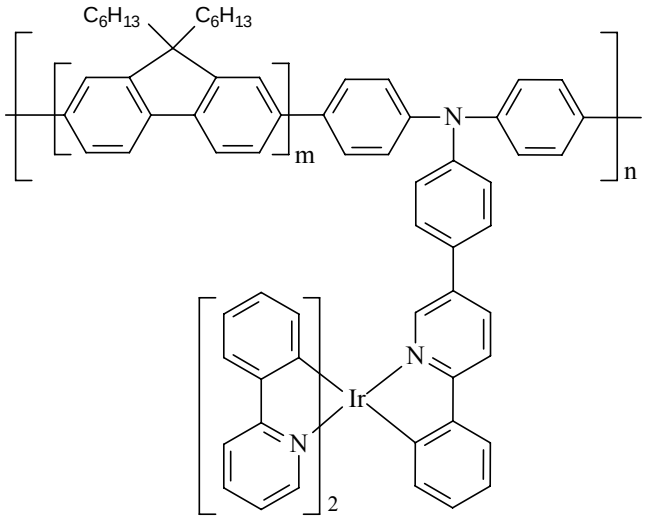

Figure 3.2. Chemical structure of polymeric Ir complexes.

3.2 Synthesis and characterization

3.2.1 Monomer synthesis

2-Phenylpyridine is commercially available, thus, only the ancillary ligand need to be synthesized. First, N,N-Diphenyl-N-(4-bromophenyl)-amine **1** was obtained from triphenylamine through N-bromosuccinimide (NBS) bromination reaction in chloroform at 0 ºC with a yield of 70%. Then N,N-diphenyl-N-(4-bromophenyl)-amine was converted into N, N-diphenyl-4-aminophenylboronic acid **2** by treating it with n-BuLi in anhydrous THF solution at -78 ºC, followed by adding trimethyl borate stirring overnight. Then the reaction was terminated with water and dilute HCl was added, the final product was obtained with a yield of 63%. 5-Bromo-2-phenylpyridine **3** was synthesized by following standard Suzuki coupling from 2,5-dibromopyridine and phenyl boronic acid in the presence of catalyst $Pd(PPh_3)_4$ with a yield of 74%. Bis(2-phenylpyridine) triphenylamine **4** was obtained by following standard Suzuki coupling reactions in anhydrous THF between compound **2** and **3** with a yield of 61%. Ancillary ligand **L1** was

obtained from **4** by following NBS bromination reaction in chloroform at 0 ºC with a yield of 85% after recrystallization from ethanol. Then a standard two-step procedure was followed to convert the ligand to the final heteroleptic complex. First, ligand 2-phenylpyridine reacts with iridium trichloride hydrate to form chloride-bridged dimmer in 2-ethoxyethanol and water mixture with the ratio of 3:1, refluxing overnight under nitrogen in a medium yield. Then the dimer reacts with the ancillary ligand **L1** in glycerol with presence of K_2CO_3 to form heteroleptic Ir complex at 200 °C under nitrogen with a yield of 41%. The heating temperature need to be higher than 200 °C, lower reaction temperature will produce more meridional conformation complexes, whose efficiency is lower than that of the facial conformation.[14] The synthetic scheme is depicted in Scheme 3.1.

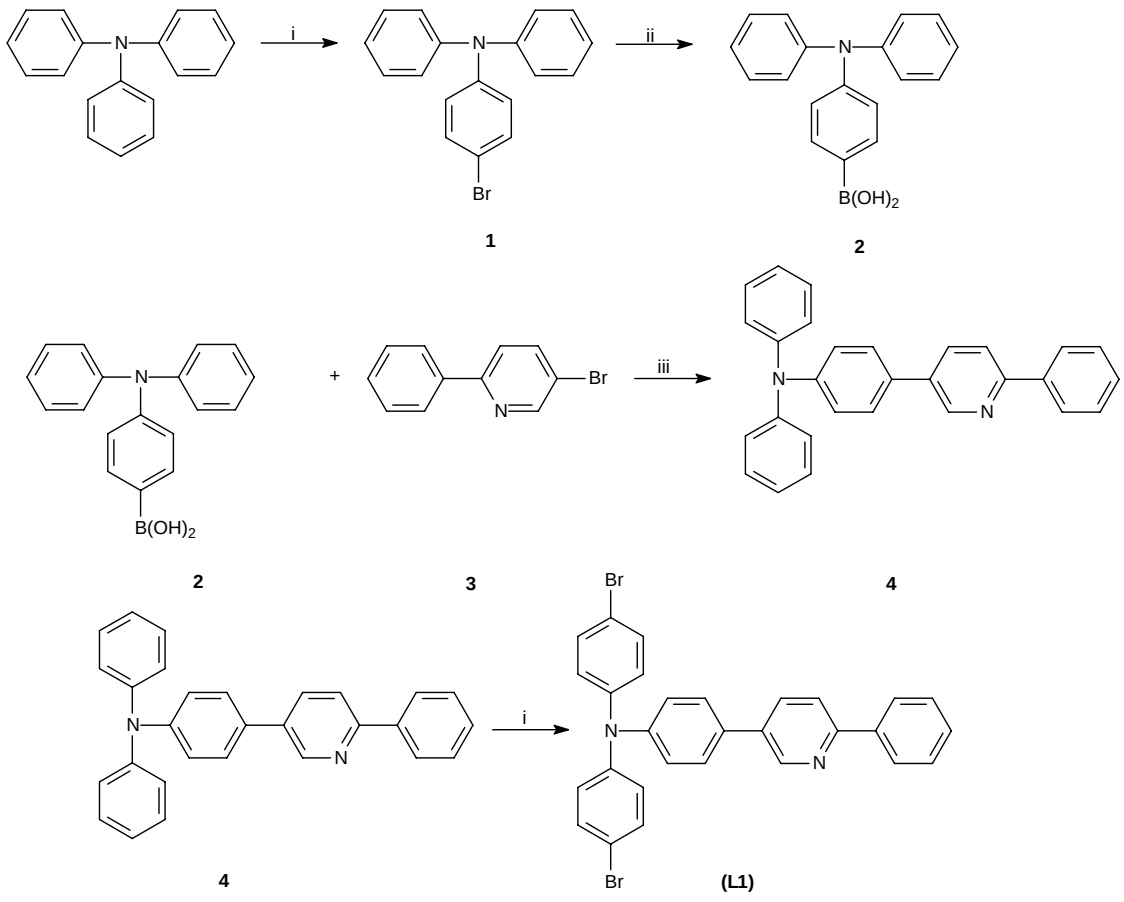

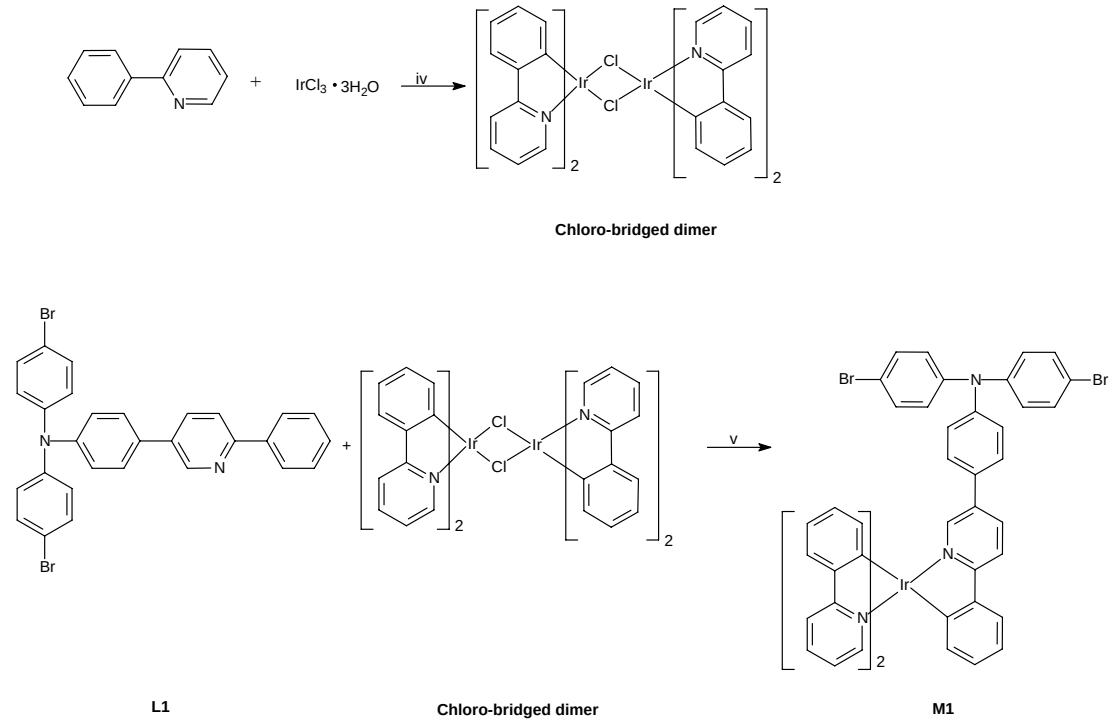

Scheme 3.1. Synthetic routes for the monomers.
Reagents and conditions: i. NBS, chloroform, 0 °C; ii. BuLi, THF, -78 °C, $B(OCH_3)_3$, H^+; iii. Na_2CO_3, THF, $Pd(PPh_3)_4$, 90 °C; iv. 2-ethoxyethanol: H_2O = 3:1, reflux, 24 h; v. K_2CO_3, glycerol, 200 °C, 24 h.

N,N-Diphenyl-N-(4-bromophenyl)-amine (1)[15]

Triphenylamine (10.0 g, 40.8 mmol) was dissolved in chloroform (50 mL) and cooled down to 0 °C. Then NBS (7.2 g, 40.8 mmol) was added slowly with small portion by several times. The mixture was stirred overnight. Then the reaction was quenched with water and extracted with dichloromethane (100 mL) 3 times. The combined organic extracts were washed with saturated brine and dried over $MgSO_4$ and concentrated in vacuo. The crude product was purified by recrystallizaiton from ethanol to provide product 9.2 g (70%) as light grey crystals.

^{1}H NMR ($CDCl_3$, 400 MHz): δ, 7.33 (d, 2H), 7.25 (m. 4H), 7.06 (m, 6H), 6.95 (d, 2H).

N,N-Diphenyl-4-aminophenylboronic acid (2)[15,16]

To a solution of N,N-diphenyl-N-(4-bromophenyl)-amine (5.82 g, 18 mmol) in anhydrous THF (90 mL) was added dropwise n-BuLi (6.5 mL, 21.6 mmol) in hexane at -78 °C, After stirring for 1 h, the mixture was transferred to a solution of trimethyl borate (23.4 mmol) in THF (10 mL) at 0 °C and stirred overnight. Then the reaction was quenched with water and diluted HCl was added, stirring for another1 h. Then the mixture was extracted with ether (100 mL) 3 times. The organic layer was combined and washed with saturated brine, dried over anhydrous $MgSO_4$, and concentrated in vacuo. The crude product was washed with hexane (50 mL) 3 times to provide the product, 3.22 g (62%), as light grey powder.

^{1}H NMR ($CDCl_3$, 400 MHz) δ, 8.03 (d, 2H), 7.24 (m, 4H), 7.17 (d, 4H), 7.02 (t, 4H).

N-Phenyl-N-(4-6-phenylpyridin-3-yl)phenyl)benzenamine (4)

A mixture of N,N-diphenyl-4-aminophenylboronic acid (2.42 g, 8.4 mmol), 5-bromo-2-phenylpyridine (1.96 g, 8.4 mmol), $Pd(PPh_3)_4$ (0.041 g, 0.035 mmol) in anhydrous THF (31 mL), aqueous sodium carbonate (2 M, 7.2 mL) was deoxygenated and heated to reflux under nitrogen, stirring for 24 h. After cooling to room temperature, the mixture was washed with water and extracted with dichloromethane (50 mL) 3 times. The combined organic layers were then washed with saturated brine, dried over $MgSO_4$ and concentrated in vacuo. The residue was purified by column chromatography (silica gel, ethyl acetate: hexane=1:20) to give light yellow crystal of the product 2.04 g (61%).

^{1}H NMR ($CDCl_3$, 400 MHz) δ, 8.92 (d, 1H), 8.05 (d, 2H), 7.93 (dd, 1H), 7.80 (d, 1H), 7.49 (m, 4H), 7.44 (m, 1H), 7.29 (m, 4H), 7.16 (t, 6H), 7.06 (t, 2H).

^{13}C NMR ($CDCl_3$, 100 MHz): δ, 155.5, 148.3, 147.6, 147.4, 138.8, 134.9, 134.8, 131.0, 129.6, 129.0, 127.8, 127.0, 125.0, 123.7, 123.6, 120.7.

MS (MALDI): 397.216 (m/z), Calcd for $C_{29}H_{21}N_2$: 397.170.

N-Bromo-N-(4-bromophenyl)-N-(4-(6-phenylpyridin-3-yl)phenyl)benzenamine (L1)

Ancillary ligand **L1** was synthesize by NBS bromination reaction of compound **4**, following the same procedure for compound **1** and purified by recrystallization from ethanol to give the product as yellow crystals with a yield of 85%.

^{1}H NMR ($CDCl_3$, 400 MHz) δ, 8.91 (d, 1H), 8.05 (d, 2H), 7.93 (dd, 1H), 7.81 (d. 1H), 7.51 (m, 4H), 7.40 (m, 5H), 7.17 (d, 2H), 7.01 (d, 4H).

^{13}C NMR ($CDCl_3$, 100 MHz): δ, 156.3, 148.1, 147.4, 146.6, 139.4, 134.9, 134.5, 132.9, 132.8, 129.4, 129.2, 128.3, 127.2, 126.3, 124.7, 120.7, 116.5.

MS (MALDI): 554.869 (m/z), Calcd for $C_{29}H_{19}N_2Br_2$: 554.989.

General procedure for Monomer M1[14]

A mixture of 2-phenylpyridine (0.97 g, 6.24 mmol), iridium chloride trihydrate (1 g, 2.84 mmol), water (30 mL) and 2-ethoxylethonal (90 mL) was deoxygenated and then heated to reflux under nitrogen for 24 h. After cooling to room temperature, the mixture was filtrated and washed with hexane, ether and ethanol to give chloride-bridged dimmer product. Then, a mixture of chloride-bridged dimer (0.43 g, 0.4 mmol), ancillary ligand **L1** (0.56 g 1 mmol), glycerol (28.7 mL) and K_2CO_3 (0.55 g, 4 mmol) was deoxygenated

and then heated to reflux under nitrogen for 24 h. After cooling to room temperature, the mixture was washed with water and extracted with dichloromethane (50 mL) 3 times. The organic layer was combined and then washed with saturated brine and dried over $MgSO_4$ and concentrated in vacuo. After column chromatography (silica gel, dichloromethane: hexane=1:1, the product was obtained as yellow powder with a yield of 41%.

MS (MALDI): 1057.013 (m/z), Calcd for $C_{51}H_{35}Br_2N_4Ir$: 1056.083.

2,7-Dibromo–(9,9-dihexyl)fluorene **5** and 2,7-bis(4,4,5,5-tetramethyl-1,3,2-dioxaborolan-2-yl)-9,9-dihexylfluorene **6** were prepared according to the published procedures.[17,18]

3.2.2 Polymer synthesis

All the polymers were synthesized through Suzuki polycondensation. A mixture of heteroleptic Ir complex monomer **M1**, 2,7-dibromo–(9,9-dihexyl)fluorene **5**, 2,7-bis(4,4,5,5-tetramethyl-1,3,2-dioxaborolan-2-yl)-9,9-dihexylfluorene **6**, and tetramethylammonium hydroxide (Me_4NOH, 25 wt%, in methanol), toluene/THF and [$Pd(PPh_3)_4$] was deoxygenated and heat to 90 °C, stirring for 3 days. Then the polymer was capped by adding 2-(4,4,5,5-tetramethyl-1,3,2-dioxaborolan-2-yl)-9,9-dihexylfluorene with continued stirring for 12 h and then 2-bromo-(9,9-dihexyl)fluorene was added, followed by stirring at 90 °C for another 12 h. In order to tune the energy level of the phosphor and reduce triplet quenching, the feed ratios of iridium complex varied froo 4%, 10%, 15% to 20% as mole fraction, and the corresponding copolymers

are respectively named as **P1**, **P2**, **P3** and **P4**. The synthetic routes of polymers were depicted in Scheme 3.2.

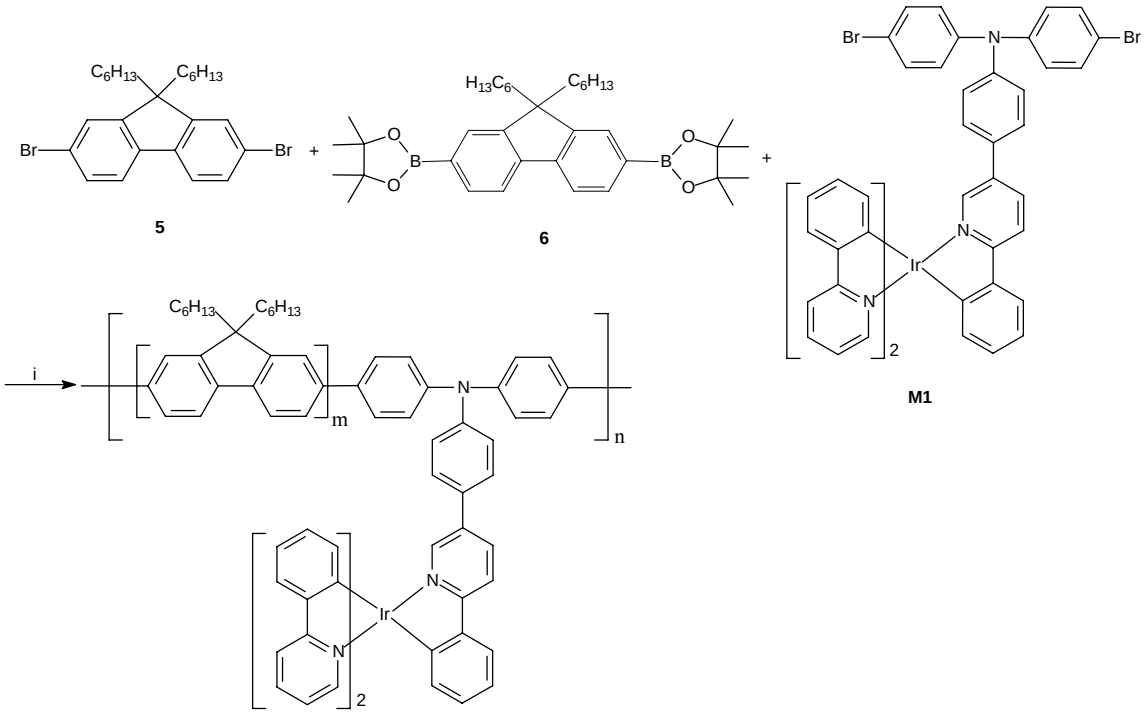

Scheme 3.2. Synthetic routes for the polymers.
Reagents and conditions: i. Me_4NOH (25 wt% in methanol), toluene/THF, $[Pd(PPh_3)_4]$, 90 °C, 72 h.

All the crude polymers were washed by water and extracted with dichloromethane, and then the organic layer was combined and then washed with saturated brine and dried over $MgSO_4$ and concentrated into 10 mL. Then the polymers were precipitated into methanol 3 times. The resulting polymers were further purified by performing a Soxhlet extraction in acetone and methanol to remove low molecular weight molecules. The purified polymers were characterized by GPC, NMR to confirm their molecular weights and chemical structures. GPC results were listed in Table 3.1. Their NMR spectra in *d*-dichloromethane were shown in Figure 3.3. The NMR of monomer 1 showed that two

kinds of isomers co-existed due to its bulky ligand structures. The NMR and GPC results of polymers demonstrated that all the polymeric Ir complexes are in high purity.

Table 3.1. Molecular weights and PDIs of phosphorescent polymers **P1**-**P4**.

Polymer	M_w (g/mol)	M_n (g/mol)	PDI
P1	59304	23674	2.5
P2	61136	16264	3.7
P3	15958	6235	2.6
P4	23439	9819	2.4

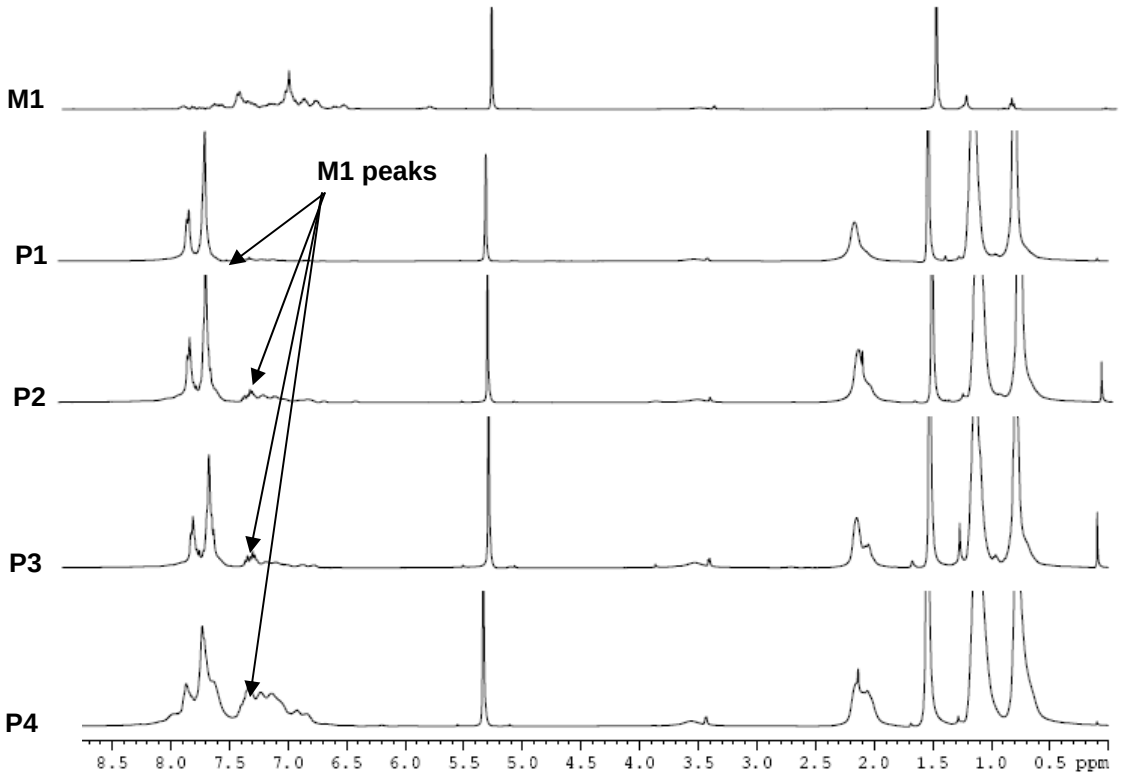

Figure 3.3. NMR spectra of phosphorescent polymer **P1**-**P4** in *d*-CD_2Cl_2.

3.3 Results and discussion

3.3.1 Polymer synthesis

It can be seen from Table 3.1 that the molecular weights of polymers decreased with the increase of Ir complex content due to the poor solubility of triphenylamine based Ir complex. When the feed ratio of Ir complex increased, the peaks from monomer increased, which can be observed from the NMR spectra in Figure 3.3.

3.3.2 Optical analysis

The UV-vis absorption and photoluminescence (PL) spectra were recorded on a Shimadzu UV 3101 spectrophotometer and Shimadzu RF-5301 PC spectrophotometer at room temperature, respectively. The spectra of Ir complex monomer and all the copolymers in anhydrous DCM solution are shown in Figure 3.4. The photophysical data are summarized in Table 3.2.

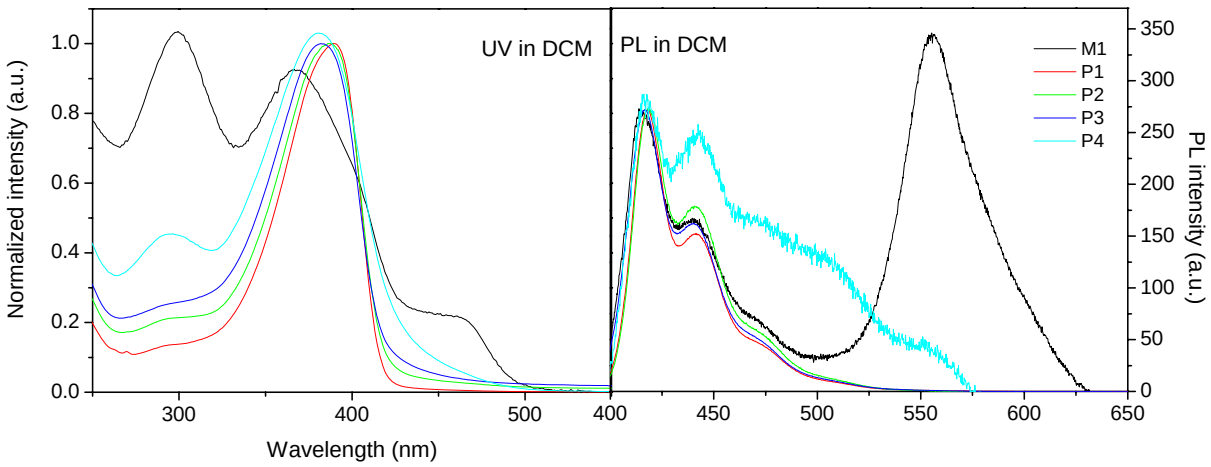

Figure 3.4. Normalized UV and PL spectra of M1 and **P1-P4** in anhydrous DCM solution.

Table 3.2. Photophysical properties of Ir complexes in anhydrous DCM.

Samples	UV-vis absorption λ_{max} (nm)	PL λ_{em} (nm)
M1	299, 369, 462	415 (441, 555)
P1	389	418 (441, 472)
P2	387	418 (441, 472)
P3	382	418 (441, 472)
P4	381	415 (441, 503)

Note: The data in the parentheses are the wavelength of shoulders and sub-peaks

It can be seen from Table 3.2 that the Ir complex monomer showed three absorption peaks due to the absorption of the ligand. The longest absorption peaks of the copolymers are blue-shifted with the increasing content of Ir complexes due to the decrease of conjugation length. However, their emission spectra are exactly the same due to the emission is totally from fluorene units in dilute solutions. For P4, due to its highest Ir complex content, weak emission from the Ir complex monomer can be seen. The Ir complex monomer showed orange light emission.

3.3.3 Thermal analysis (TGA)

The thermal stability of Ir complexes in nitrogen was evaluated by thermogravimetric analysis (TGA) using TGA Q500 instrument (heating rate of 10 °C·min^{-1}). The TGA traces of polymer **P1** to **P4** are shown in Figure 3.5.

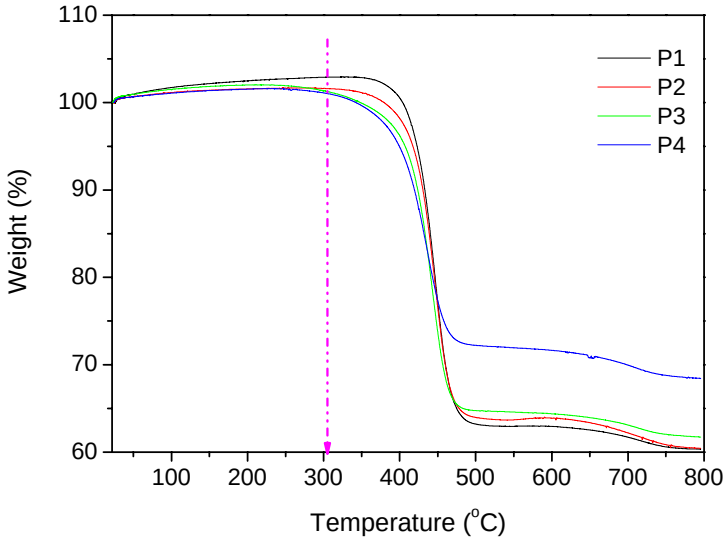

Figure 3.5. Thermogravimetric analyses of copolymers under nitrogen atmosphere.

As can be seen from the TGA data, all the copolymers exhibited excellent thermal stability. All the onset temperatures of weight loss are higher than 300 °C, and temperatures for 5% weight loss are higher than 400 °C. It was noticed that with the increases of Ir complex content, the thermal stability decreased. The onset and 5% weight loss temperatures of all the copolymers are summarized in Table 3.3.

Table 3.3. Onset temperature of weight loss and temperature for 5% weight loss under N_2.

Polymers	T_{on} (°C)	$T_{5\ wt\%}$ (°C)
P1	366	422
P2	341	417
P3	314	407
P4	307	400

3.3.4 Electrochemical properties

The redox properties of the polymers were investigated by the cyclic voltammetry (CV). The CV measurements were performed by coating the film on working electrodes in a solution of 0.1 M tetrabutylammonium hexafluorophosphate ($TBAPF_6$) in acetonitrile at a scan rate of 0.1 V/s at room temperature under the protection of nitrogen. The CV curve of **P1** is shown in Figure 3.6 as an example. All the electrochemical data in acetonitrile is summarized in Table 3.4.

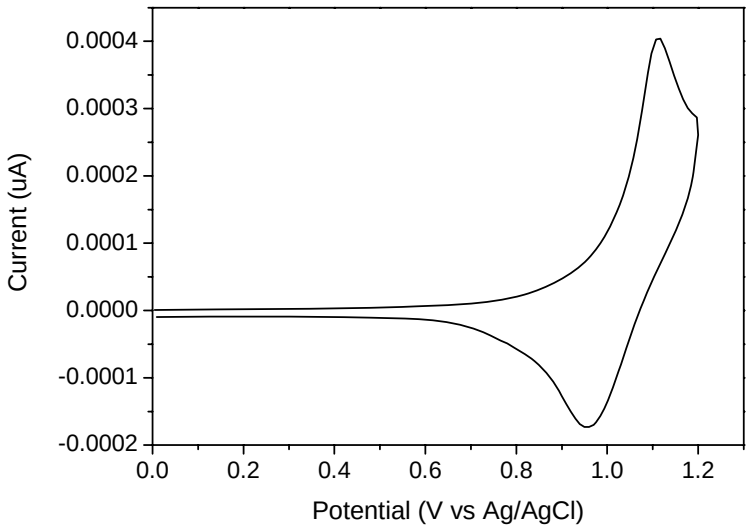

Figure 3.6. Cyclic voltammagrams of P4 films in acetonitrile solution at room temperature under nitrogen.

Table 3.4. Electrochemical properties of the copolymers films in acetonitrile.

Samples	E_{onset} (eV)	HOMO (eV)	LUMO (eV)	E_g (eV)
M1	0.68	-5.08	-2.57	2.51
P1	0.94	-5.34	-2.35	2.99
P2	0.94	-5.34	-2.49	2.85
P3	0.87	-5.27	-2.46	2.81
P4	0.93	-5.33	-2.72	2.61

All the copolymers showed obvious oxidation peaks and underwent a reversible one-electron oxidation process, demonstrating excellent electrochemical stability of their cations. However, no reduction peak was observed. Thus, all the energy band gaps were estimated from the long-wavelength absorption edge data collected from spectroscopic method as described in Chapter 2. It was found that with the increasing of Ir complex in polymers, the energy gap of the polymers decreased. It confirmed that the energy levels of the polymers were tuned by the ratio of Ir complex.

3.4 Conclusion

Ir complex monomer based on 2-phenylpyridine main ligands and triphenylammine ancillary ligand was synthesized, which is orange emitter. A series of phosphorescent polymers containing Ir complexes pendants and polyfluorene backbones has been synthesized. The molecular weights of the polymers largely increased compared with literature reported polymers with Ir complex pendants. With the increase of Ir complex feed ratio, the molecular weights of polymers decreased due to the bulky structure of Ir complex. All the polymers exhibited excellent thermal stability up to 300 °C. The energy

levels of the polymers were tuned by changing the Ir complex feed ratios. Efficient energy transfer is expected to be realized from blue light-emitting polyfluorenes to orange light-emitting Ir complex pedants. Thus, good device performances are expected from these phosphorescent polymers.

3.5 Outlook

Due to bulky structure of ancillary ligand for Ir complex, its solubility was not very good, thus the molecular weights and PDIs of the copolymers were affected. In order to improve its solubility and enhance the molecular weight, alkyl chain can be introduced into the main ligand for Ir complexes. Dihexylfluorene can also be replaced by didodecylfluorene to improve the solubility further.

In order to improve energy transfer further, 2-phenylisoquinoline can be used as the main ligand instead of 2-phenylpyridine for Ir complexes, which will shift the light emission to red region. Energy transfer from polymer to Ir complex will be more efficient due to lower energy level of Ir complex. Another way to improve energy transfer between polymer backbones to Ir complex is to enhance the triplet energy level of the polymers, which can be realized by copolymerizing it with carbazole moieties or other partially conjugated building blocks.

The current designed copolymers could also achieve white light emission when appropriate ratio between the polymer backbone and the Ir complex pendants is achieved.[19,20] Here the singlet excitons from polymer backone will emit blue light, while the triplet excitons trapped by Ir complex pendants will emit orange light. Such a design can result in white OLEDs in a simple device structure.

References

1. Y. Fu, Z. Bo, *Macromol. Rapid Commun*. **2005**, *26*, 1704.
2. X. Pan, S. Liu, H. S. O. Chan, S.-C. Ng, *Macromolecules* **2005**, *38*, 7629.
3. H.-J. Su, F.-I. Wu, Y.-H. Tseng, C.-F. Shu, *Adv. Funct. Mater*. **2005**, *15*, 1209.
4. X. H. Yang, F. Jaiser, B. Stiller, D. Neher, F. Galbrecht, U. Scherf. *Adv. Func. Mater*. **2006**, *16*, 2156.
5. F.–C. Chen, Y. Yang, M. E. Thompson, J. Kido, *Appl. Phys. Lett.* **2002**, *80*, 2308.
6. X. Gong, M. R. Robinson, J. C. Ostrowski, D. Moses, G. C. Bazan, A. J. Heeger, *Adv. Mater*. **2002**, *14*, 581.
7. A. Beeby, S. Bettington, I. D. W. Samuel, Z. Wang, *J. Mater. Chem*. **2003**, *13*, 80.
8. J.-P. Duan, P.-P.Sun, C.-H. Cheng, *Adv. Mater*. **2003**, *15*, 224.
9. S.-C. Loh, N. A. H. A. Male, J. P. J. Marham, S. W. Magennis, P. L. Burn, O. V. Salata, I. D. W. Samuel, *Adv. Mater*. **2002**, *14*, 975.
10. B. W. D'Andrade, R. J. Holmes, S. R. Forrest, *Adv. Mater*. **2004**, *16*, 624.
11. S. Tokito, T. Iijima, Y. Suzuri, H. Kita, T. Tsuzuki, F. Sato, *Appl. Phys. Lett*. **2003**, *83*, 569.
12. J. Li, T. Sano, Y. Hirayama, T. Tomita, H. Fujii, K. Wakisaka, *Jpn J. Appl. Phys*. **2006**, *45*, 5232.
13. K. Ono, M. Joho, K. Saito, M. Tomura, Y. Matsushita, S. Naka, H. Okada, H. Onnagawa, *Eur. J. Inor. Chem*. **2006**, 4676.
14. A. B. Tamayo. B. D. Alleyne, P. I. Djurovich, S. Lamansky, I. Tsyba, N. N. Ho, R. Bau, M. E. Thompson, *J. Am. Chem. Soc*. **2003**, *125*, 7377.
15. P. Pudzich, J. Salbeck, *Synth. Met.* **2003**, *138*, 21.

16. Z. H. Li, M. S. Wong, *Org. Lett*. **2006**, *8*, 1499.

17. J. K. Lee, G. Klaerner, R. D. Miller, *Chem. Mater*. **1997**, *9*, 1083.

18. M. Ranger, D. Rondeau, M. Leclerc, *Macromolecules* **1997**, *30*, 7686.

19. Y. Xu, X. Zhang, J. Peng, Q. Niu1 Y. Cao, *Semicond. Sci. Technol*. **2006**, *21*, 1373.

20. V. Adamovich, J. Brooks, A. Tamayo, A. M. Alexander, P. I. Djurovich, B. W. D'Andrade, C. Adachi, S. R. Forrest, M. E. Thompson, *New J. Chem*. **2002**, *26*, 1171.

1. Introduction

1.1 Block copolymers

Different from homopolymer that only one monomer is included, copolymer is formed by two or more different types of monomers linked together by covalent bonds. The properties of copolymers can be modified and improved by selecting different monomer compositions and designing their arrangement. Thus, copolymerization offers a more flexible method to design and synthesize novel materials with desired performances.

Since a copolymer consists of at least two types of repeating units, copolymers can be classified to five types based on how these units are arranged (architectures) along the chain: block copolymer (BCP), random copolymer, alternative copolymer, graft copolymer, and star copolymer (shown in Figure 1.1). Undoubtedly, the chain architecture of copolymers will affect the chemical and physical properties of copolymers greatly.[1]

The arrangement of alternative, random and block copolymers is linear. Alternative copolymers are more like homopolymers due to their monomers can be regarded as the combination of two kinds of units. Block copolymers consist of blocks of different polymerized monomers. The individual segment species of block copolymers exercise independent roles in the overall properties of the materials and the copolymer will show combined performances of all the blocks. The possibility of tuning their properties by varying either the kind of monomer or proportion of the constituting blocks and the architecture of polymer chains renders their wide range of applications in industry, such as thermoplastic elastomers and spandex elastic fibers due to their elastomeric

properties.[2] Currently, block copolymers have been widely used as stabilizer, surfactants, blending agents, antistatic agents and impact-resistance modifiers.[3-7]

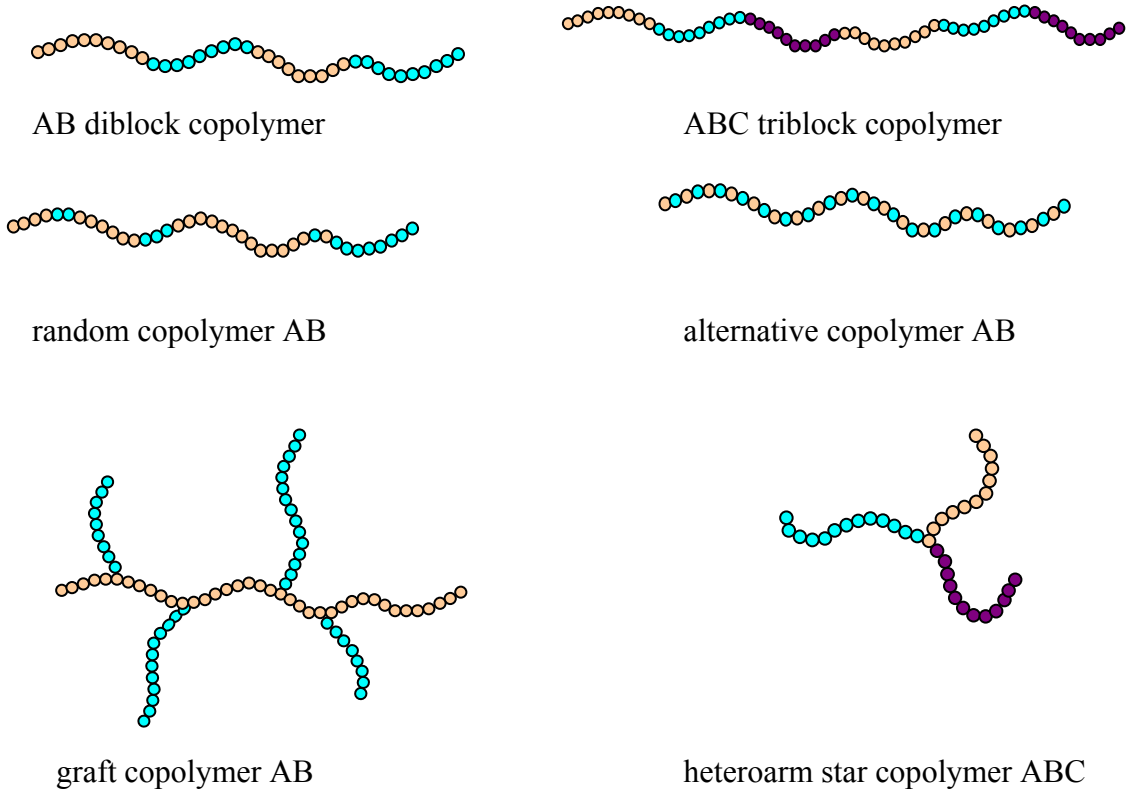

Figure 1.1. Architecture of copolymer chains.

The ability to form a rich variety of nanoscaled structures spontaneously, such as lamellar, hexagonal-packed cylinder etc., amphiphilic block copolymers (ABCs) extends their applications to nanotechnology and attracted numerous attention. The unique self-associated properties of ABCs results from the block incompatibility and microscopic phase separation in selective solution.[8-12] The ability to synthesize amphiphilic block copolymers with desired architecture facilitates the ability to manipulate their aggregation behavior, thus provides them wider and more flexible applications in nanotechnology. So far, a variety of self-assembling amphiphilic block copolymers have been synthesized,

investigated, and applied in nanotechnology. Polystyrene(PS)-*b*-poly(4-vinylpyridine)(4-PVP),[13,14] PS-*b*-poly(methyl methacrylate)(PMMA),[15] poly(vinyl alcohol)(PVA)-*b*-PS,[16,17] poly(n-hexylisocyanate)(PHIC)-*b*-poly(2-vinylpyridine),[18] (P2VP)-*b*-poly(n-hexyl isocyanate)[19]were good representatives of amphiphilic block copolymers. Poly(ethylene oxide) (PEO) based amphiphilic block copolymers, such as PEO-*b*-PS diblock and triblock copolymers,[20,21] and poly(propylene oxide) (PPO)–*b*-PEO,[22-26] have been systematic investigated as typical model copolymers for the study of self-assembly systems due to the excellent water solubility and biocompatibility of PEO blocks.

The arrangement of graft and star-shaped copolymers is radial. Both of them can also self-assemble into nanostructures since they are composed of different polymerized blocks. In comparison with block copolymers, graft and star-shaped copolymers are less popular due to their more complicated structures and synthetic procedures. However, in some cases, graft copolymers can be obtained through simple synthesis and achieve different morphologies. Some graft copolymers with simple structures have been studied, such as, PS-*g*-PEO,[27] which can form reverse micelles in toluene. Poly(acrylic acid)-*g*-polystyrene graft copolymer (PAA-*g*-PS)[28] has been used as nanoreactors for synthesis of gold clusters.

Amphiphilic oligomers which have lower molecular weight than polymers, have also been synthesized and their nanostructural morphologies at different conditions have been investigated.[29.30]

1.1.1 Preparation techniques for micelles

Morphology of polymeric micelle will be affected by preparation methods. Polymeric micellar samples are generally prepared by two procedures.[8,9,17,31] The first technique is to dissolve the block copolymer in the selective solvent directly and then to anneal it by stirring or speed up the process by heating the sample, then cool down to room temperature. The prerequisite for this approach is that the copolymer has some solubility in the selective solvent. The second technique is to dissolve the block copolymer in a good/common solvent in which all blocks are soluble. Then conditions such as temperature or composition of the solvent are altered gradually until the solvent completely change from good solvent to selective solvent. Dialysis technique is recommended for changing the composition of the solvent continuously from the common solvent to the selective solvent. An alternative method is to add the selective solvent into the good solvent gradually and eliminate the good solvent by evaporation. It is worth to mention that once a successful micelle preparation protocol has been developed, the procedure is usually found to be reliable and reproducible.

1.1.2 Critical aggregation concentration (CAC)

Micelles only exist when the solution concentration reaches a threshold-critical micelle concentration (CMC), which is also called critical association/aggregation concentration (CAC) for polymeric micelles. Micelles from block copolymer are aggregates that resemble many properties of micelles formed from low-molecular-weight surfactants.[10] Thus some of the available characterization methods for surfactants are applicable to block copolymer micellar systems. CAC can be regarded as a turning point

and micellization will affect solution properties. The onset of the micellization often induces a dramatic change of a number of properties such as surface tension, viscosity of solution or light scattering intensity. According to the methods used for surfactants, a variety of methods are offered to determine the CAC of a colloid solution, e.g. surface tension, electrical conductivity, light scattering, refractive index, dye solubilization, diffusion coefficient, and viscosity, etc.[32]

Surface tension method is based on the fact that surface tension of aqueous solutions of the surface-active agents decreases very rapidly until the CAC is reached and then stays constant above the CAC. Thus CAC value can be located as the point at which the surface tension becomes essentially independent of concentration.[33,34] It is necessary to mention that surface tension method is very sensitive to dust impurities, since it only measures the change of surface tension and cannot detect the presence of micelles. Therefore, it is recommended that other techniques should be applied to confirm the CAC values.

Dye solublization or fluorescent probe techniques are widely used for measuring CAC.[35-37] This method is not sensitive to dust in the solution and therefore it is widely used for CAC measurement. Hydrophobic pyrene is usually used as probe to measure CACs because its PL spectrum is very sensitive to the environment. When micelles present in solution, pyrene will enter the core of micelles, its PL spectrum will show intensity change.

Static light scattering (SLS) can also be applied to measure CAC.[38-42] The abrupt increases of intensity denotes the threshold concentrations for micellization. Due to the presence of particles will affect the light scattering intensity, careful elimination of dust

particles and bubbles from solution is necessary since the presence of only small amount of them will result in significant errors.

1.1.3 Morphology of amphiphilic block/graft copolymers in selective solvents

Amphiphilic block/graft copolymers comprise of chemically distinct building blocks that are covalently jointed. The inherent immiscibility between different blocks and the competing thermodynamic effects give rise to various nanostructures ranging from spheres to cylinders to lamellae, in selective solvents (good solvent for one block and poor for the other). Diblock copolymers are the most common and simplest block copolymers and thus have been intensively investigated. Figure 1.2 shows an overview of nanostructures formed from diblock copolymers.[31,43,44] With the increasing efforts put in the investigation ABCs, more variety of nanostructural morphologies have been obtained from block copolymers. Nanoring[45] and nanowire[46] structures formed from dumbbell-shaped amphiphilic molecules and V-shaped PS_{40}-PEO_{50} amphiphiles have been reported recently.

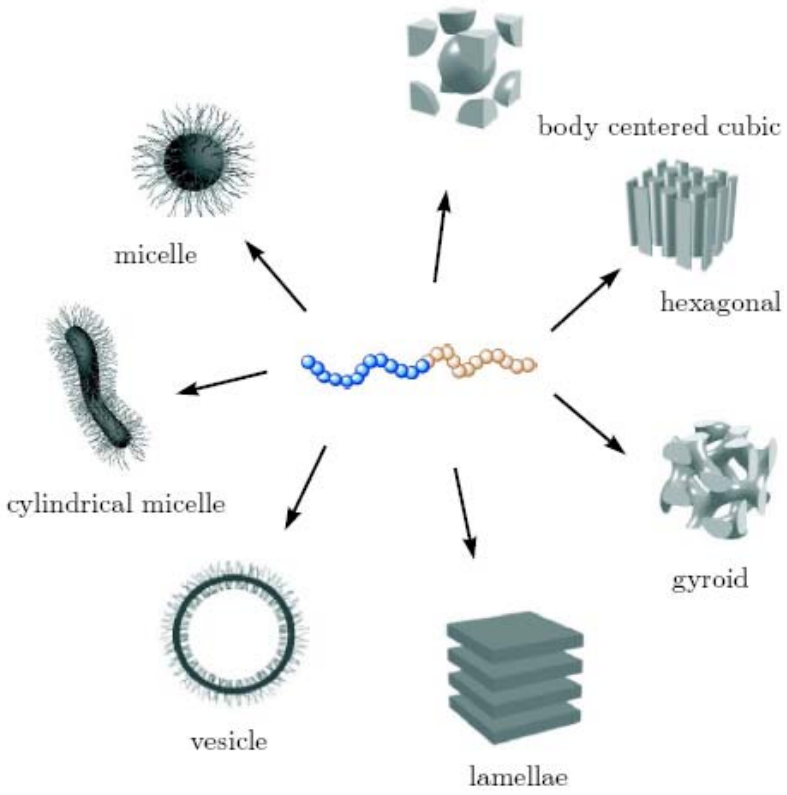

Figure 1.2. Schematic representations of the most common self-organized structures of diblock copolymers in solution**.**

The morphology of block copolymers in solution and solid state largely depends on volume fraction of monomers, chemical composition, segmental interaction between building blocks and molecular weight of copolymers as well as the architectures.[11,47] Besides the block copolymers themselves, solvent is another factor that affects the morphology of block copolymers in solution. Any macromolecule assumes a conformation in solution that is directed by the balance between the strengths of interaction of the polymer segments and macromolecules with the solvent molecules. For block copolymers, it is a kind of balance among lyophilic and lyophobic blocks with the solvents. This balance is generically called solvent quality. Thus selection of solvent system is a key factor to tune the morphology of block copolymers in solutions.

Cosolvent system was often adopted to tune the morphologies and properties of nanostructures of block copolymers.[48]

Because self-assembly is a kind of response to the stimuli, the morphology (shape and size) of nanoparticles also relies on the solution conditions such as concentration, temperature, pH value,[49] ionic strength, presence of impurities, etc.[50,51] Some groups have reported the environmental responsive micelles[52] and photoresponsive micelles from amphiphilic copolymer with Azo side chains.[53]

Among all the morphologies of block copolymers, micelle is the most popular one. The micellar structure can be spherical, elliptical, cylindrical and worm-like micelles. In selective solvents, micelles form core-shell or core-corona structure. The cores of micelles consist of the insoluble blocks, while the shells are composed of swollen soluble blocks. In comparison with the compact core, the shell is diffuse to protect the hydrophobic core and prevent them to contact with solvent, therefore reduce the energy of system. That means that the hydrophobic core is stabilized by the hydrophilic shell. With closer observation, the core-shell micellar structure can be divided into two classical types, core/shell model and star model. Their basic difference lies in the density profile $\varphi(r)$ of the corona, which is a constant for the core/shell model and scales as $\varphi \sim r$ in the star model.[14,54] Generally, the micelle structure is looser at low concentration compared with the structure at high concentration.

Micelles spontaneously form when the concentration of the block copolymer is higher than the CAC.[55] CAC is an important parameter for block copolymers and it denotes the lowest concentration that nanostructures start to be formed. Below CAC, only independent polymer chains (unimers) are presented. Above CAC, multimolecular

micelles are in equilibrium with single molecular unimers. However, if the solution concentration is much higher than CAC, micelles will aggregate. Figure 1.3 shows the micellization process and it illustrates that micelles only exist within a certain concentration range. Besides concentration, temperature is another critical parameter for the formation of micelles. At a fixed concentration, when temperature is at or beyond the critical micelle temperature (CMT), micelles can also form. Both of CAC and CMT are the basic critical parameters for block copolymer solutions. CAC is more commonly used than CMT because most of the microstructures are widely used at room temperature or within small temperature range[8,56]

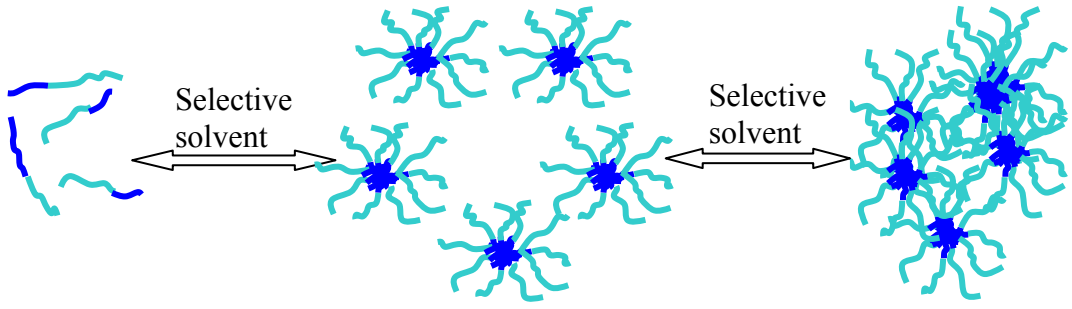

Figure 1.3. Schematic representation of micellization process.

The key morphological parameters of micelle include hydrodynamic radius R_h and gyration radius R_g, aggregation number (N),[57] aggregation/apparent molecular weight ($M_{w,\,agg}$).[37] It is known that R_g is responsive to the mass distribution of the micelle. R_h is responsive to the hydrodynamics of the micelle, which includes the contribution from the

solvent molecules upon hydration. The ratio of R_g/R_h is defined as ρ, which is related to the spatial density distribution and the degree of draining of a particle in solution.[58] ρ indicates the morphology of microstructure of micelles and determines the deviation of particle shape from the sphere, whether they are spherical, elliptical or worm-like. For ideal sphere, ρ is 0.75. With the increase of this value, large anisomeric objects are observed. If ρ is between 1.5 and 2.1, it indicates a worm-like structure of the micelles.[59,60] The association number, or aggregation number, is the number of molecules included in one single micelle. Aggregation molecular weight is the molecular weight of one micelle. From the above parameters, a clear morphology about micelles is obtained.

It is worthy to note that the micelle size is not unique, it is a distribution. The particle size distribution of the micelle is crucially affected by the polydispersity of the constituent block copolymers, indicating the importance of establishing a reliable synthetic route for block copolymers to obtain micelles with a narrow polydispersity.[61]

Micelle stability needs to be considered because the association progress relies on the interaction of hydrophilic polymers with solvents. They undergo thermal fluctuations and Brownian motion. As a result, micelles are dynamic and equilibrium structures, so they are able to rearrange in response to change of environmental conditions. Thus, the micellization is a reversible process. If the concentration is decreased to below CAC, micelles can disassociate back to unimers. Luckily, compared with traditional surfactant, micelles have relatively high stability due to the fact that the micelles are thermodynamically equilibrated aggregates.

1.2 Characterization methods

1.2.1 Chemical structure characterization

For the synthetic block copolymers, their structure, molecular weight and molecular weight distribution must be confirmed with some of the routine characterization methods for polymers, i.e., NMR and GPC.

1.2.1.1 Nuclear magnetic resonance (NMR)

Nuclear magnetic resonance (NMR) is a widely used characterization method to confirm the chemical structures, for both small molecules and polymers. It can be used to obtain physical, chemical, electronic and structural information about a molecule. NMR is a physical phenomenon based upon the magnetic property of an atom's nucleus, different nuclear environment will give different chemical shift, and structures can be confirmed from the NMR spectrum. Proton NMR and carbon 13 NMR are the most commonly used for hydrocarbons, while phosphor, silicon, nitrogen, oxygen NMR will be needed for some chemicals that contain such atoms. In most of cases, one dimension NMR is enough to tell the chemical structure. However, sometimes 1D NMR spectra are far too complex for interpretation as most of the signals overlap heavily. By introduction of additional spectral dimensions, these spectra are simplified and some extra information is obtained. For 1H spectra of organic compounds (except polymers), the quantity of material required is about several milligrams. The sample is dissolved in deuterated solvents and refilled to an NMR tube to 4.5 cm and 5.5 cm of height. The commonly used solvents for NMR are *d*-chloroform, *d*-acetone and *d*-tetrahydrofuran (THF).

^{1}H NMR can also be used for micelle characterization. NMR can provide further evidence for the formation of micelles. Due to the high mobility of corona of micelles, the peaks from corona can be seen in micellar NMR spectra. However, the signals from core can only be seen in unimers and will be absent in the micelles.[62,63] Thus, NMR also can be used to monitor the appearance of micelles.[64,65]

1.2.1.2 Gel permeation chromatography (GPC)

Gel permeation chromatography (GPC), also called size exclusion chromatography (SEC) and gel filtration offers rapid and useful method to determine molecular weights and molecular weight distributions (MWD) of polymer. GPC approach utilizes columns containing finely divided microporous particles and solvent (mobile phase, eluent) is forced through the column at fixed flow rate. Polymer molecules that are smaller than the pore sizes in the particles can enter the pores, and therefore have a longer path and longer transit time than larger molecules that cannot enter the pores. Motion in and out of the pores is statistical, being governed by Brownian motion. Thus, the larger molecules elute earlier in the chromatogram, while the smaller molecules elute later. This is largely an entropically governed phenomenon. Since GPC is a relative method, it needs to be calibrated with polymer standard with known molecular weight and narrow molecular weight distribution, such as PS standard or PEG standard. The schematic spectrum of GPC is shown in Figure 1.4.

The molecular weight of a polymer is not an exact number, but a dispersion. There are two kinds of molecular weights: number average molecular weight (M_n) and weight average molecular weight (M_w). The ratio M_w/M_n is defined as weight distributions of

polydispersity index (PDI). Lower PDI means narrower molecular weight distribution. The ideal PDI value is 1; however, PDI values will increase with increasing molecular weight.

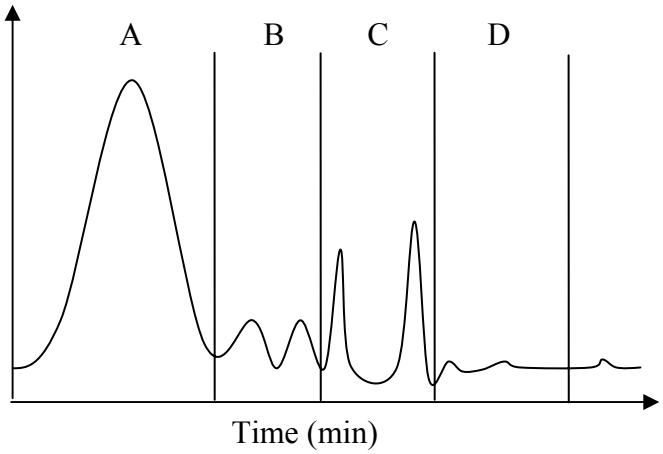

Figure 1.4. Schematic diagram of GPC.

1.2.2 Optical property

1.2.2.1 UV-vis absorption spectroscopy

Because most molecules absorb ultraviolet (UV) or visible (vis) light, UV-vis spectroscopy becomes a common characterization method for measuring the wavelength and intensity of absorption of ultraviolet and visible light by a sample. UV-vis are energetic enough to promote outer electrons to higher energy levels of the molecular orbital. UV-vis absorption spectroscopy is usually applied to molecules and inorganic ions or complexes in solution or thin film on quartz. The UV-vis spectrum has broad features that are of limited use for sample identification but are very useful for quantitative measurements. Different molecules absorb radiation of different wavelengths. An absorption spectrum will show a number of absorption bands corresponding to structural groups within the molecule. For conjugated molecules, the absorption spectrum

will show change of effective conjugation length because longer conjugation will shift the absorption peak to longer wavelength.

1.2.2.2 Photoluminescence (PL)

Photoluminescence is a process in which a chemical compound absorbs photons (electromagnetic radiation), electrons within the compound are transited to a higher electronic energy state (excited state), and then radiate photon back to a lower energy state (ground state). The energy of the emitted light (photoluminescence) relates to the difference in energy levels between the two electron states: the excited state and the ground state, involved in the transition process. PL is widely used to measure the emission wavelength and PL efficiency of semiconducting materials. PL is a powerful and nondestructive optical method used for probing the electronic structure of materials.

The conformation of the conjugated polymers strongly affects their effective conjugation length. Therefore, their optical properties are also influenced by the conformation of the molecules. The molecular packing in micelles is different from the packing in good solvents. It was expected that their packing resembles the packing in solid state. Thus PL spectra of micelle solution offer information about intermolecular interaction and packing.

Fluorescence lifetime measurement can also offer further information about the intermolecular packing because the close packing among molecules causes excimer formation, which can be confirmed by the appearance of long fluorescence lifetime.

1.2.3 Light scattering

Light scattering is a well-known, efficient and non-invasive method for characterizing polymers and a wide range of particles in solution. When a beam of coherent light (such as laser) passes through a colloidal dispersion, the particles or droplets scatter some of the light in all directions. The technique of light scattering involves the measurement of the intensity of the light scattered from the solution. For particle characterization, light scattering can be applied to measure CAC, hydrodynamic radius (R_h), radius of gyration (R_g), aggregation number (N_{agg}), apparent molecular weight ($M_{w,agg}$), and second virial coefficient (A_2) of polymer solutions. It is a convenient technique to study the shape of micelles and the polymer-solvent interaction in polymer solutions.[66-68]

There are two types of light scattering technologies, dynamic light scattering (DLS) and static light scattering (SLS) depends on the light intensity collection modes. These two techniques often have complementary roles and they can be carried out simultaneously using the same instrument.

1.2.3.1 Static light scattering (SLS)

Static light scattering (SLS), also known as "classical" or "Rayleigh" light scattering, was derived by Lord Rayleigh. Light is elastically scattered at the same wavelength as the incoming light and the scattered light is measured as a function of angle and solute concentration.[69,70] SLS is a multi-angle light scattering. The intensity is averaged over a sufficient long time interval (more than 0.1s). This time scale is longer than that of molecular motion, so it can be seen that the system is in thermodynamic equilibrium and accordingly, it is called static light scattering. The intensity of scattered light is directly

proportional to the weight-average molar mass and the concentration of samples, thus SLS allows the determination of average molecular weight, radius of gyration (R_g), second virial coefficient (A_2) and shape information for the particles.

The molecular weight is determined by measuring the samples at different concentrations and applying the Rayleigh equation:

$$\frac{KC}{R_\theta} = (\frac{1}{M_w} + 2A_2C)P(\theta)$$

$R(\theta)$: Rayleigh ratio, the ratio of scattered light to incident light of sample at given angle

M_w: Weight-average molecular weight

A_2: Second virial coefficient

C: Sample concentration

$P(\theta)$: Angular dependence of scattered light

K: Optical parameter

The typical way for data analysis is Zimm plot, which describes the angular (θ) and the concentration (c) dependence of $Kc/\Delta R_\theta$. By extrapolating the total excess scattered intensity to zero scattering angle and zero sample concentration, the molecular weight together with the radius of gyration (R_g) and the second virial coefficient (A_2) were determined from the intercept and the slopes of the graph.

1.2.3.2 Dynamic light scattering (DLS)

Dynamic light scattering (DLS), which is also known as "photon correlation spectroscopy" (PCS) or "quasi-elastic light scattering" (QELS), uses the scattered light to

measure the rate of diffusion of the nanoparticles.[62,71,72] Contrary to SLS, the scattered intensity in DLS is not averaged over a period but correlated. It is a technique measures the time-dependent or real-time fluctuations in the intensity of scattered light which occurs because the particles are undergoing random, Brownian motion. An important feature of Brownian motion for DLS is that small particles move quickly and large one move more slowly. DLS is an experimental method which uses the intensity and polarization of light scattered from a solution to characterize the size, shape, and interactions of the particles in a solution. The motion data of the particles are conventionally processed to derive a size distribution for the sample, where the size is given by the "Stokes radius" or "hydrodynamic radius" of the particle, R_h. This hydrodynamic size depends on both mass and shape (conformation). Analysis of the time dependence of the intensity fluctuation can therefore yield the diffusion coefficient of the particles from which, via the Stokes-Einstein equation,[8] knowing the viscosity of the medium, the hydrodynamic radius or diameter of the particles can be calculated. Traditionally, DLS experiments are performed at an angle of 90 degrees.

1.2.4 Microscopy

Microscope extends our vision to micro-world and nano-world, which visualizes the nanostructure vividly. Scanning electron microscopy (SEM) has a large depth of field, which allows large area of the sample to be in focus at one time. It also produces surface images with high resolution, which means that closely spaced features can be examined at a high magnification.[4,73-75] Transmission electron microscope (TEM) can be used to look at a wide variety of materials at very high magnifications and is ideal for imaging,

displaying the nanostructure size and shape clearly. Especially for the core-shell micelles, the core and shell can be differentiated. Atomic force microscope (AFM) is one of the most extensively used imaging techniques for characterization of surfaces on the molecular and atomic scale, which offers visualization in three dimensions, including direct measurements of height, volume, phase and 3D display. The effective combination of the above three methods will offer a completed description of micelle morphology in solid state.

1.2.4.1 Atomic force microscopy (AFM)

AFM is a very high-resolution type of scanning probe microscope. It was invented by Binnig, Quate and Gerber in 1986, and is one of the foremost tools for imaging, measuring and manipulating matter at the nanoscale. AFM measures topography with a force probe. It is a very versatile and non-destructive tool used to probe the local physical and chemical properties of surfaces.[76]

AFM operates by measuring attractive or repulsive forces between a tip (mounted on a cantilever) and the sample. In this technique, a very tiny tip (5 – 50 nm), attached to the underside of a cantilever, is scanned over a surface. The movement of the sample is performed by means of a precise piezo-electric crystal, which is capable of sub-angstrom resolution in three dimensions. AFM tips are micromachined probes and a consistent tip will give good resolution and reproducibility. So far, many AFM modes have appeared for special purpose while the technique of AFM is becoming mature. According to the interaction between tip and sample surface, AFM operation modes can be classified into three principle modes: contact mode, non-contact mode, and tapping mode. In the contact

mode, the tip scans the sample in close contact with the surface. The force on the tip is repulsive with a mean value of 10^{-9} N. Contact mode is suitable for hard samples that won't be damaged by the force. In the non-contact mode, the tip hovers 50 - 150 Angstrom above the sample surface. Attractive Van der Waals forces acting between the tip and the sample are detected, and topographic images are constructed by scanning the tip above the surface. This mode is used under the condition that the tip contact might alter the sample in subtle ways. Tapping mode is a key advance in AFM. This potent technique allows high resolution topographic imaging of sample surfaces that are easily damaged, loosely hold to their substrate, or difficult to image by other AFM techniques. The measurement can be conducted in air and in fluid.[31,77] Tapping mode is the best choice for fragile, soft matter surfaces such as polymers and biological tissues.

1.2.4.2 Transmission electron microscopy (TEM)

Transmission electron microscopy (TEM) is an imaging technique whereby a beam of electrons is focused onto a specimen causing an enlarged version to appear on a fluorescent screen or layer of photographic film, or to be detected by a charge-coupled diode (CCD) camera. The first practical transmission electron microscope was built by Albert Prebus and James Hillier at the University of Toronto in 1938 using concepts developed earlier by Max Knoll and Ernst Ruska.

So far, TEM has been used heavily in both material science and the biological science. In both cases the specimens must be very thin and able to withstand the high vacuum present inside the instrument.

An additional class of these instruments is the electron cryomicroscope (Cryo-TEM), it includes a specimen stage capable of maintaining the specimen at liquid nitrogen or liquid helium temperatures. This allows imaging specimens prepared in vitreous ice, the preferred preparation technique for imaging individual molecules or macromolecular assemblies.

Since the polymeric TEM samples are not conductive, they need be stained by some reagent and put on conductive carbon-coated copper grid and the thickness of sample layer should be smaller than 100 nm.

1.3 Application of block copolymer micellar systems

Polymeric micelles formed from amphiphilic block copolymers have found a rich variety of applications in nanotechnology as solubilizers, surface modifiers, nanoreactors[28] as well as gene and drug delivery vehicles.

A distinguishing feature of micellar systems is their ability to enhance the solubility of compounds that otherwise show very low solubility in some solvents. This occurs because the core of the micelle, which is incompatible with the solvent, provides a suitable microenvironment for the solubilizate, which is also incompatible with the solvent. Consequently, the extent of dissolution of the solubilizate in micellar solutions is dramatically enhanced when compared to that in the pure solvents. This phenomenon, known as solubilization or microemulsification, is one of large number of the basic practical applications of surfactants.[78]

The surface properties of block copolymers make them practical interest as dispersants, emulsifier, wetting agents, foam stabilizers, flocculants, demulsifiers, etc., in

many industrial and pharmaceutical preparations. It is known that many nano structural materials, such as carbon nanotubes, metal oxide nanorods, quantum dots (QDs), all present poor solubility and processibility. Consequently, their applications are severely restricted. After surface modification of the nano-scale materials, they can be better dispersed and thus more applications can be explored because of the improved solubility. The micelles formed from block copolymers also have been employed as templates for the fabrication of inorganic nanparticles including ZnS[79], Ag[80] and Au[81], etc.

Amphiphilic block copolymer micellar systems also have application in controlled delivery of drugs, diagonistic agents and gene transfections.[82-85] Suitable and controllable size, good stability and low toxicity make block copolymer micelle applicable for drug delivery. The polymeric micelle drug delivery systems largely account for their flexibility and physicochemical properties. The drugs, which are usually hydrophobic in nature, can be trapped in the hydrophobic cores of the micelles and make use of the excellent aqueous solubility of hydrophilic shells to delivery the drugs to targets. The molecular architecture of block copolymers greatly influences self-assembling properties and is a key factor in determining the stability and drug loading capacities. In order to load drugs, there are three different methods can be considered: first, the micelle can form conjugates between drugs and block copolymers, which means that the drugs are covalently linked to the copolymers. If the drugs are loaded through covalent bonding, functionalization of the micellar cores is necessary for drug loading. Second, the drugs can also be non-covalently incorporated into the micelles with formation of microcontainers. The last one is to form complexes between drugs and block copolymers by electrostatic interactions.

For drug delivery, lower CAC is favorable for drug retention in the micelle in vivo under considerable dilution.[61]

1.4 Luminescent materials and their applications in biolabelling

Fluorescence is a luminescence that occurs where the energy is supplied by electromagnetic radiation, usually ultraviolet or visible light. The energy source stimulates an electron of an atom from a lower energy state (ground state) into a higher energy state (excited state), and then the electron releases the energy (decay) in the form of light (luminescence) when it falls back to ground state. Briefly, it contains three continuous stages, absorption, excitation and emission. Fluorescence is the property of some atoms and molecules to absorb light at a particular wavelength and to subsequently emit light of longer wavelength after a brief interval, termed the fluorescence lifetime. The wavelengths of absorption and emission are determined by chemical structure and internal energy level.

Optical imaging is unequivocally the most versatile and widely used visualization modality in clinical practice and research. It is of great benefit in many types of biological research and industry to mark microscopic structures (cells, bacteria, drug molecules etc) with fluorescent materials in order to track their movements and activities within an organism or other medium, and portray the image of cells, drug encapsulants, etc.) (Figure 1.5). The advantages of fluorescence probes are their high sensitivity, fast response and easy operation. Fluorescence microscopy and imaging have received particular attention due to the increasing availability of organic dyes, fluorescent proteins and probes that visualize the study of gene expression, protein function, protein-protein

interactions, and a large number of cellular processes. There are two main categories of fluorescent materials used for bioimaging: organic and inorganic fluorescent probes.

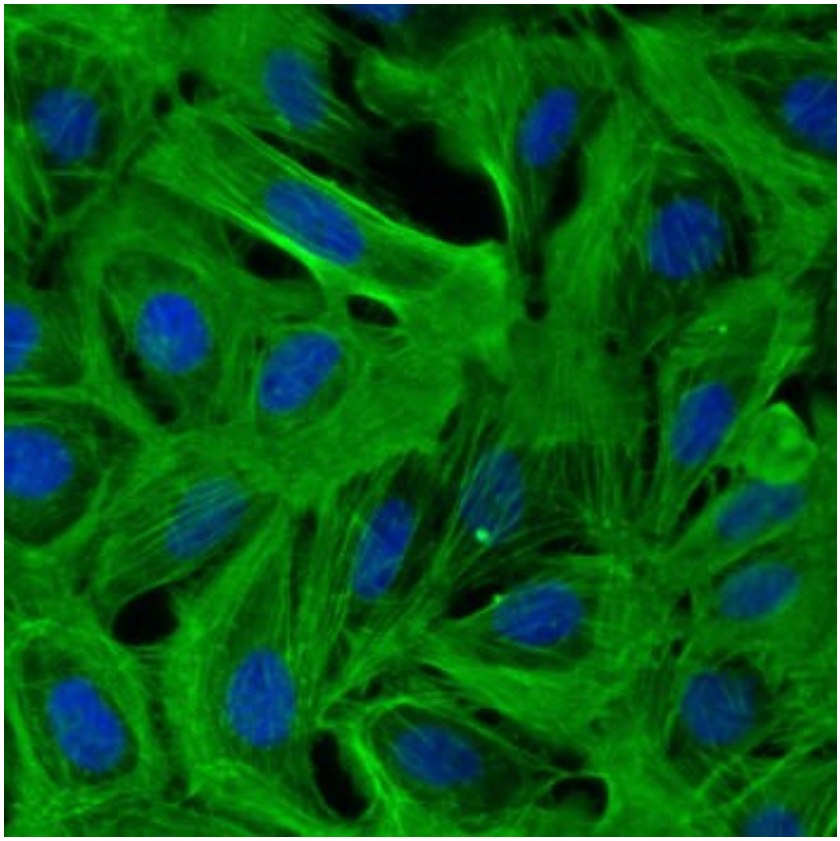

Figure 1.5. Fluorescent image of tissues.

1.4.1 Organic fluorescent probes

1.4.1.1 Organic dyes

Traditionally the favored materials for fluorescent probes are organic dyes, which can be chemically engineered to adhere to a diverse variety of cellular structures. After the dyes come into contact with the proper cellular structure, light with a certain wavelength can be used to excite the dye into fluorescence, whereby it emits radiation at a peak wavelength.

Rhodamine derivatives and fluorescein are the first generation of fluorophores used as fluorescence probes in life science research (Figure 1.6).[86-89] However, their disadvantages restricted their application. When organic dye molecules are conjugated to biocompatible molecules, modification of the organic dye structure to introduce a suitable coupling group is essential and the synthetic procedure could be very complicated and extremely tedious.[90] Another limitation of organic dye fluorescence probes is that they are susceptible to surrounding environment, e.g., pH value, ionic species and strength, which may affect the fluorescence response sensitivity and selectivity. For instance, diaminofluoresceins could be used as fluorescence indicators imaging nitric oxide products in vivo. The suitable pH value for fluorescence imaging is > pH7. In an acidic environment, the fluorescence intensity of these compounds will dramatically decrease or fluorescence even completely loses.[91]

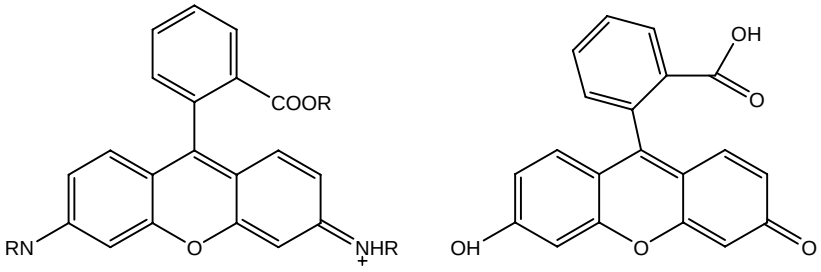

Figure 1.6. Chemical structures of rhodamine and fluorescein.

1.4.1.2 Fluorescent proteins

Fluorescent proteins are recently developed fluorophores for bio-application. A number of mutants of fluorescent proteins with different emission wavelength have been developed.

Green fluorescent proteins (GFP) and their variants are widely applied for visualization of recombinant protein expression and/or localization in single living cells.[92] A number of GFP mutants with different emission wavelength have been developed which could be useful for simultaneous comparisons of multiple protein fates, developmental lineages and gene expression levels.[93,94]

The most advantage of fluorescent proteins is their biocompatibility, which allows them to monitor gene expression and protein localization in vivo, in situ, and in real time. However, their disadvantages are vital. The disadvantages of fluorescent proteins are (1) the luminescence is not very efficient, especially for blue and red; (2) synthetic procedure is very complicated and also difficult for scale up, thus limit their commercial applications; (3) fluorophores are susceptible to surrounding environment, most of the fluorescent proteins are not pH resistance and couldn't be used for probing acidic cellular environments, which restricted their application.

1.4.2 Inorganic fluorescent materials

1.4.2.1 Quantum dots (QDs)

In the bioimage and fluorescent label field, semiconductor QDs are the most investigated potential fluorescent markers for bio-applications, which are stable and could be used for multicolor emission. QDs are nanocrystals composed of atoms from groups II-VI or III-V of the periodic table. For example, CdS, CdSe, CdTe, and CdSe/ZnS, etc are inorganic semiconductor nanocrystals (2 - 100 nm) with unique optical and electrical properties.[95,96] They demonstrate narrow, size tunability, symmetric emission spectra and are photochemically stability. These features, in addition to their

binding compatibility with DNA and proteins, render QDs prime candidates to replace fluorophores as biological labeling agents.

QDs consist of a core, a shell and a coating. The core contains the key material (i.e. CdSe, CdTe), defining the optical properties of the particle. A shell (ZnSe, ZnS) is used for passivation and as energy barriers to optimize radiative relaxation. The coating allows to functionalize the particles and to make them compatible with the application.

Because the QDs emission frequency is dependent on the size of the QDs (Figure 1.7); the direct limitation is that the emission frequency and size can not be tune separately. In addition, blue light-emitting QDs are not stable result from their ultra small particle sizes.

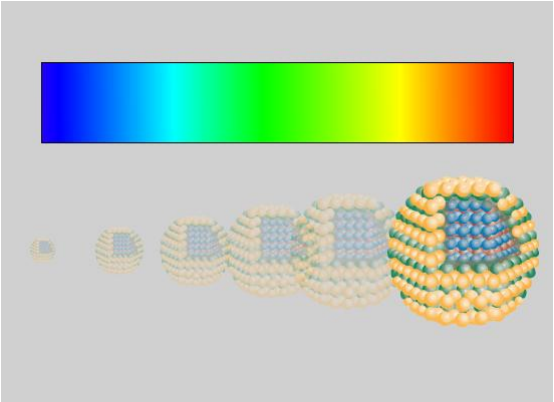

Figure 1.7. Size dependent color of QDs.

The most attractive advantage of QDs over other fluorescent probes is its absorption spectrum is very wide but emission spectrum is very sharp. This feature makes it possible to achieve multicolour emission under one light source.[97-99] However, their synthesis is normally carried out in organic solvents at high temperatures (>300 °C) in the presence of surfactants, followed by replacing or covering the inorganic hydrophobic nanoparticles with hydrophilic layers to render their biocompatibility. The last big problem for QDs is their uncertain toxicity. Assessing QDs exposure routes and potential

toxicity is not a simple matter due to each individual type of QD possessing its own physicochemical properties.[100] So far, the toxicity of QDs is uncertain.

1.4.2.2 Silica nanoparticles (SNs)

Dye-doped silica nanoparticles are another category of candidate for biolabelling. Usually, the SNs need to be porous, which facilitates the later surface modification. Surface coating of nanostructural Si materials is indispensable, aiming to increase the PL stability and their dispersibility in solvents. Alkyl chains, macromolecules and polymers all have been used to modify the porous silica particle surface.[101,102]

SNs are synthesized by reverse microemulsion, comprise numerous organic dye molecules in a silica matrix.[103,104] Unique core-shell-structured silica nanoparticles have been reported, in which the fluorophore molecules in the core are protected and separated from the conjugated biomolecules. These nanoparticles are stable in both aqueous electrolytes and organic solvents, hence they do not aggregate.

The SNs have tunable fluorescence, high PL efficiency, excellent photostability and sensitivity. However, they still showed some limitations associated with the encapsulated fluorophores.

1.5 Objectives and significance

Tracing drug delivery or label organ tissues can offer more useful information for clinical applications. One of the methods for drug tracing is to use fluorescence to monitor fluorescent drugs.[60] However this method is only applicable to a very limited number of drugs because most of the drugs are non-fluorescent. At the same times, the available

fluorescent probes all showed some limitations coupled with their complicated synthetic procedure. For drug delivery tracing, it makes strategic sense to combine the properties of drug delivery with optical labeling.[104] Due to the application of amphiphilic block copolymers in drug delivery, luminescent polymeric micelles can be used for drug delivery and biolabeling. Thus in this project, we aim to find a simple, flexible and effective approach to fluorescent polymeric micelles with intense fluorescence, excellent biocompatibility and nontoxicity that can find applications not only in drug delivery, but also in tracing and bioimaging of bio-species.

In order to guarantee the fluorescent properties, the materials for core or shell must be fluorescent. The inclusion of conjugated oligomers/polymers will introduce fluorescent property for micelles. Efficient luminescence and easy functionalization are the requirements for core materials. Oligofluorenes (OFs) are well-known light-emitting materials for organic light emitting diodes due to their high efficient luminescence, good stability, and facile structural tunability for both backbones and side chains. Due to the hydrophobicity of conjugated molecules, they will form the core of polymeric micelles

Good water solubility, nontoxicity and biocompatibility are first consideration for the hydrophilic segments, which will contact with tissues and organs in human body directly. Among all the polymeric micelles, PEG-containing micelles have been intensively investigated due to the highly hydrophilic properties, excellent biocompatibility, non-cytotoxicity and commercial availability of PEGs with a variety of molecular weights. Due to the above mentioned properties, PEGs have been widely used as hydrophilic blocks for amphiphilic copolymers. Thus, graft copolymers based on OF backbones and

PEG side chains are developed, which can self aggregate into fluorescent micelles in aqueous solution.

It is expected that a new series of amphiphilic graft copolymers should be realized through simple synthesis and purification process. Tunable size and size dispersion could be achieved by modifying the architecture, hydrophilic/hydrophobic ratio and molecular weight of the molecules. The most important is the stability of micelles formed from them, which can be obtained by tuning the composition/ratio of the hydrophobic fluorene backbone and the hydrophilic PEG side chains to balance the hydrophobicity and hydrophilicity of the polymers.

In comparison with the existing inorganic and organic fluorescent probes, fluorescent polymeric micelles can be realized through simple synthetic procedure. Templates are not necessary and each block can be designed in an optimum way based on the functional and environmental requirements. In addition, micelle size and light emission can be tuned conveniently and separately. It was expected that these fluorescent micelles are good complement and improvement for fluorescent probes and polymeric micelles.

References

1. G. H. Michler, F. J. Balta Calleja, I. Puente, M. E. Cagiao, K. Knoll, S. Henning, R. Adhikari, *J. Appl. Polym. Sci.* **2003**, *90*, 1670.
2. I. Goodman, *Developments in block copolymers-1*, London: Applied Science, **1982**.
3. D. Urban, M. Gerst, P. Rossmanith, H. Schuch, *Polym. Mater. Sci. Eng*. **1998**, *79*, 440.
4. J. M. Lee, B. H. Lee, S. Choe, *Polymer* **2006**, *47*, 3838.
5. S. W. Mork, G. D. Rose, D. P. Green, *J. Surf. Detergents* **2001**, *4*, 127.
6. F. O. M. S. Abreu , M. M. C. Forte, S. A. Liberman *J. Appl. Polym. Sci.* **2004**, *95*, 254.
7. X. Li, R. Liu, L. Zhong, L. Gu, *J. Appl. Polym. Sci.* **2003**, *89*, 1696.
8. G. Riess, *Prog. Polym. Sci.* **2003**, *28*, 1107.
9. S. E. Webber, *J. Phys. Chem. B* **1998**, *102*, 2618.
10. S. E. Webber, P. Munk, Z. Tuzar, *Solvents and Self-organization of polymers*, NATO ASI Series, Series E: Applied Science **1996**, Vol. 327.
11. P. S. Goyal, V. K. Aswal, *Curr. Sci.* **2001**, *80*, 972.
12. C. Park, J. Yoon, E. L. Thomas, *Polymer* **2003**, *44*, 6725.
13. M. Antonietti, S. Heinz, M. Schimdt, C. Rosenauer, *Macromolecules* **1994**, *27*, 3276.
14. S. Förster, M. Zisenis, E. Wenz, M. Antonietti, *J. Chem. Phys.* **1996**, *104*, 9956.
15. A. A. Khaydarov, I. W. Hamley, T. M. Legge, S. Perrier, *Eur. Polym. J.* **2007**, *43*, 789.
16. H. Li, Y. M. Zhang, M. Z. Xue, Y. G. Liu, *Polym. J.* **2005**, *37*, 841.

17. G.-H. Li, C.-G. Cho, *Colloid Polym. Sci*. **2005**, *283*, 946.

18. J.-H. Kim, M. S. Rahman, J.-S. Lee, J.-W. Park, *J. Am. Chem. Soc*. **2007**, *129*, 7756.

19. M. S. Rahman, S. Samal, J.-S. Lee, *Macromolecules* **2006**, *39*, 5009.

20. R. Xu, M. A. Winnik, G. Riess, B. Chu, M. D. Croucher, *Macromolecules* **1992**, *25*, 644.

21. K. Yu, A. Eisenberg, *Macromolecules* **1996**, *29*, 6359.

22. N. J. Jain, V. K. Aswal, P. S. Goyal, P. Bahadur, *Colloids Surf. A* **2000**, *173*, 85.

23. K. Mortensen, J. S. Pedersen, *Macromolecules* **1993**, *26*, 805.

24. M. Almgren, W. Brown, S. Hvidt, *Colloid Polym. Sci*. **1995**, *273*, 2.

25. S. L. Nolan, R. J. Phillips, P. M. Cotts, S. R. Dungan, *J. Colloid. Interface Sci.* **1997**, *191*, 291.

26. J. James, C. Ramalechume, A. B. Mandal, *Chem. Phys. Lett.* **2005**, *405*, 84.

27. Z. Xu, C. Yi, S. Cheng, L. Feng, *Polym. Bull*. **2003**, *44*, 115.

28. G. Carrot, J. C. Valmalette, C. J. G. Plummer, S. M. Scholz, H. Hofmann, J. G. Hilborn, *Colloid Polym. Sci.* **1998**, *276*, 853.

29. Y. Koizumi, S. Seki, S. Tsukuda, S. Sakamoto, S. Tagawa, *J. Am. Chem. Soc*. **2006**, *128*, 9036.

30. D. W. Chang, L. Dai, *J. Mater. Chem*. **2007**, *17*, 364.

31. S. Kubowicz, *Design and Characterization of Multicompartment Micelles in Aqueous Solution*, Dissertation, Potsdam, April **2005**.

32. K. Holmberg, *Handbook of Applied Surface and Colloidal Chemistry*, John Wiley & Sons Ltd., Chichester, **2002**, Chapter 13 & 15.

33. J. Zhao, W. Brown, *Langmuir* **1996**, *12*, 1141.

34. C. Price, E. K. M. Chan, A. L. Hudd, R. B. Stubbersfield, *British Polym. J.* **2007**, *18*, 57.

35. N. Bhattarai, S. R. Bhattarai, H. K. Yi, J. C. Lee, M. S. Khil, P. H. Hwang, H.Y. Kim, *Pharm. Res.* **2003**, *20*, 2021.

36. K. Y. Mya, X, Li, L. Chen, X. Ni, J. Li, C. He, *J. Phys. Chem. B* **2005**, *109*, 9455.

37. X. Li, K. Y. Mya, X. Ni, C. He, K. W. Leong, J. Li, *J. Phys. Chem. B*. **2006**, *110*, 5920.

38. C. A. Gracia, S. Gómez-Barreiro, A. González-Pérez, J. Nimo, J. R. Rodríguez, *J Colloid Interface Sci*. **2004**, *276*, 408.

39. C. Hitscherich Jr, V. Aseyev, J. Wiencek, P. J. Loll, *Acta Crystallogr. Sect. D* **2001**, *7*, 1020.

40. K. Khougaz, Z. S. Gao, A. Eisenberg, *Macromolecules* **1994**, *27*, 6341.

41. J. P. Vernille, L. C. Kovell, J. W. Schneider, *Bioconjugate Chem*. **2004**, *15*, 1314.

42. S. Rangelov, P. Petrov. I. Berlinvoa, Ch. Tsvetanov, *Polym. Bull.* **2004**, *52*, 155.

43. S. Forster, T. Plantenberg, *Angew. Chem. Int. Ed.* **2002**, *41*, 688.

44. T. P. Lodge, J. Bang, Z. Li, M. A. Hillmyer, Y. Talmon, *Faraday Discuss* **2005**, *128*, 1.

45. J.-K. Kim, E. Lee, Z. Huang, M. Lee, *J. Am. Chem. Soc*. **2006**, *128*, 14022.

46. E. R. Zubarev, J. Xu, A. Sayyad, J. D. Gibson *J. Am. Chem. Soc*. **2006**, *128*, 15098.

47. C. Park, J. Yoonb, E. L. Thomas, *Polymer* **2003**, *44*, 6725.

48. A. Choucair, A. Eisenberga, *Eur. Phys. J. E* **2003**, *10*, 37.

49. (a) X. Feng, D. Taton, R. Borsali, E.L. Chaikof, Y. Gnanou, *J. Am. Chem. Soc.* **2006**, *128*, 11551. (b) X. Jiang, S. Luo, S. P. Armes, W. Shi, S. Liu, *Macromolecules* **2006**, 39, 5987.

50. P. Alexandridis, L. Yang, *Macromolecules* **2000**, *33*, 5574.

51. S. Krishnamoorthy, R. Pugin, J. Brugger, H. Heinzelmann, C. Hinderling, *Adv. Funct. Mater.* **2006**, *16*, 1469.

52. Y. Chang, E. S. Powell, H. R. Allcock, *J. Pharm. Sci.* **2003**, *92*, 2912.

53. Y. Deng, Y. Li, X. Wang, *Macromolecules* **2006**, *39*, 6590.

54. A. Halperin, *Macromolecules* **1987**, *20*, 2943.

55. M. Hans, K. Shimoni, D. Danino, S. J. Siegel, A. Lowman, *Biomacromolecules* **2005**, *6*, 2708.

56. M. Phil. Hazrat Hussain, *Amphiphlic Block Copolymer of Poly(ethylene oxide) and Poly(perfluorohexylethyl methacrylate): from Synthesis to Applications*, Dissertation, **2004**.

57. W. Brown, K. Schillen, M. Almgren, S. Hvidt, P. Bahadur, *J. Phys. Chem*. **1991**, *95*, 1850.

58. T. Nie, Y. Zhao, Z. Xie, C. Wu, *Macromolecules* **2003**, *36*, 8825.

59. B. Herzog, K. Huber, A. R. Rennie, *J. Colloid Interface Sci.* **1994**, *164*, 370.

60. Y. Kim, P. Dalhaimer, R. A. Chritian, D. E. Discher, *Nanotechnology* **2005**, *16*, S484.

61. K. Yasugi, Y. Nagasaki, M. Kato, K. Kataoka, *J. Controlled Release* **1999**, *62*, 89.

62. F. Liu, G. Liu, *Macromolecules* **2001**, *34*, 1302.

63. C. Booth, D. Attwood, *Macromol. Rapid Commun*. **2000**, *21*, 501.

64. D. W. Chang, L. Dai, *J. Mater. Chem*. **2007**, *17*, 364.

65. K. K. Jette, D. Law, E. A. Schmitt, G. S. Kwon, *Pharm. Res*. **2004**, *21*, 1184.

66. W. Brown, *Laser Light Scatttering, Principles and Developments*; Clarendon Press: Oxford, **1996**.

67. R. Palaniswamy, C. Wang, K. C. Tam, L. H. Gan, *Macromolecules* **2003**, *36*, 173.

68. G. Guerin, J. Raez, I. Manners, M. A. Winnik, *Macromolecules* **2005**, *38*, 7819.

69. A. Ramzi, M. Sutter, W. E. Hennink, W. Jiskoot, *J. Pharm. Sci*. **2006**, *95*, 1703.

70. P. Taboada, D. Attwood, J. M. Ruso, M. Garcia, V. Mosquera, *Phys. Chem. Chem. Phys*. **2000**, *2*, 5175.

71. F. Wang, M.-Y. Han, K. Y. Mya, Y. Wang, Y.-H. Lai, *J. Am. Chem. Soc*. **2005**, *127*, 10350.

72. C. Tsitsilianis, D. Voulgaris, *Langmuir* **2000**, *16*, 6868.

73. I. W. Hamley, *Nanotechnology* **2003**, *14*, R39.

74. Y. Ma, L. Qi, J. Ma, H. Cheng, *Adv. Mater*. **2004**, *16*, 1023.

75. L. Liu, Y.Niu, X. Zhu, X. Sun, G. Wang, Z. Jiang, *Colloid Polym. Sci*. **2006**, *284*, 556.

76. G. Bar, Y. Thomann, M.-H. Whangbo, *Langmuir* **1998**, *14*, 1219.

77. L. Tian, P. T. Hammond, *Chem. Mater.* **2006**, *18*, 3976.

78. (a)R. Nagarajan, K. Ganesh, *Macromolecules* **1989**, *22*, 4312. (b) M. Antonietti, S. Forster, J. Hartmann, S. Oestreich, *Macromolecules* **1996**, *29*, 3800.

79. Y. Ma, L. Qi, J. Ma, H. Cheng, *Langmuir* **2003**, *19*, 4040.

80. D. Zhang, L. Qi, J. Ma, H. Cheng, *Adv. Mater*. **2002**, *14*, 1499.

81. M. S. Wong, J. N. Cha, K.-S. Choi, T. J. Deming, G. D. Stucky, *Nano Lett*. **2002**, *2*, 583.

82. M. L. Adams, A. Lavasanifar, G. S. Kwon, *J. Pharm. Sci*. **2003**, *92*, 1343.

83. G. B. Sukhorukov, H. Mohwald, *Trends in Biotech*. **2007**, *25*, 93.

84. V. P. Torchilin, *Cell. Mol. Life. Sci*. **2004**, *61*, 2549.

85. V. Schmit, C. Giacomelli, F. Lecolley, J. Lai-Kee-Him, A. R. Brisson, R. Borsali, *J. Am. Chem. Soc*. **2006**, *128*, 9010.

86. S. N. Letuta, G. A. Ketsle, L. V. Levshin, A. N. Nikiyan, O. K. Davydova, *Optics and Spectroscopy* 2002, *93*, 844.

87. K. L. Holmes, L. M. Lantz, *Methods Cell Biol*. **2001**, *63*, 185.

88. F. Wang, W. B. Tan, Y. Zhang, X. Fan, M. Wang, *Nanotechnology* **2006**, *17*, R1.

89. S. C Hung, J. Ju, R. A. Mathies, A. N. Glazer, *Anal. Biochem*. **1996**, *238*, 165.

90. H. Kojima, M. Hirotani, N. Nakatsubo, K. Kikuchi, Y. Urano, T. Higuchi, Y. Hirata, T. Nagano, *Anal. Chem*. **2001**, *73*, 1967.

91. H. Kojima, Y. Urano, K. Kikuchi, T. Higuchi, Y. Hirata, T. Nagano, *Angew. Chem. Int. Ed.* **1999**, *38*, 3209.

92. J. L. Schwartz, G. H. Patterson, *Science* **2003**, *300*, 87.

93. R. Heim, R. Y. Tsien, *Curr. Biol.* **1996**, *6*, 178.

94. C. J. Daly, J. C. McGrath, *Pharmacol. Therap*. **2003**, *100*, 101.

95. V. Ntziachristos, *Annu. Rev. Biomed. Eng*. **2006**, *8*, 1.

96. W. J. Parak, T. Pellegrino, C. Plank, *Nanotechonolgy* **2005**, *16*, R9.

97. M. Bruchez Jr., M. Moronne, P. Gin, S. Weiss, A. P. Alivisatos, *Science* **1998**, *281*, 2013.

98. W. C. W. Chan, S. Nie, *Science* **1998**, *281*, 2016.

99. M. Han, X. Gao, J. Z. Su, S. Nie, *Nature Biotech*. **2001**, 19, 631.

100. R. Hardman, Environmental Health Perspectives 2006, 114, 165.

101. Z. F. Li, E. Ruckenstein, *Nano Lett.* **2004**, *4*, 1463.

102. I. Sokolov, Y. Y. Kievsky, J. M. Kaszpurenko, *Small* **2007**, *3*, 419.

103. N. C. Tansil, Z. Gao, *Nanotoday* **2006**, *1*, 28.

104. R. Savic, L. B. Luo, A. Eisenberg, D. Maysinger, *Science* **2003**, *300,* 615.

2. Design and synthesis of fluorescent amphiphilic graft copolymer

2.1 Molecular design

With the aim to explore new amphiphilic block/graft copolymers that combine the properties of fluorescence and amphiphilicity, amphiphilic molecules based on polyfluorene and oligofluorene grafted with PEGs were designed. Another consideration for the molecular design is to simplify the synthesis and purification procedure, which will favor commercial applications. In order to investigate the architecture effect on the morphology and properties of polymeric micelles, the ratio of hydrophilic/hydrophobic blocks, molecular weight and architecture were changed to tune CAC, particle morphology and properties.

Hydrophilic segments in amphiphilic copolymers offer them water solubility and their presence will also increase the residence time of micelles in systemic circulation. Their property will affect the nanostructure shape, size and their interaction with aqueous environments. The surface properties of self-assembled micelles are highly dependent on hydrophilic blocks. As we know, acids, alcohols, ethers, esters and some strong polyelectrolytes have good water solubility. However, they will show different response to stimuli. Some of them are sensitive to temperature, such as poly(ethylene oxide) (PEO), which shows hydrophilicity at $T < 80$ °C. Some blocks are pH-value responsive, such as Na-salts of polyelectrolytes and some will be affected by ionic strength, e.g. peptides. The well-known hydrophilic segments include poly(methacrylic acid) (PMAA), poly(acrylic acid) (PAA), poly(vinyl alcohol) (PVA) and PEO, which have been used as hydrophilic building blocks widely.

PEO is also often referred to as poly(ethylene glycol) (PEG),–[CH_2–CH_2–O–]$_n$–CH_2–CH_2–OH. PEO has a perfect balance between the hydrophobic methylene (CH_2) group and hydrophilic oxygen (O) group, which can be sensed from its unexpected water solubility or ‘‘hydrophilicity’’. Other analogs, such as polymers that contain more methylene group, e.g. poly(propylene oxide) (PPO) or poly(butylene oxide) (PBO), do not have such good water solubility. PEG also exhibits other unique and versatile properties such as chemical stability, aqueous media and various organic solvents solubility, nontoxicity, ion-transporting ability, nonbiodegradability and nonrecognition by the immune system (stealth effect). PEG is also permitted to be covalently attached to biologically active molecules (PEGylation). Thus PEG is the most frequently used hydrophilic segment in bio-applicable amphiphilic molecules.[1,2]

PEGs are synthesized by anionic ring opening polymerization of ethylene oxide initiated by nucleophilic attack of a hydroxide ion on the epoxide ring. They are commercially available with a variety of molecular weights. Their solubility in water is inversely proportional to their molecular weight. Compared with other polymers, PEGs have a relatively narrow polydispersity (PDI = M_w/M_n) in the range of 1.01 for low molecular weight PEGs (<5 kDa) to 1.1 for high molecular weight PEGs (>50 kDa).[3] Although PEGs are known to be non-biodegradable, yet they are readily excretable after administration into living organisms. Below a molecular weight of about 20 kDa, the molecule can be excreted from the kidneys and is cleared in the urine, and higher molecular weight between 20 kDa and 50 kDa PEGs are cleared more slowly in the urine and feces.[3] Thus, accumulation toxicity may not become a problem unless PEGs with a M_w higher than the critical value is used in the polymerization process. The non-toxic

nature of PEGs and nonrecognition by the immune system has been exploited to conjugate biologically active molecules to increase the in vivo stability and therapeutic efficacy.[1]

In addition, PEGs also demonstrate excellent pharmacokinetic and biodistribution behavior. When they are injected into animal body, they show high persistence in blood compartment and low accumulation in reticuloendothelial system (RES) organs, e.g. liver and spleen.[4] Their ability to alter the interactions of cells and proteins is desired. PEGs also present the ability to precipitate proteins, to exclude proteins and cells from surfaces, and to reduce immunogenicity and antigenicity and prevent degradation by mammalian cells and enzymes.[3]

PEGs are generally considered to be inert and possess a low order of toxicity in animals and humans. Thus PEGs are highly investigated polymers and have a great promise for covalent modification of biological macromolecules (PEGylation), drug delivery systems for many pharmaceutical and biotechnical applications.[3-5] PEGs also have been widely used in food and food packaging. They were also used as plasticizers, solvents, water-soluble lubricants for rubber molds; wetting or softening agents, antistatics in the production of urethane rubber, components of detergents, etc. In medicine, PEGs are used in ointments, suppositories, in ophthalmic solutions and sustained-released oral pharmaceutical applications. In this project, PEG with lower molecular weight (M_w = 2 kDa) was chosen as hydrophilic blocks to build fluorescent amphiphilic copolymers. The reason is that the PEG with M_w = 2 kDa (~ 45 repeating units) is solid flake, not viscous liquid and it can be easily processed for anhydrous reactions.

Hydrophobic blocks in amphiphilic copolymers form the core of micelles in aqueous solution. They will determine the properties of micellar cores. When micelles are used in drug delivery, functionalized hydrophobic blocks will help to recognize molecules and the functional groups are the key factor for drug loading and delivery. Thus their applications also depend on the design of hydrophobic segments.

It is well known that organic conjugated molecules have fluorescent properties. So far a variety of organic fluorescent molecules have been synthesized and widely used in organic electronics, such as organic light-emitting diodes (OLEDs), field effect transistors (FET) and organic photovoltaic devices. Oligofluorene[6,7], polyfluorene (PF) and their derivatives are a class of widely investigated blue light-emitting conjugated molecules.[8-13] They are well-known light-emitting materials for organic light emitting diodes due to their high efficient luminescence, good stability, and facile structural tunability for both backbones and side chains. The availability of specific and highly regioselective coupling reactions also provide a rich variety of tailored polyfluorene-based polymers and copolymers.[14-19] Another attractive property of fluorene-based polymers is that their light emission can be conveniently tuned from blue to green and red by simple structure modification.[20-23]

Oligo/polyfluorenes (OFs/PFs) can also be functionalized with water soluble groups/segments, which will enable the materials water solubility and can extend their application to biotechnology.[24,25]

In this project, polyfluorene/oligofluorene will be selected as hydrophobic backbones. PEG will be grafted as side chains of polyfluorene/oligofluorene. Thus, graft copolymers based on OF/PF backbones and PEG side chains are developed, which can self-aggregate

into fluorescent micelles in aqueous solution. These fluorescent micelles can be used for bio-labeling and bio-marker as well as drug delivery vehicles.

To obtain tunable CAC, particle size and size dispersion, graft copolymers with different molecular weights and hydrophilic/hydrophobic block ratios and architectures were designed. Since fully conjugated oligofluorene and polyfluorene backbones are rigid, their aggregation behavior should be different from polymers with flexible backbones. To investigate the rigidity/flexibility of the polymer backbone on micellization, flexible moieties were introduced into the polymer backbones and acted as co-monomer for polymers. The chemical structures of the designed oligomers and polymers are shown in Figure 2.1.

Series A: PEG grafted OFs/PFs rigid backbones

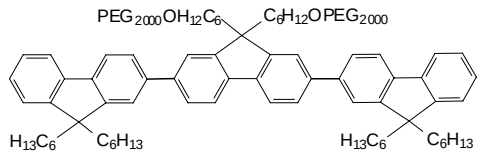

OFP1

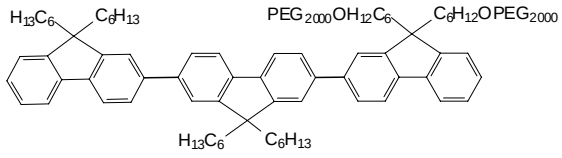

OFP2

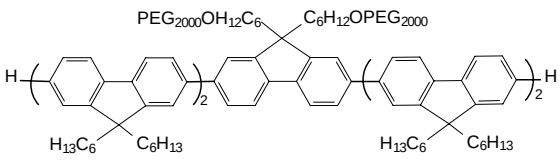

OFP3

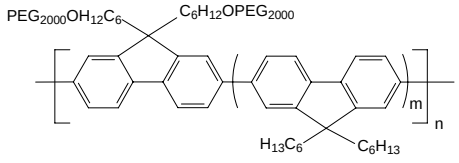

RFP

Series B: PEG grafted PFs containing flexible units in the backbones

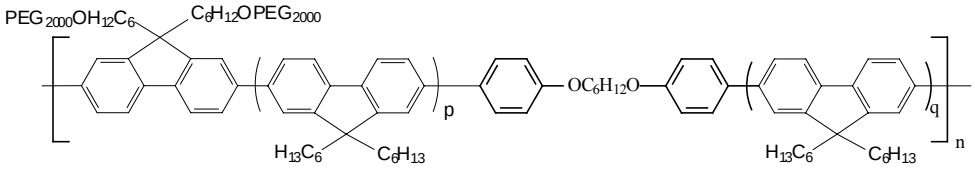

p+q=6, FFP1
p+q=10, FFP2
p+q=20, FFP3

Figure 2.1. Structures of fluorescent amphiphilic graft copolymers.

2.2 Experimental details

Reagents and chemicals including mono and dibromofluorene, 1-bromohexane, 1,6-dibromohexane were purchased from Lancaster Company. Other chemicals including 2-isopropoxy-4,4,5,5-tetramethyl-1,3,2-dioxaborolane were purchased from Sigma-Adrich Chemical Company. Catalyst tetrakis(triphenylphosphine)palladium(0) $Pd(PPh_3)_4$ was purchased from STREM Company. All the above chemicals were used directly without further purification. The anhydrous solvent tetrahydrofuran (THF) was distilled from sodium-benzophenone immediately prior to use.

The ^1H NMR and ^{13}C NMR spectra were recorded in solution of *d*-$CDCl_3$ on a Bruker DPX (400 MHz) NMR spectrometer with tetramethylsilane (TMS) as the internal standard. GPC analysis was conducted on a Shimadzu SCL-10A and LC-8A system equipped with two Phenogel 5 μm, 50 and 1000 Å columns (size 300 x 4.6 mm) in series and a Shimadzu RID-10A refractive index detector. Tetrahydrofuran (THF) was used as eluent at a flow rate of 0.20 mL/min at 45 ˚C. Monodispersed poly(ethylene glycol) standards (M_n: 400 - 70,000 g.mol^{-1}) were used to obtain a calibration curve. UV-vis-NIR absorption spectroscopy was measured by Shimadzu UV-3101 PC spectrometer at room

temperature. Fluorescence spectra were measured by Shimadzu RF-5301 PC spectrophotometer at room temperature.

The general synthetic routes are outlined in Scheme 2.1. Monobromosubstituted and dibromosubstituted fluorene were alkylated with 1,6-dibromohexane or bromohexane in 50 wt% strong base solution in the presence of phase transfer catalyst tetrabutylammonium bromide with yields of 75% for **1** and **2** and 98% for **3** and **4**. Compound **1** and **2** were further reacted with excess amount of PEG (M_w = 2 kDa) at room temperature in anhydrous THF solution with the presence of excess strong base NaH to afford compound **5** and **6**, respectively. Due to the coil PEG, the reactions were stirred for 1 week to guarantee completion of the reaction. Compound **7** and **8** were obtained by standard n-butyl lithium reaction at -78 °C in anhydrous THF solution, followed by adding 2-isopropoxy-4,4,5,5-tetramethyl-1,3,2-dioxaborolane with around 60 - 70% yields. Compound **9** was obtained by refluxing p-bromophenol and 1,6-dibromohexane in acetone/K_2CO_3 with a medium yield of 46%.

All the oligomers and polymers were obtained by following standard Suzuki coupling reaction, which was carried out in a mixture of toluene and aqueous sodium carbonate solution (2 M) containing 1 mol % $Pd(PPh_3)_4$ under nitrogen, stirring at 90 °C for 3 - 5 days. Purification was performed by repeated precipitation. Impurities trapped in the precipitated polymer matrix were eliminated by subsequent steps, such as ultrafiltration and dialysis in water.

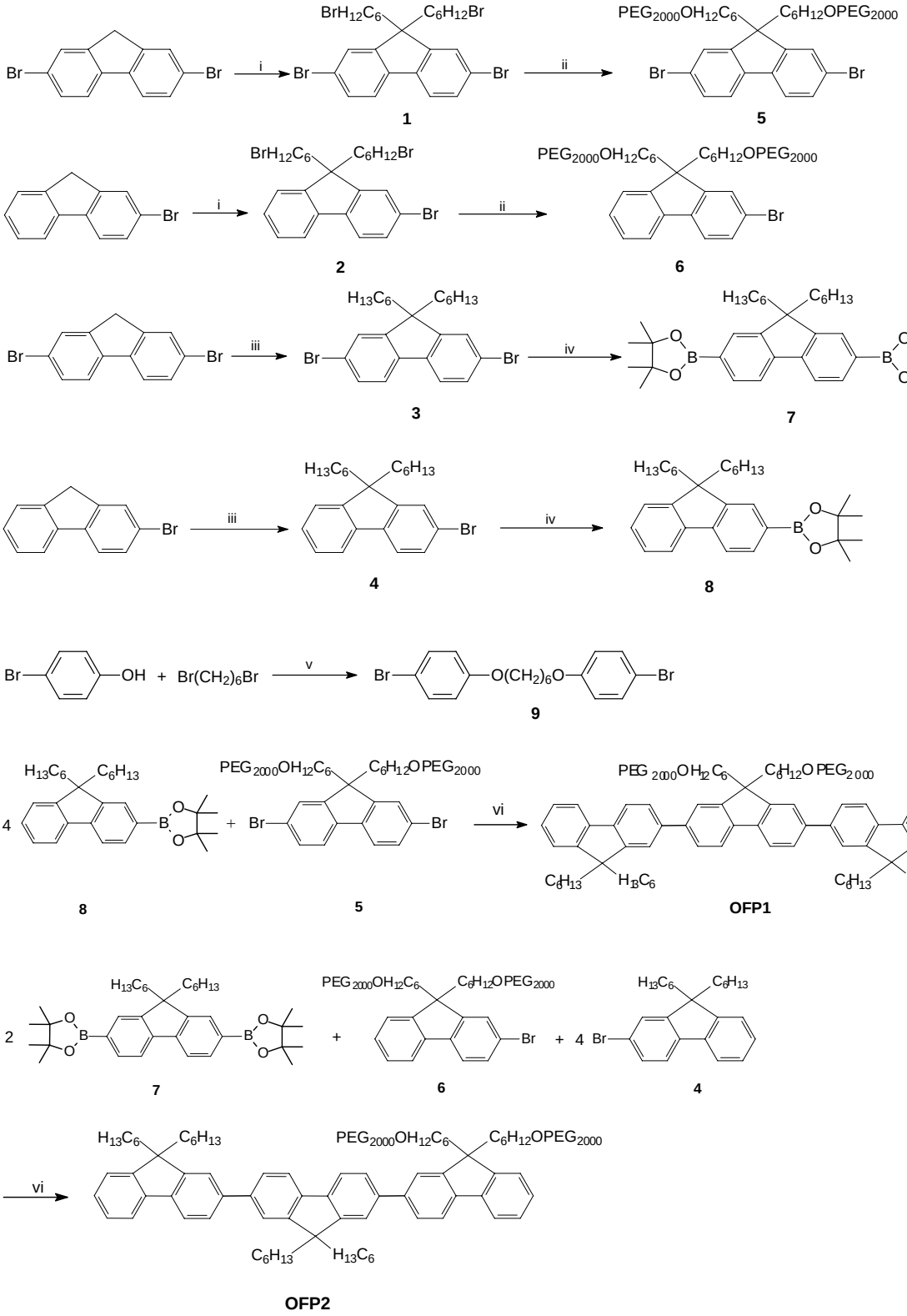
Br
i
BrH12C6
C6H12Br
ii
PEG2000OH12C6
C6H12OPEG2000
1
5
2
6
iii
H13C6
C6H13
iv
3
7
4
8
OH + Br(CH2)6Br
v
O(CH2)6O
9
vi
OFP1
OFP2

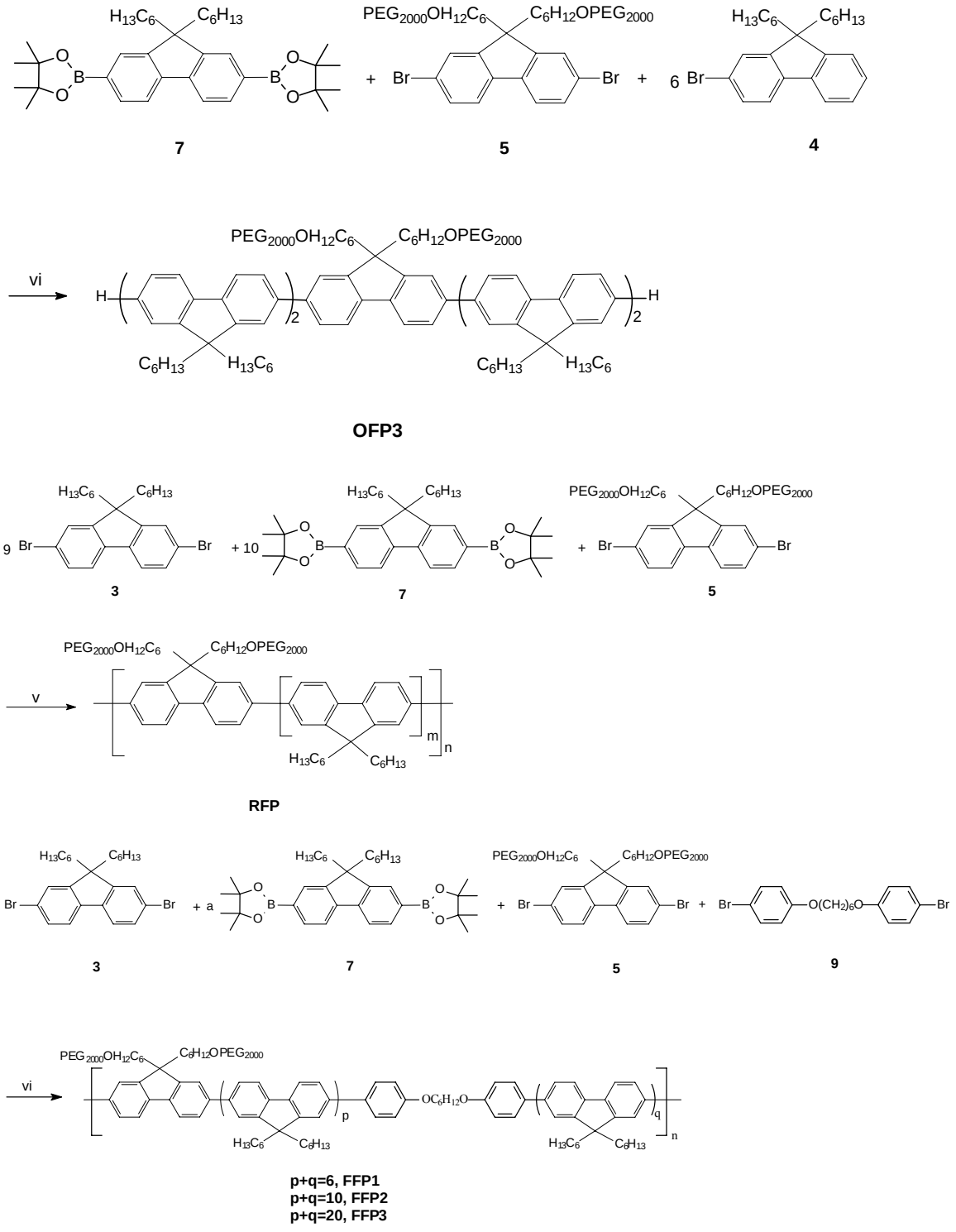

Scheme 2.1. Synthetic route of amphiphilic graft copolymers
Reagents and conditions: i. n-$BrC_6H_{12}Br$, 50% KOH, Bu_4NBr, 75 °C, 1.5 h; ii. NaH, THF, r. t., 1 week; iii. n-$C_6H_{13}Br$, 50% NaOH, Bu_4NBr, 80 °C, 5 h; iv. n-BuLi, THF, -78 °C, 2-isopropoxy-4, 4, 5, 5-tetramethyl-1, 3, 2-dioxaborolane; v. K_2CO_3, acetone, 8 h; vi. toluene, Na_2CO_3, $Pd(PPh_3)_4$, 90 °C, 3 - 5 days.

2,7-Dibromo-9,9-bis(6'-bromohexyl)fluorene (1)[26]

2,7-Dibromofluorene (0.97 g, 3 mmol) was added to a mixture of aqueous potassium hydroxide (60 mL, 50%), tetrabutylammonium bromide (0.20 g, 0.6 mmol), and 1,6-dibromohexane (7.32 g, 30 mmol) at 75 °C. After stirring for 15 mins, the mixture was cooled down to room temperature. After extraction with dichloromethane, the combined organic layers were washed with water, aqueous HCl, water, and brine, and then dried over anhydrous $MgSO_4$. After removal of the solvent and the excess 1,6-dibromohexane, the residue was purified by silica gel column using hexane to chloroform 9:1 as the eluent to provide 1.47 g (75%) of the title compound as a white solid.

^{1}H NMR ($CDCl_3$, 400 MHz) δ, 7.54 (d, 2H), 7.48-7.43 (m, 4H), 3.30 (t, 4H), 1.93 (m, 4H), 1.69-1.65 (m, 4H), 1.20 (m, 4H), 1.08 (m, 4H), 0.61 (m, 4H).

^{13}C NMR ($CDCl_3$, 100 MHz) δ, 152.6, 139.5, 130.8, 126.5, 122.0, 121.6, 56.0, 40.4, 34.1, 33.0, 29.3, 28.1, 23.9.

2-Bromo-9,9-bis(6'-bromohexyl)fluorene (2)

Following the same synthetic procedure and column chromatography as compound **1**, compound **2** was obtained as light yellow viscous liquid with a yield of 75%.

^{1}H NMR ($CDCl_3$, 400 MHz) δ, 7.67 (m, 1H), 7.55 (m, 1H), 7.45 (m, 2H), 7.32 (m, 3H), 3.28 (t, 4H), 1.94 (m, 4H), 1.66 (m, 4H), 1.19 (m, 4H), 1.07 (m, 4H), 0.60 (m, 4H)

2,7-Dibromo–(9,9-dihexyl)fluorene (3)[27]

2,7-Dibromofluorene (9.72 g, 30 mmol) was added to a mixture of aqueous sodium hydroxide (54.3 mL, 50%), tetrabutylammonium bromide (1.82 g, 5.63 mmol, 0.2 equiv),

and 1-bromohexane (25.4 mL, 180 mmol, 6 equiv) at 80 °C. After stirring for 5 hrs, the mixture was cooled down to room temperature. After extraction with dichloromethane, the combined organic layers were washed with water, aqueous HCl, water, brine, and then dried over anhydrous $MgSO_4$. After removal of the solvent and the excess 1-bromohexane, the residue was purified by silica gel column using hexane as the eluent to provide 14.55 g (98%) of the title compound as a white crystal.

^{1}H NMR ($CDCl_3$, 400 MHz) δ, 7.51 (m, 6H), 1.91 (m, 4H), 1.12 (m, 12H), 0.78 (t, 6H), 0.58 (m, 4H).

^{13}C NMR ($CDCl_3$, 100 MHz) δ, 152.8, 139.3, 130.3, 126.4, 121.6, 121.3, 55.9, 40.3, 31.6, 29.7, 23.8, 22.7, 14.1.

2-Bromo-(9,9-dihexyl)fluorene (4)

Following the same synthetic procedure and column chromatography as compound **3**, compound **4** was obtained as light yellow viscous liquid with a yield of 98%.

^{1}H NMR ($CDCl_3$, 400MHz) δ, 7.70 (m, 1H), 7.59 (d, 1H), 7.47 (m, 2H), 7.35 (m, 3H), 1.97 (m, 4H), 1.11 (m, 12H), 0.80 (t, 6H), 0.63 (m, 4H).

^{13}C NMR ($CDCl_3$, 100 MHz) δ, 153.1, 150.4, 140.3, 140.1, 130.0, 127.6, 127.0, 126.2, 123.0, 121.1, 121.0, 119.8, 55.5, 40.4, 31.6, 29.8, 23.8, 22.7, 14.1.

Compound 5[28]

In a three-necked 150 mL flask under argon atmosphere was placed sodium hydride (0.96 g, 40 mmol) and anhydrous THF (30 mL) and then PEG (8 g, 4 mmol, M_w = 2 kDa) in THF (50 mL) was dropped in at room temperature. After the solution was stirred for 4

hrs, 2,7-dibromo-9,9-bis(6'-bromohexyl) fluorene (0.65 g, 1 mmol) was added and stirred at room temperature. TLC showed that the reaction completed after one week. Water was added drop by drop to terminate the reaction. The mixture was evaporated off to remove THF and the residue was dissolved in 20 mL dichloromethane and 4 mL methanol. Then the solution was precipitated in 500 mL ether, stirring for 1 h. After centrifuging off all the solvent, the solid was dissolved in dichloromethane/methanol again and precipitated in ether. After repeating the procedure of dissolution/precipitation/centrifugation 3 times, the final solid was dissolved in dichloromethane and loaded into dialysis tube to remove the salts and unreacted PEGs. After dialysis for one week, the aqueous solution was freeze dried and 1 g (50%) of monomer as white powder was obtained. GPC (254 nm, THF), M_w = 4396, PDI = 1.02.

Compound 6

Following the same procedure as compound **5**; compound **6** was obtained as white powder. GPC (254 nm, THF), M_w = 4167, PDI = 1.01.

2-(4,4,5,5-Tetramethyl-1,3,2-dioxaborolan-2-yl)-9,9-dihexylfluorene (7)

To a solution of 2-bromo-(9,9-dihexyl)fluorene (6.2 g, 15 mmol) in anhydrous THF (100 mL) was added dropwise n-BuLi (22.5 mL, 27 mmol) at -78 ºC. The reaction was stirred for 1 h, then 2-isopropoxy-4,4,5,5-tetramethyl-1,3,2-dioxaborolane (3.9 mL, 18.75 mmol) was added. The mixture was stirred overnight. Then the reaction was quenched with water and extracted with dichloromethane (100 mL) 3 times. The organic layer was combined and washed with saturated brine and dried over $MgSO_4$ and concentrated in

vacuo. After purification by silica gel column chromatography (ethyl acetate: hexane 1: 20), 5.83 g yellow viscous liquid was obtained with a yield of 84.5%.

^{1}H NMR ($CDCl_3$, 400 MHz) δ, 7.81 (m, 1H), 7.75 (m, 3H), 7.32 (m, 3H), 1.99 (m, 4H), 1.39 (s, 12H), 1.02 (m, 12H), 0.75 (m, 6H), 0.60 (m, 4H).

2,7-Bis(4,4,5,5-tetramethyl-1,3,2-dioxaborolan-2-yl)-9,9-dihexylfluorene (8)

Compound **8** was synthesized by following the same synthetic procedure of compound **7**, it was purified by recrystallization from ethanol to provide 1.82 g white solid product with a yield of 62%.

^{1}H NMR ($CDCl_3$, 400MHz) δ [ppm]: 7.79 (d, J=7.6 Hz, 2H), 7.74 (s, 2H), 7.73 (d, J=7.6 Hz, 2H), 2.00 (m, 4H), 1.39 (s, 24H), 1.06 (m, 12H), 0.74 (t, 6H), 0.55 (m, 4H).

^{13}C NMR ($CDCl_3$, 100 MHz) δ, 150.7, 144.1, 133.8, 129.1, 119.5, 83.9, 55.3, 40.2, 31.6, 29.8, 25.1, 23.8, 22.7, 14.1.

Compound 9

A mixture of 4-bromophenol (2.63 g, 15 mmol), dibromohexane (1.22 g, 5 mmol) and anhydrous potassium carbonate (1.38 g, 10 mmol) was dissolved in acetone and heated to reflux. After stirring for 8 hours, water was added to terminate the reaction. The solution was extracted with ether (50 mL) 3 times. The combined organic layer was successively washed with 2 M sodium hydroxide solution and brine. Then it was dried over anhydrous $MgSO_4$. After removal of the solvent, the residue was recrystallized from ethanol to give white crystals 1.15 g, with a yield of 46%.

^{1}H NMR ($CDCl_3$, 400 MHz) δ, 7.37-7.35 (d, J=8.8 Hz, 4H), 6.78-6.75 (d, J=8.8 Hz, 4H), 3.93 (t, 4H), 1.80 (m, 4H), 1.53 (m, 4H).

^{13}C NMR ($CDCl_3$, 100 MHz) δ, 158.4, 132.4, 116.5, 112.9, 68.3, 29.3, 26.0.

Graft copolymers

All the graft copolymers were synthesized by following the standard Suzuki coupling reaction, which was carried out in a mixture of toluene and aqueous sodium carbonate solution (2 M) containing 1 mol % [$Pd(PPh_3)_4$] under nitrogen, stirring at 90 °C for 3 days. Purification was performed by precipitation; the procedure is the same as that used to prepare the monomers. Precipitation is the principal method for polymer purification. However, impurities can be trapped in the precipitated polymer matrix. Subsequent steps, such as dialysis and/or ultrafiltration, were carried out to further eliminate impurity residues trapped in the polymers.

Synthesis of rigid copolymers taking OFP1 as an example

A mixture of compound **8** (0.46 g, 1 mmol), compound **5** (1.12 g, 0.25 mmol), [$Pd(PPh_3)_4$] (50 mg, 0.04 mmol), aqueous sodium carbonate (2 M, 1.24 mL), and toluene (10 mL) was deoxygenated and then heated to reflux under nitrogen. The mixture was stirred for 2 days and then cooled down to room temperature. The organic solvent in the mixture was allowed to evaporate. The residue was dissolved in 20 mL of dichloromethane, and mixed with 800 mL of ether to form a precipitate. The solvents were removed by centrifuge. The precipitation process was repeated 3 times. The crude product was dissolved in dichloromethane and subject to dialysis using an 8 k dialysis

tube for about one week. The solution was freeze-dried to form a pale powder product, which was amphiphilic graft copolymer **OFP1**. The yield of the process was 50%.

^{1}H NMR ($CDCl_3$, 400 MHz) δ, 7.80-7.73 (m, fluorene), 7.66-7.62 (m, fluorene), 7.52 (s, fluorene), 3.64 (s, PEG).

OFP2 was synthesized with a yield of 42% as pale powder.

^{1}H NMR ($CDCl_3$, 400 MHz) δ, 7.69-7.61 (m, fluorene), 7.55-7.20 (t, fluorene), 7.47-7.31 (m, fluorene), 7.30 (sw, fluorene), 3.64 (s, PEG).

OFP3 was synthesized with a yield of 37% as pale powder.

^{1}H NMR ($CDCl_3$, 400 MHz) δ, 7.82-7.67 (m, fluorene), 7.52 (s, fluorene), 7.00 (s, fluorene), 3.64 (s, PEG).

Synthesis of flexible copolymers FFP1

A mixture of compound **3** (147 mg, 0.30 mmol), compound **5** (674 mg, 0.06 mmol), compound **7** (351 mg, 0.60 mmol), [$Pd(PPh_3)_4$] (96.1 mg, 0.08 mmol), compound **9** (75 mg, 0.15 mmol), aqueous sodium carbonate (2 M, 2.6 mL), and toluene (7.8 mL) was deoxygenated and then heated to reflux under nitrogen. The mixture was stirred for 3 days and then cooled down to room temperature. The organic solvent in the mixture was allowed to evaporate. The residue was dissolved in 8 mL of dichloromethane, and mixed with 300 mL of ether to form a precipitate. The solvents were removed by centrifuge. The precipitation process was repeated 3 times. The crude product was dissolved in dichloromethane and subject to dialysis using a 10 k dialysis tube for about one week.

The solution was freeze-dried to form a pale powder product, which was amphiphilic graft copolymer **FFP1**. The yield of the process was 21%.

^{1}H NMR ($CDCl_3$, 400 MHz) δ, 8.58 (sw, fluorene), 7.93 (s, fluorene), 7.66 (m, fluorene), 7.66 (m, fluorene), 7.52 (s, fluorene), 7.44 (d, flexible units), 7.00 (s, fluorene), 4.05-4.00 (m, flexible unit), 3.64 (s, PEG), 2.20 (m, fluorene), 1.80 (m, fluorene), 1.30 (m, fluorene), 0.90-0.69 (m, fluorene)

Synthesis of flexible copolymers FFP2

A mixture of compound **3** (160 mg, 0.32 mmol), compound **5** (360 mg, 0.08 mmol), compound **7** (280 mg, 0.48 mmol), $[Pd(PPh_3)_4]$ (106 mg, 0.09 mmol), compound **9** (40 mg, 0.08 mmol), aqueous sodium carbonate (2 M, 2.1 mL), and toluene (6.5 mL) was deoxygenated and then heated to reflux under nitrogen. The mixture was stirred for 3 days and then cooled down to room temperature. The organic solvent in the mixture was allowed to evaporate. The residue was dissolved in 8 mL of dichloromethane, and mixed with 300 mL of ether to form a precipitate. The solvents were removed by centrifuge. The precipitation process was repeated 3 times. The crude product was dissolved in dichloromethane and subject to dialysis using a 10 k dialysis tube for about one week. The solution was freeze-dried to form a pale powder product, which was amphiphilic graft copolymer **FFP2**. The yield of the process was 24%.

^{1}H NMR ($CDCl_3$, 400 MHz) δ, 7.82 (m, fluorene), 7.66 (m, fluorene), 7.52 (s, fluorene), 7.00 (s, fluorene), 4.08-4.05 (m, flexible unit), 3.65 (s, PEG), 2.18 (m, fluorene), 1.87-1.84 (m, fluorene and flexible units), 1.27 (m, fluorene), 0.82-0.61 (m, fluorene).

Synthesis of flexible copolymers FFP3

A mixture of compound **3** (266 mg, 0.54 mmol), compound **5** (270 mg, 0.06 mmol), compound **7** (387 mg, 0.66 mmol), [$Pd(PPh_3)_4$] (106 mg, 0.09 mmol), compound **9** (30 mg, 0.06 mmol), aqueous sodium carbonate (2 M, 3.0 mL), and toluene (9.2 mL) was deoxygenated and then heated to reflux under nitrogen. The mixture was stirred for 3 days and then cooled down to room temperature. The organic solvent in the mixture was allowed to evaporate. The residue was dissolved in 8 mL of dichloromethane, and mixed with 300 mL of ether to form a precipitate. The solvents were removed by centrifuge. The precipitation process was repeated 3 times. The crude product was dissolved in dichloromethane and subject to dialysis using a 10 k dialysis tube for about one week. The solution was freeze-dried to form a pale powder product, which was amphiphilic graft copolymer **FFP3**. The yield of the process was 37%.

^{1}H NMR ($CDCl_3$, 400 MHz) δ, 7.82 (m, fluorene), 7.66 (m, fluorene), 7.52 (s, fluorene), 7.00 (s, fluorene), 4.08-4.05 (sw, flexible unit), 3.64 (s, PEG), 2.17 (s, fluorene), 1.87-1.84 (m, fluorene and flexible units), 1.25 (m, fluorene), 0.90-0.63 (m, fluorene).

The NMR spectra of copolymers with oligofluroene (**OFP1**, **OFP2** and **OFP3**) backbones can not be used for confirming their structures due to the unbalance ratio of PEG to terfluorene and pentafluorene. GPC was applied to confirm the molecular weights and number of PEG side chains. PL spectra were used to confirm structure of oligofluorene backbones due to the PL high sensitivity to conjugation length of oligofluorenes, which will be discussed in the next chapter. For rigid and low PEG content flexible copolymers, their structures can be easily confirmed by GPC and NMR. Figure 2.2 shows the ^{1}H NMR of rigid polymer **RFP**. GPC results are listed in Table 2.1.

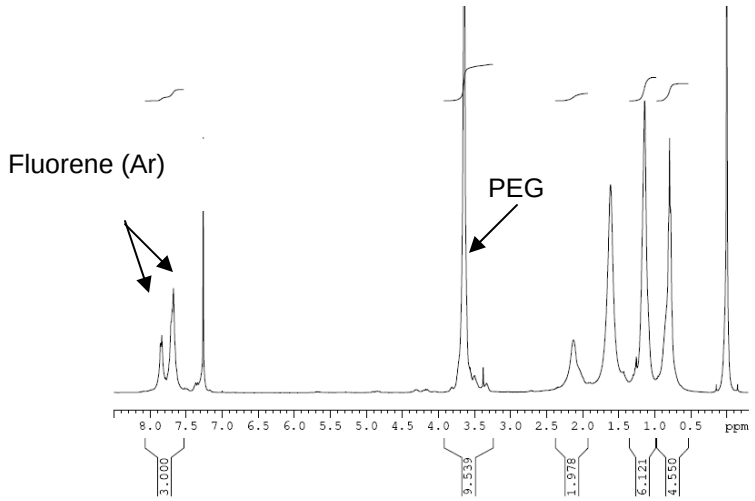

Figure 2.2 ^{1}H NMR spectrum of **RFP** in *d*-chloroform.

Table 2.1. Molecular weights and PDIs of all the amphiphiles.

Sample	M_w (g/mol)	M_n (g/mol)	PDI= (M_w/M_n)
5	4396	4300	1.02
6	4167	4112	1.01
OFP1	4123	3969	1.04
OFP2	4096	3666	1.12
OFP3	4409	3919	1.13
RFP	19585	9886	1.98
FFP1	9839	8441	1.17
FFP2	8528	6740	1.27
FFP3	14223	11057	1.29

References

1. X. Feng, D. Taton, R. Borsali, E. L. Chaikof, Y. Gnanou, *J. Am. Chem. Soc*. **2006**, *128*, 11551.
2. F. Zeng, C. Allen, *Macromolecules* **2006**, *39*, 6391.
3. M. J. Roberts, M. D. Bentley, J. M. Harris, *Adv. Drug Del. Rev.* **2002**, *54*, 459.
4. S. Zalipsky, *Adv. Drug Del. Rev.* **1995**, *16*, 157.
5. J. Israelachvili, *Proc. Natl. Acad. Sci.* **1997**, *94*, 8378.
6. Y. Geng, S. W. Culligan, A. Trajkovska, J. U. Wallace, S. H. Chen, *Chem. Mater*. **2003**, *15*, 542.
7. K.-T. Wong, R.-T. Chen, F.-C. Fang, C.-C. Wu, Y.-T. Lin, *Org. Lett.* **2005**, *7*, 1979.
8. D. Katsis, Y. H. Geng, J. J. Ou, S. W. Culligan, A. Trajkovska, S. H. Chen, L. J. Rothberg, *Chem. Mater*. **2002**, *14*, 1332.
9. Z. H. Li, M. S. Wong, Y. Tao, J. Lu, *Chem. Eur. J*. **2005**, *11*, 3285.
10. A. D.-Bouillud, I. Levesque, Y. Tao, M. D'Iorio, *Chem. Mater*. **2000**, *12*, 1931.
11. K.-T. Wong, Y.-M. Chen, Y.-T. Lin, H.-C. Su, C.-C. Wu, *Org. Lett*. **2005**, *7*, 5361.
12. K.-T. Wong, Y.-L. Liao, Y.-T. Lin, H.-C. Su, C.-C. Wu, *Org. Lett*. **2005**, *7*, 5131.
13. H. Meng, Z. Bao, A. J. Lovinger, B. C. Wang, A. M. Mujsce, *J. Am. Chem. Soc*. **2001**, *123*, 9214.
14. G. Zeng, *Macromolecules* **2002**, *35*, 6904.
15. U. Scherf, E. J. W. List, *Adv. Mater*. **2002**, *14*, 477.
16. Z. H. Li, M. S. Wong, Y. Tao, J. Lu, *Chem. Eur. J.* **2005**, *11*, 3285.
17. R. Grisorio, P. Mastrorilli, C. F. Nobile, G. Romanazzi, G. P. Suranna, E. W. Meijer, *Tetrahedron Lett.* **2004**, *45*, 5367.
18. J. Jo. C. Chi, S. Hoger, G. Wegner, D. Y. Yoon, *Chem. Eur. J*. **2004**, *10*, 2681

19. C.-W. Wu, H.-C. Lin, *Macromolecules* **2006**, *39*, 7232.

20. N. S. Cho, D.-H. Hwang, J.-I. Lee, B.-J. Jung, H.-K. Shim, *Macromolecules* **2002**, *35*, 1224.

21. W. Wu, M. Inbasekaran, M. Hudack, D. Welsh, W. Yu, Y. Cheng, S. Wang, S. Kram, M. Tacey, M. Bernius, R. Fletcher, K. Kiszka, S. Munger, J. O'Bren, M*icorelectronics J.* **2004**, *35*, 343.

22. H.-J. Su, F.-I. Wu, Y.-H. Tseng, C.-F. Shu, *Adv. Funct. Mater.* **2005**, *15*, 1209.

23. D. Nether, *Macromol. Rapid Commun*. **2001**, *17*, 1365.

24. S. Wang, B. Liu, B. S. Gaylord, G. C. Bazan, *Adv. Funct. Mater*. **2003**, *13*, 463.

25. S. Wang, J. W. Hong, G. C. Bazan, *Org. Lett.* **2005**, *7*, 1907.

26. B. Liu, B. S. Gaylord, S. Wang, G. C. Bazan, *J. Am. Chem. Soc.* **2003**, *125*, 6705.

27. J. C. Ostrowski, M. R. Robinson, A. J. Heeger, G. C. Bazan, *Chem. Commun*. **2002**, 784.

28. J. H. Choi, J. S. Choi, H. Suh, J. S. Park, *Bull Korean Chem. Soc*. **2001**, *22*, 46.

3. Results and discussion

3.1 Synthesis and characterization

3.1.1 Monomer synthesis

The synthetic routes directly affect the yield and purification procedure. There are two possible ways to synthesize the final amphiphilic graft copolymers. The first route is to synthesize oligofluorene or polyfluorene backbones first, then PEG was grafted onto the backbone as side chains (e.g. **OFP1**, Scheme 3.1). In this route, the by product with a single PEG side chain is difficult to be removed from the desired product, which is attached with two PEG chains. Thus, PEG side chains must be grafted onto fluorene unit first as depicted in Chapter 2. The major product with two PEG chains (i.e. compound **5** and **6**) from the second route can be easily separated from the unreacted free PEGs and monosubstituted by product by dialysis.

Scheme 3.1. Alternative synthetic route for **OFP1**.

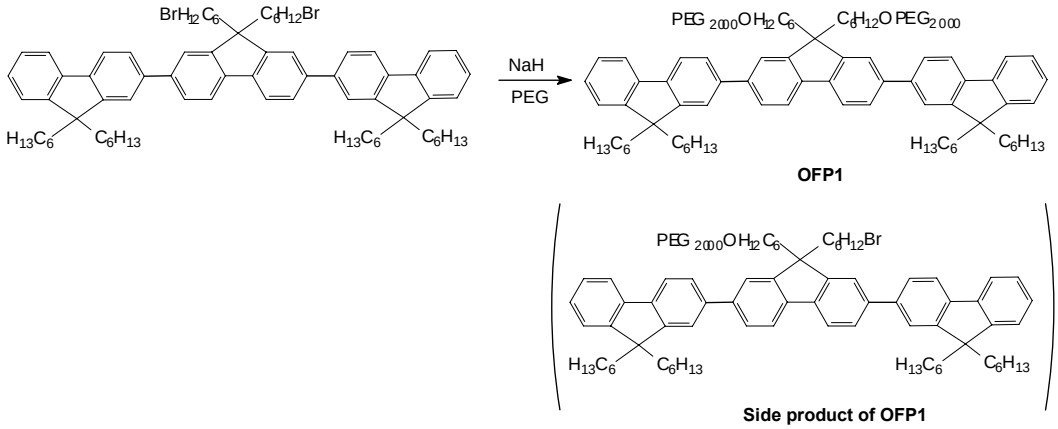

3.1.2 Polymer synthesis and characterization

Although dibromofluorene unit with two PEG side chains guarantee the Suzuki coupling reaction with fluorenyl diboronic ester, the bulky PEG side chains only offer good yields for copolymers with low hydrophilic/hydrophobic ratios. For example, copolymer **RFP** with hydrophilic/hydrophobic segment ratio of 1:18 can be easily synthesized and purified. When the hydrophilic/hydrophobic segment ratio increased to 1:9, more polyfluorenes were obtained in the final copolymers as side products. In order to improve the yield and simplifying purification procedure for the amphiphilic copolymers, steric hindrance effect must be reduced further, thus flexible unit compound **9** was introduced. The GPC results showed that the raw products of flexible copolymers were purer than the crude product of copolymer **RFP** with rigid backbone, which facilitates the purification procedure. The improved synthetic route also offers a flexible method to tune the molecular weight and hydrophilic/hydrophobic ratio.

GPC results indicate that **OFP1**, **OFP2** and **OFP3** contain two PEG chains, which means that the two oligomers contain only one fluorine unit with PEG side chains. In comparison of the PL spectra of **OFP1**, **OFP2** with the PL spectra of reference samples bifluorene (**BF**), terfluorene (**TF**) in dilute solution (as shown in Figure 3.1), we can find that the PL spectra of **OFP1**, **OFP2** and **TF** overlapped very well, indicating that **OFP1** and **OFP2** contain 3 fluorene repeat units. Similarly, when we compare the PL spectrum of **OFP3** with reference reported data of pentafluorene, we found that both of the compounds have similar PL spectra and same peak wavelength (410 nm).[1] Thus we can confirm that **OFP3** contains 5 fluorene repeat units.

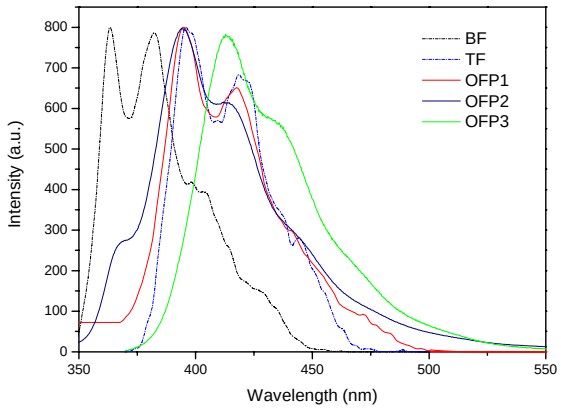

Figure 3.1. PL spectra of **BF**, **TF** (dash lines), **OFP1**, **OFP2** and **OFP3** (solid lines) in THF.

The GPC curves of rigid polymer **RFP** and flexible polymer **FFP3** are shown in Figure 3.2 and 3.3, respectively. Due to purer raw product, the purification of flexible polymers facilitated the purification process, which is one of their advantages. Another advantage for flexible polymers is their narrow PDIs than that of the rigid polymers, which will offer more uniform micelles.

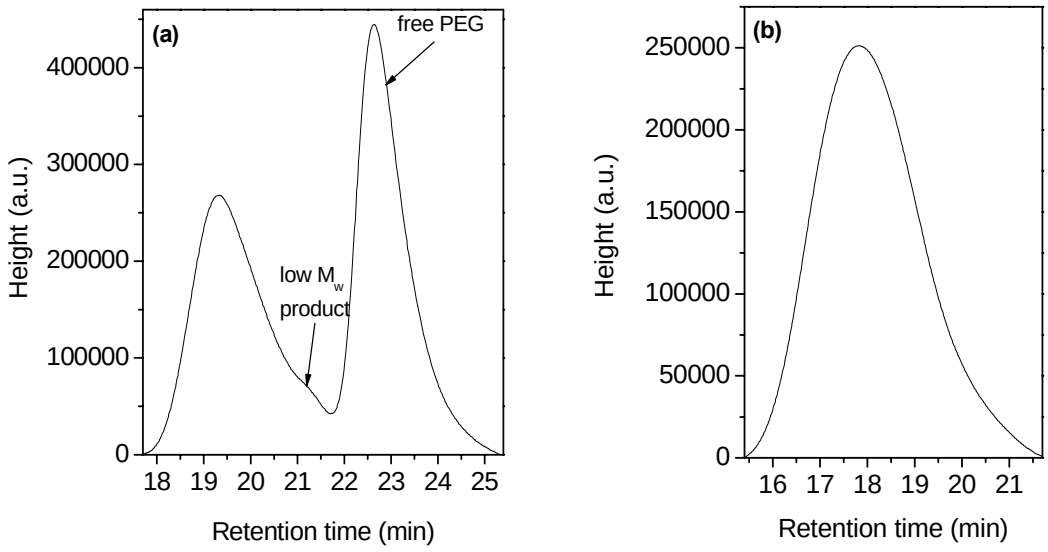

Figure 3.2. GPC curves of **RFP** (a) before purification and (b) after purification.

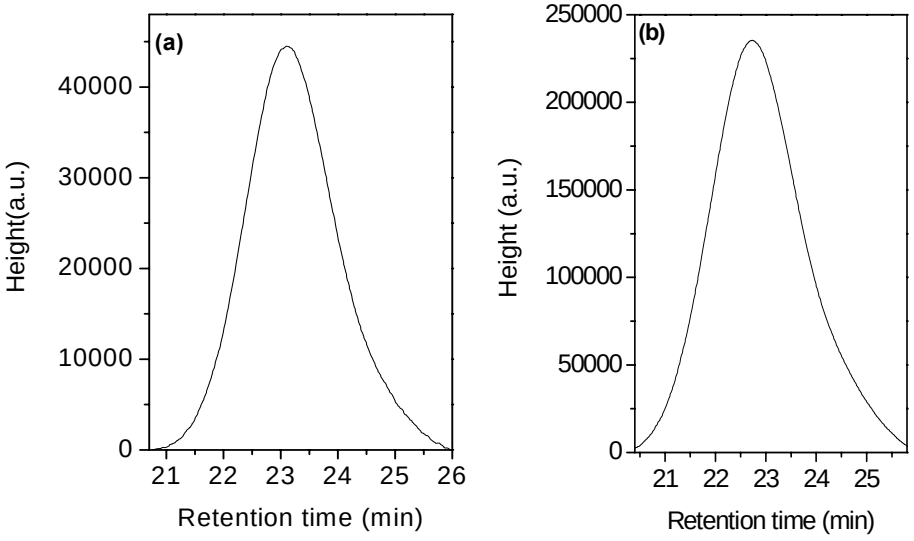

Figure 3.3. GPC curves of **FFP3** (a) before purification and (b) after purification.

The combination of GPC and ^{1}H NMR measurement was used to confirm the structure and molecular weight of polymer **RFP**, **FFP1** and **FFP2**. By calculating the ratio of the integration of protons in PEG chains and the aromatic protons from the NMR spectrum of **RFP**, we can estimate that the ratio between the fluorene with PEG chains and the fluorene without PEG chain is 1:18, which is very close to the feed ratio for the polymerization (feed ratio is 1:19). GPC measurement indicates M_n of **RFP** is 9886, which corresponds to 1 fluorene units with 2 PEG side chains and 18 fluorene repeat units with hexyl groups as side chains. The GPC result is in very good agreement with the NMR measurement. Analysis of NMR spectrum of **FFP1** - **FFP3** confirmed that the flexible units have been incorporated into the polymer backbone.

3.2 Light scattering measurements

Light scattering is a well-known and efficient method for characterization of nanoparticles in solution. It was applied to measure *CAC*, hydrodynamic radius (R_h), radius of gyration (R_g), aggregation number (N_{agg}), apparent molecular weight, and second virial coefficient (A_2) of polymer solutions. A Brookhaven light scattering instrument with BI-200SM multiangle goniometer and BI-APD detector was used to perform dynamic light scattering measurements. The light source was a 35-mW He-Ne laser emitting vertically polarized light of 632.8 nm wavelength. The sample cells were mounted in a temperature-controlled, refractive index matched bath filled with cis-trans decahydronaphthalene (decalin). Prior to both DLS and SLS measurements, all the solvents were filtered through 0.2 μm Millipore membrane filters (Whatman) to remove dust particles and the solutions were centrifuged at 8,000 rpm for 30 min and then filtered

with 0.2 μm Millipore filters directly into the light scattering cell. All the measurements were taken at 25 °C and the measured intensity correlation functions were analyzed by double exponential fit where bimodal distribution of relaxation time is considered. For SLS studies, Zimm plot was used to determine the radius of gyration (R_g), apparent molecular weight of polymer aggregates ($M_{w,agg}$), and second virial coefficient (A_2) of graft copolymers in aqueous solution. The critical aggregation concentration (*CAC*) of graft copolymers was determined by light intensity measurement.

3.2.1 CAC measurement and size distribution

The critical aggregation concentration (*CAC)* values indicate starting point of micelles formation. A variety of methods can be used to determine the *CAC* of polymeric surfactants. The fluorescent probe is the most widely used method due to its convenience and easy operation. However, due to the fluorescent properties of the micelles, fluorescent probe (pyrene) method for measuring *CAC* can not be used for current fluorescent nanoparitcle system because energy transfer happened between blue light-emitting micelles and pyrene. Thus, *CAC* values were measured by light scattering measurement. It is known that the amount of scattered light depends on particle size and number in the solution. Below *CAC*, only unimers exist and no or very weak scattering light was detected. Thus once micelles are formed in solution, excess scattered light intensity will experience an abrupt increase.[2,3] When more and more micelles were formed in solution with increasing the concentration of sample above *CAC*, the scattering light intensity showed linear increase vs. the concentration. The abrupt increases at the threshold concentrations from the intensity vs. copolymer concentration curves were

denoted as the *CAC* values. Scattering intensity of samples with different concentrations was measured. Figure 3.4 shows a typical *CAC* curve of **RFP** determined by SLS. Amphiphilic copolymers **OFP1**, **OFP2**, **OFP3** and **FFP3** showed very good water solubility and can be dissolved in water directly. Due to lower hydrophilic/hydrophobic ratio, other polymer samples (**RFP**, **FFP1** and **FFP2**) can not be dissolved in water directly and they were prepared by dialysis method. The solid sample was dissolved in THF first, and then the solvent system was changed from THF to pure water continuously by dialysis method. All the *CAC* values and particle sized of amphiphilic copolymers are summarized in Table 3.1.

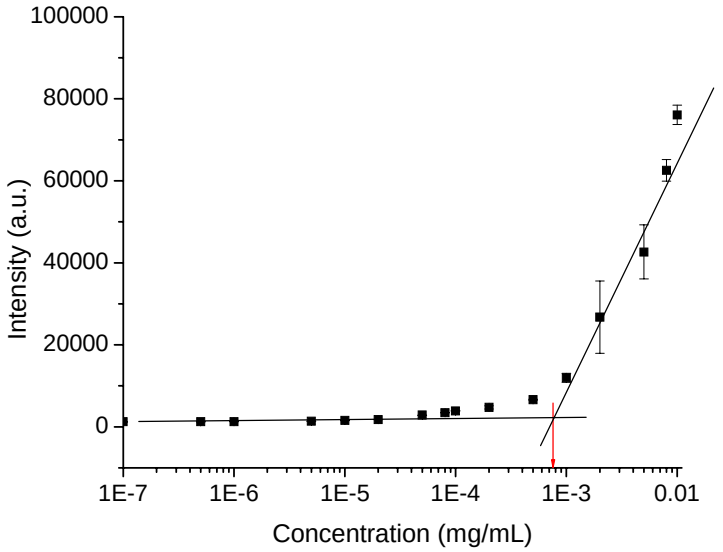

Figure 3.4. Variation of scattering light intensity as a function of sample concentration of **RFP**, red arrow shows *CAC* value.

Table 3.1. *CAC* values and radii of hydrodynamic (R_h) of amphiphilic polymers in aqueous solution at room temperature.

Sample	Theory M_w (g/mol)	M_w(Hydrophobic)/ M_w(Hydrophilic)	No. of fluorene units in the backbone	CAC (mg/mL)	R_h
5	4492	0.248	1	$8x10^{-2}$	60
OFP1	4996	0.249	3	$1x10^{-1}$	65
OFP2	4996	0.249	3	$5x10^{-2}$	66
OFP3	5660	0.415	5	$8x10^{-2}$	85
RPF	10640	1.66	19	$8x10^{-3}$	43
FFP1	11312	1.828	7	$4.5x10^{-4}$	89
FFP2	7992	0.998	11	$3.2x10^{-4}$	77
FFP3	6664	0.666	21	$4x10^{-4}$	54

It can be seen from Table 3.1, *CAC* values varied with the change of hydrophobic/hydrophilic ratio, molecular weight and architecture of molecules. *CAC* will decrease with the increase of hydrophobic/hydrophilic ratio, which was confirmed by the *CAC* values in the order of **OFP1**, **OFP3** and **RFP**. It was found that **OFP2** has lower *CAC* value (0.05 mg/mL) than **OFP1** (0.1 mg/mL). This indicates that the tendency to form the copolymer aggregates in **OFP2** is higher than that in **OFP1**. Figure 3.5 shows the particle size distributions of **OFP1**, **OFP2**, **OFP3**, **RFP** and **FFP3** in aqueous solution measured at the angle of 90° with a concentration above their *CAC*s. It was found that **OFP1** and **OFP2**, which possess the same backbone but with PEG side chains

linked at different positions, exhibited different physicochemical properties in aqueous solutions. The observation of two size distribution peaks of **OFP1** and **OFP2** in Figure 3.5(a) and (b) revealed the coexistence of unassociated single copolymer chains together with copolymer aggregates. The *CAC* result was confirmed by particle size distributions which exhibited equal size distribution of unassociated single copolymer chains and copolymer aggregates in **OFP1,** while a small amount of single polymer chains (< 10%) was observed in **OFP2**. It is reasonable to explain by the structure effect on intermolecular packing, which will be further confirmed by the measurement of apparent molecular weight (M_w) and aggregation number (N_{agg}) of the **OFP1** and **OFP2** micelles. It was also found that the value of R_h increased from 65 nm in **OFP1** to 89 nm in **OFP3** with the extension of the hydrophobic backbone chain length. As expected, the value of *CAC* decreased in **OFP3** (0.08 mg/mL) as compared to **OFP1** (0.1 mg/mL) due to the longer hydrophobic backbone. In addition, only monodispersed micelles were formed in **OFP3** and **RFP**.

Comparison of the *CAC* values of rigid polymers and flexible polymers indicated that the *CAC* of flexible polymers are two orders magnitudes smaller than that of rigid polymer **RFP**, which indicates that their micelles are more stable than rigid polymers and more easily micellize at low concentration. It is believed that the flexible units allow more intramolecular bending and intermolecular packing, and thus decrease the CACs greatly. For all the three flexible polymers, their *CAC*s were similar although their molecular weights and hydrophobic/hydrophilic ratios are different. The reason is supposed to be the flexible units playing more important roles in affecting micellization.

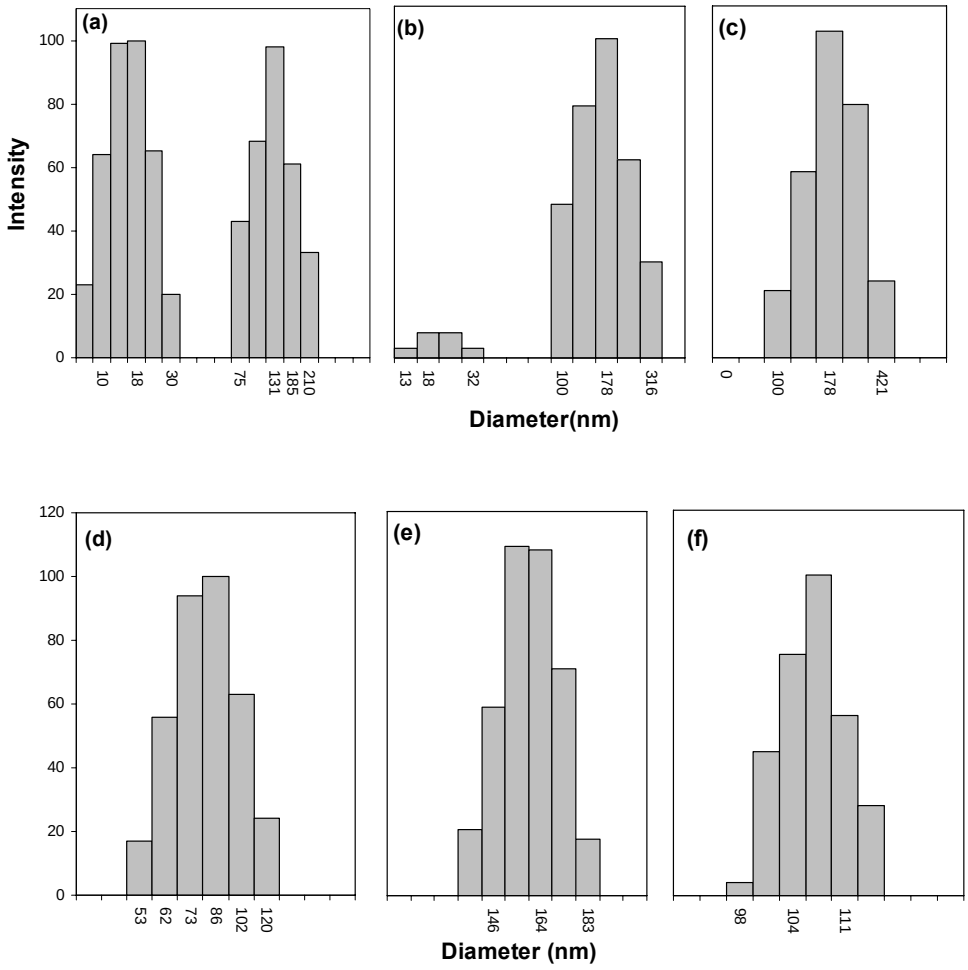

Figure 3.5. Hydrodynamic diameter distributions of (a) **OFP1** at 1 mg/mL concentration, (b) **OFP2** at 1 mg/mL concentration (c) **OFP3** at 1 mg/mL concentration, (d) **RFP** at 0.1 mg/mL concentration, (e) **FFP1** at 0.01 mg/mL concentration and (f) **FFP2** at 0.01 mg/mL concentration in H_2O at room temperature.

In most cases, the micelles are not ideal spheres and can be elliptical. The ratio of radius of gyration (R_g) to radius of hydrodynamic (R_h), i.e. $\rho=R_g/R_h$ is used to describe the morphology of micelles. The value of ρ is related to the spatial density distribution and the degree of draining of a particle in solution.[4] The ρ values for **OFP1** (0.88) and **OFP2** (0.92) are higher than 0.78 expected for a non-draining sphere particle,[5] revealing that such formed graft copolymer micelles are partially draining and contain loosely

aggregates due to the hydrophilic PEG blocks.[6] The value of ρ = 0.76 for **OFP3** is slightly lower than the non-draining sphere particle (0.78), which indicates that the hydrophobic backbone is tightly packed and therefore, the core is more condensed than the hydrophilic shell.

3.2.2 Aggregation number and apparent molecular weight measurement

SLS study can also provide the apparent molecular weight of polymer aggregate ($M_{w,agg}$) and size (radius of gyration R_g) of macromolecules in solution. The amount of light scattered is directly proportional to the product of the weight-average molar mass and the concentration of the macromolecule. The average aggregation number of graft copolymers aggregates were evaluated from the ratio of apparent molecular weight of aggregates determined by static light scattering and the molecular weight of unassociated single graft copolymers obtained by GPC measurements ($N_{agg} = M_{w,agg}/M_{w,0}$). Aggregation number indicates the number of molecules that are included in one micelle. In order to know the micelle molecular weight and aggregation number, a batch mode experiment was carried out to obtain $M_{w,agg}$ R_g, N_{agg} and the second virial coefficient A_2. The second virial coefficient is a measure of macromolecule-solvent interactions, which can be helpfully used to describe the thermodynamic behavior of macromolecules in solution. Second virial coefficient, also reflects the quality of solvent. Large positive A_2 value means that the solvent is a good solvent for the polymer, negative or small positive value means poor solvent.[7] Water-soluble copolymers **OFP1**, **OFP2** and **OFP3** were used for investigation. The sample was injected directly into the flow cell and then measured the amount of scattered light at different angles. The data collected for each

sample are processed simultaneously using the Zimm formalism. A typical experiment requires several (at least four) samples of macromolecule at different concentrations (in the range of mg/mL). The scattering angle ranges from 30 to 120 degree. The values of apparent molecular weight ($M_{w,agg}$) were estimated by extrapolation of c and θ to zero; A_2 and R_g were estimated from the slope of the angular and concentration dependence of Zimm plots, respectively. Figure 3.6 shows the angular (θ) and the concentration (c) dependence of $Kc/\Delta R_\theta$ (Zimm plot) of **OFP1**.

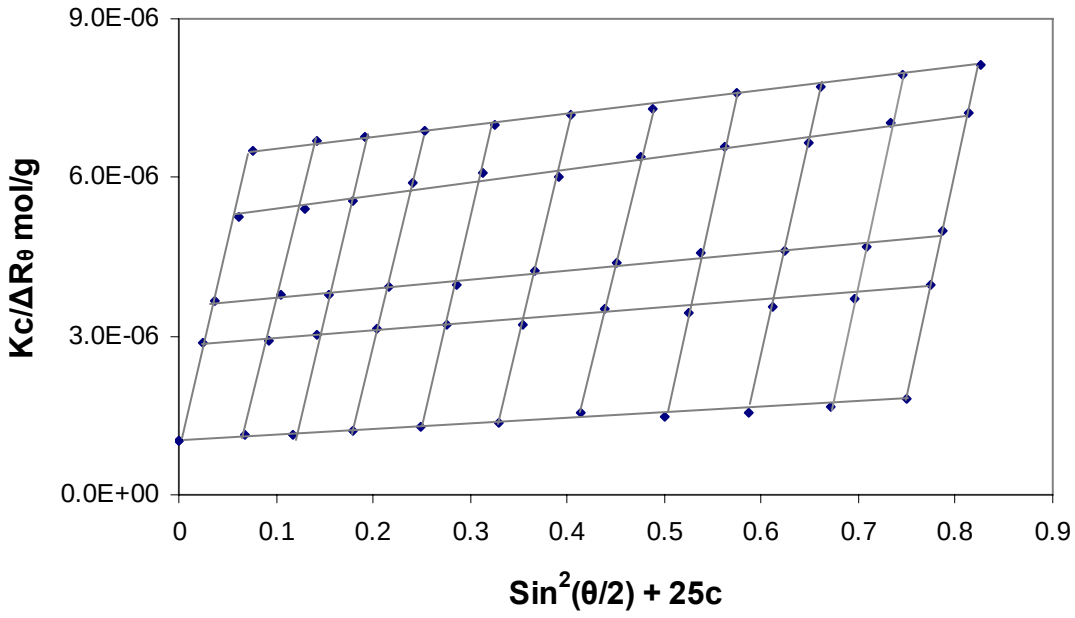

Figure 3.6. Zimm plot of **OFP1**, the concentration c changes from 1.0 to 3.0 mg/mL in water at 25 °C. Lines are drawn to align the data points.

It was found that the N_{agg} of **OFP3** (145) is much larger than **OFP1** (34) and **OFP2** (66) due to the longer hydrophobic chain length in **OFP3**. **OFP2** showed not only lower *CAC* value than **OFP1** but also double aggregation number. It is worthy to note that the hydrophilic blocks in **OFP2** were linked to the end of the backbone while the hydrophilic

blocks in **OFP1** resided at the center of the molecular backbones. The architecture of **OFP2** favored better intermolecular packing and therefore, it showed much higher aggregation number than **OFP1**. Moreover, the possession of longer hydrophobic backbones in **OFP3** graft copolymer supported a better intermolecular packing than **OFP1** and **OFP2**. The positive values of second virial coefficients (A_2) exhibit the favorable graft copolymer-solvent interaction, influenced by high molecular weight of PEG.

3.3 Morphology characterization

To confirm the polymeric micelle morphology predicted by light scattering measurements, the direct observation of micelles was illustrated by atomic force microscopy (AFM) and transmission electron microscopy (TEM). Micelle samples were prepared by following the standard dialysis procedure mentioned in Chapter 1.

3.3.1 Atomic force microscopy (AFM)

AFM samples were prepared from dilute sample solutions, which were dropped on freshly cleaved mica surface and air-dried overnight. AFM measurements were performed on a Nano-Scope IIIa Microscope (Digital Instruments, USA) using a 10*10 μm cantilever. The tips are micromachined monolithic silicon probes, exhibiting excellent uniformity, and a sharp tip radius. The consistent tip radius of less than 10 nm gives good resolution and reproducibility. All measurements were carried out with tapping mode at room temperature in air.

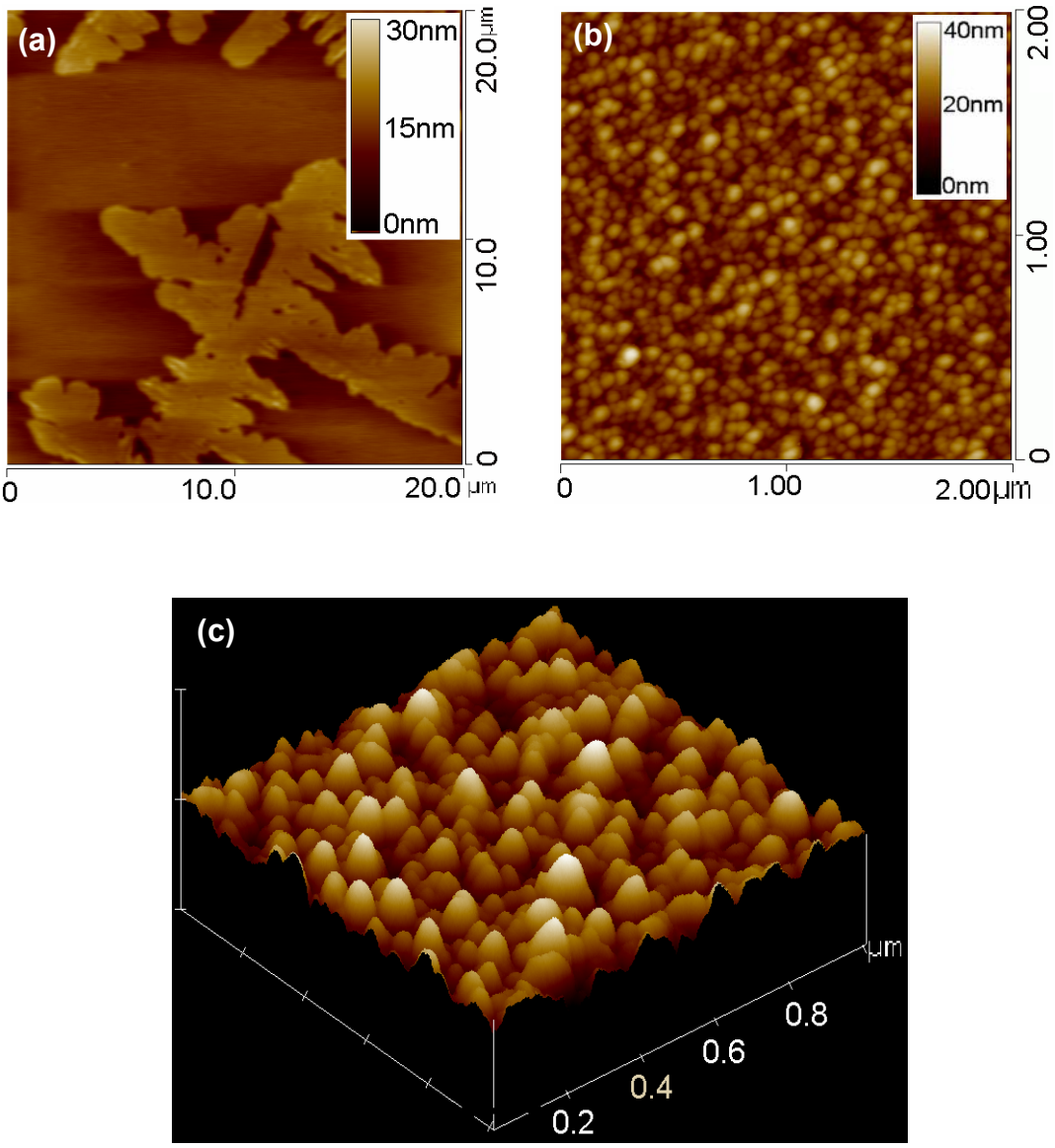

Figure 3.7. AFM height images (tapping mode) on mica of **OFP1** with the concentration of (a) 1 mg/mL, (b) 0.5 mg/mL and (c) 3-D image at the concentration of 0.5 mg/mL.

OFP1 contains more PEG than other polymers, so it forms much softer micelles. It was found that micelles tended to aggregate at low concentration (1 mg/mL) in solid state (*CAC*: 0.1 mg/mL). When the sample was prepared with a concentration of 1 mg/mL, its AFM microscopy showed severe aggregation. No micelle particles can be found. Only

when the sample concentration diluted to 0.5 mg/mL, **OFP1** formed soft elliptical micelles with the average diameter of 10 nm and 105 nm (Figures 3.7b), which is completely coincident with the results obtained from DLS measurement. The same phenomenon happened to **OFP2** and **OFP3** in solid state. Even when the sample concentrations were as low as their *CAC*s, severe aggregation occurred. Figure 3.8 shows the AFM image **OFP3** at the concentration of 0.08 mg/mL, the same as its *CAC*.

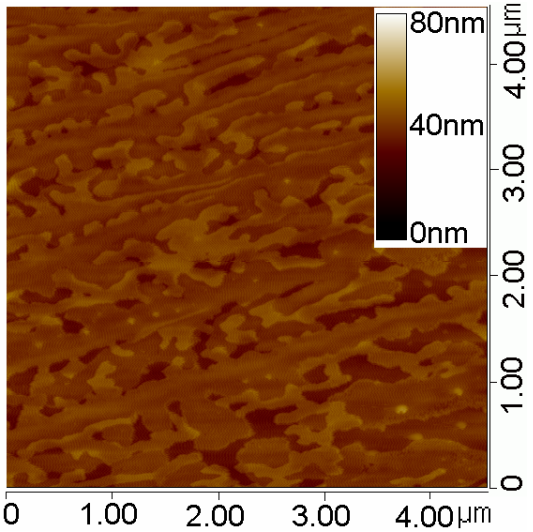

Figure 3.8. AFM height images (tapping mode) on mica of **OFP3** with the concentration of 0.08 mg/mL.

In comparison with **OFP1**, **OFP2** and **OFP3**, the balanced hydrophilic/hydrophobic ratio and higher molecular weight of polymer **RFP** force the amphiphiles to form uniform and densely packed micelles with thin shell layer in large area (See Figure 3.9a). The AFM images of **RFP** showed clear particle boundaries and revealed uniformly dispersed spherical objects possessing an average diameter of 60 nm (Figures 3.9b). The AFM images of **RFP** revealed uniformly dispersed spherical objects possessing an average diameter of 60 nm, which is in good agreement with the particle size measured

by LS, 85 nm in solution. The micelle size on film should be smaller than their sizes in solution due to shrinkage after they dry in air, while the shell of micelles will be outspread in aqueous solution. Polymer **RFP** has relatively low PEG content, so the formed micelle is hard and the particle borders are clearer than soft micelles, such as **OFP1** and **OFP2.**

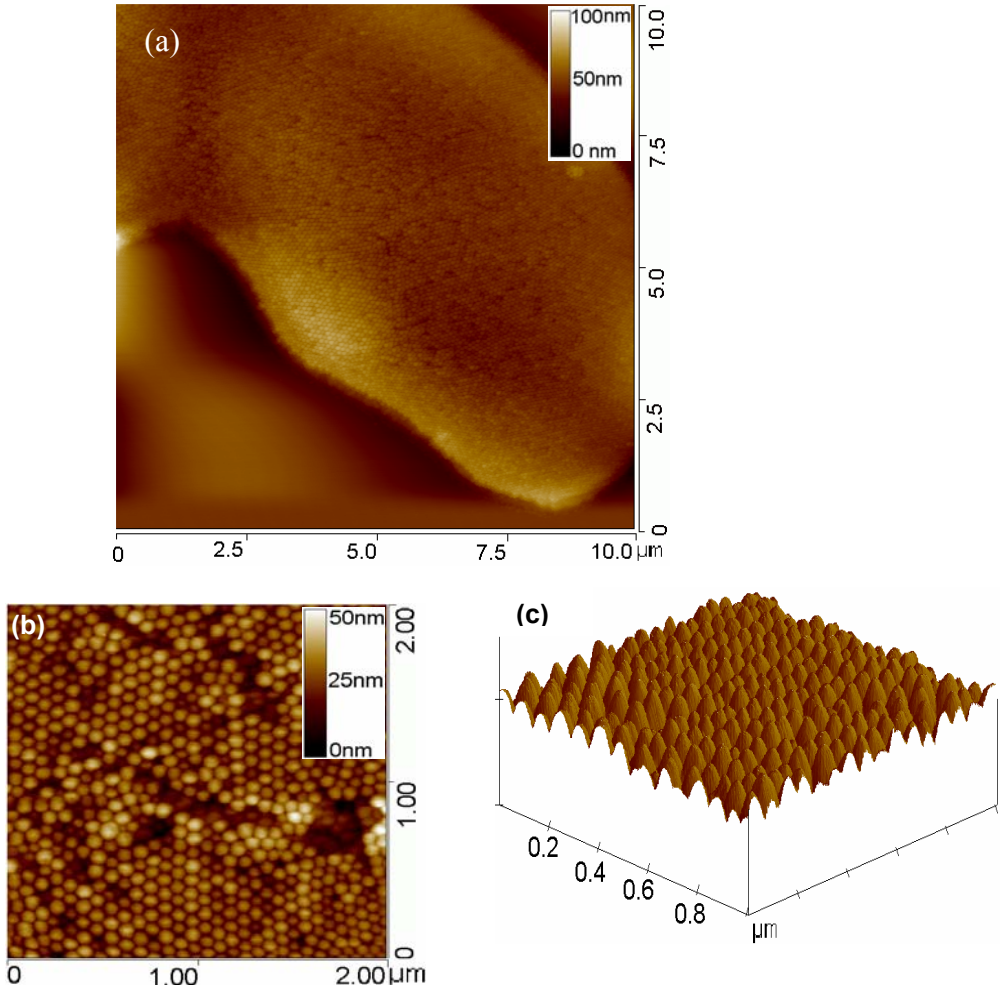

Figure 3.9. AFM height image (tapping mode) of **RFP** at concentration of 0.6 mg/mL on mica (a) 10 µm* 10 µm, (b) 2 µm* µm, (c) 3-D image.

The PEG content of flexible copolymer **FFP1** is similar as the rigid copolymer **OFP3**, its higher PEG content is the reason for its tendency of aggregation at low concentration

in solid state. Figure 3.10 shows the AFM image of **FFP1** at the concentration of 0.008 mg/mL, 25 times of its *CAC* value (0.00032 mg/mL).

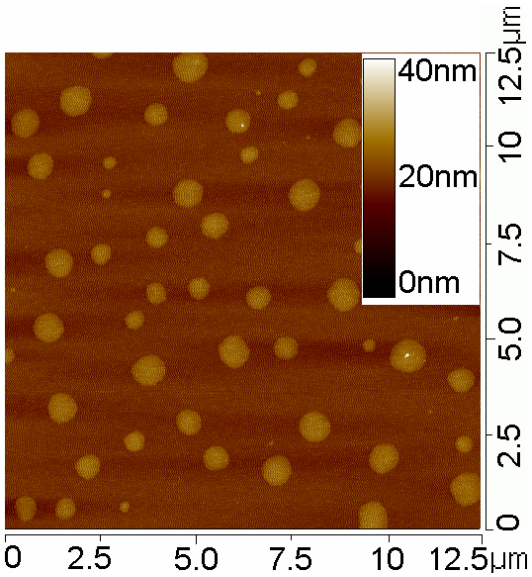

Figure 3.10. AFM height image of **FFP1** at the concentration of 0.008 mg/mL on mica.

Figure 3.11 shows the AFM image of micelles formed by flexible polymer **FFP3** at the concentration of 0.01 mg/mL. Its PEG content is similar with the rigid polymer **RFP**. Uniform micelles were formed from **FFP3**. The particle boundaries are clear although they look not as hard as that of **RFP** due to the introduction of flexible units. The micelle size in solid states is smaller than their size in solution due to shell shrinkage after they are dried in air. The micelle diameter of **FFP3** in thin film was around 74 nm, the diameter decreased 34 nm comparing with the particle size in solution (108 nm). For rigid polymer **RFP**, its diameter shrunk 25 nm from solution to thin film, whose size decreased from 85 nm to 60 nm. The micelle formed from flexible polymer shrink more than the micelles formed from rigid polymer, the reason is supposed to be its flexible

units offer more space for squeeze. It can be deduced that more flexible units, more shrinkage from solution to thin film.

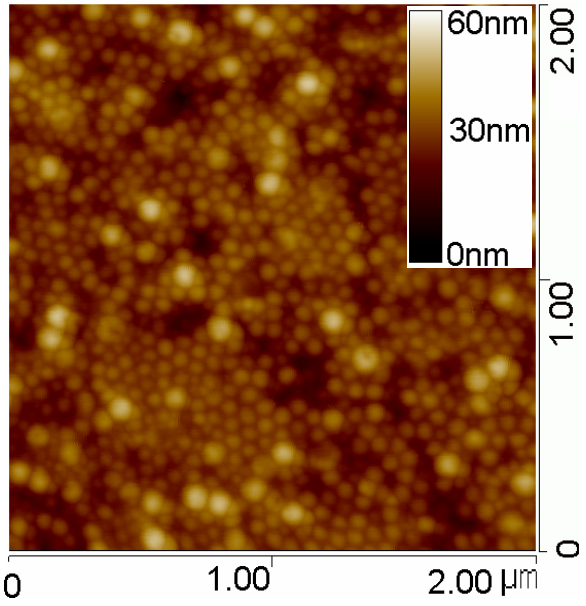

Figure 3.11. AFM height image of **FFP3** on mica at the concentration of 0.01 mg/mL.

3.3.2 Transmission electron microscopy (TEM)

AFM offer the particle size and size distribution in solid state, TEM can offer more information about the morphology of micelles. It can show the core and shell of the micelles clearly. TEM images were obtained on a JEOL JEM 2010F at transmission electron microscope operating at 300 kV accelerating voltage. Polymeric TEM samples need to be stained due to their nonconducting property. Phosphotungstic acid (PTA) was used as staining agent for these PEG-containing micelle samples. A 90 µL sample solution was mixed with 10 µL 1% PTA aqueous solution by vortex. A drop of solution mixture was then put onto a 400-mesh carbon-coated copper grid and air-dried overnight.[8] After the sample was dropped on the grid, micelles sedimentate on the grid,

however, they will prefer the more hydrophilic places and thus the micelles won't be well distributed on the grid surface and the size was also affected to some extent. The TEM images of micelle **OFP1**, **OFP2**, **RFP** and **FFP3** are shown in Figure 3.12 - 3.14, respectively.

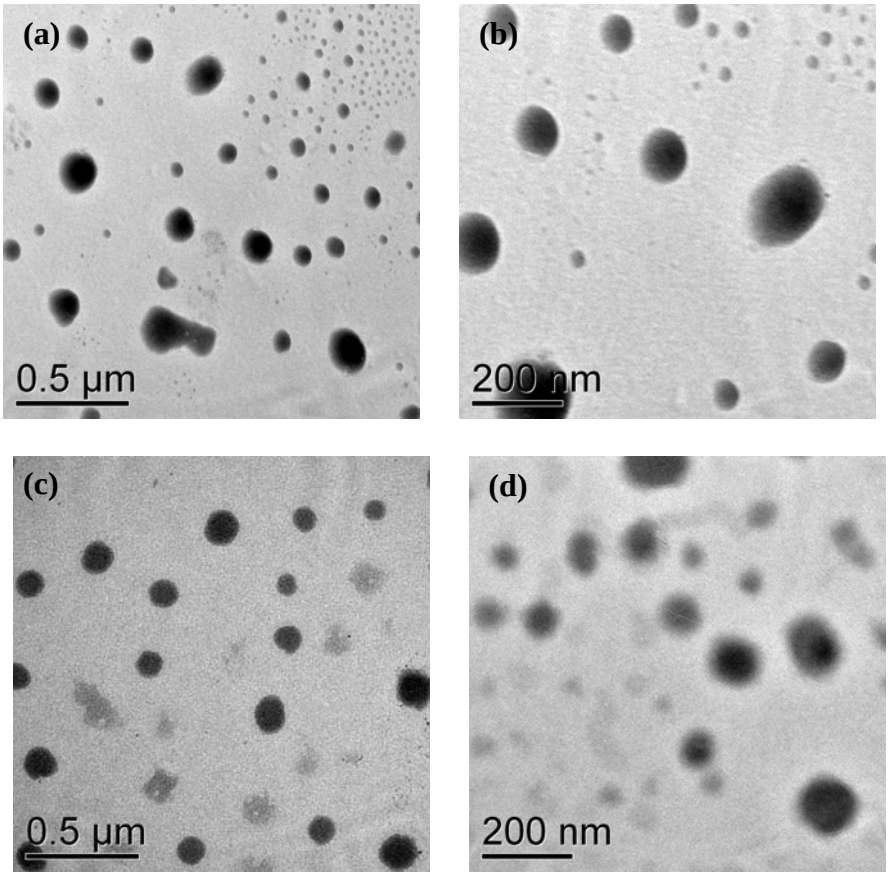

Figure 3.12. Stained TEM micrographs of (a) & (b) **OFP1** and (c) & (d) **OFP2** on 400-mesh carbon-coated copper grid at the concentration of 0.5 mg/mL.

From the TEM images of **OFP1** and **OFP2**, soft and loose packed core-shell structures are clearly exhibited. Due to their higher hydrophilic content, PEG was stained by staining reagent and micelles look dark. Similar to the light scattering results, different sizes of **OFP1** (Figure 3.12a & b) micelles were observed in the TEM image, which are

found to have the diameter of ~ 10 and 86 nm (the radii of the particles are ~ 5 and 43 nm). **OFP2** (Figure 3.12c & d) displayed more uniform particle size, in agreement with the LS and AFM results. The shrinkage of the micelles particle size from the solution to the solid state was estimated and the shrinkages in particle diameters were found to be 29% and 11% for **OFP1** and **OFP2**. The more obvious shrinkage in the aggregate size of **OFP1**, as compared to **OFP2**, is due to the much looser packing of **OFP1** in solution, which has been confirmed by the aggregation number of **OFP1** (N_{agg} = 34) and **OFP2** (N_{agg} = 66).

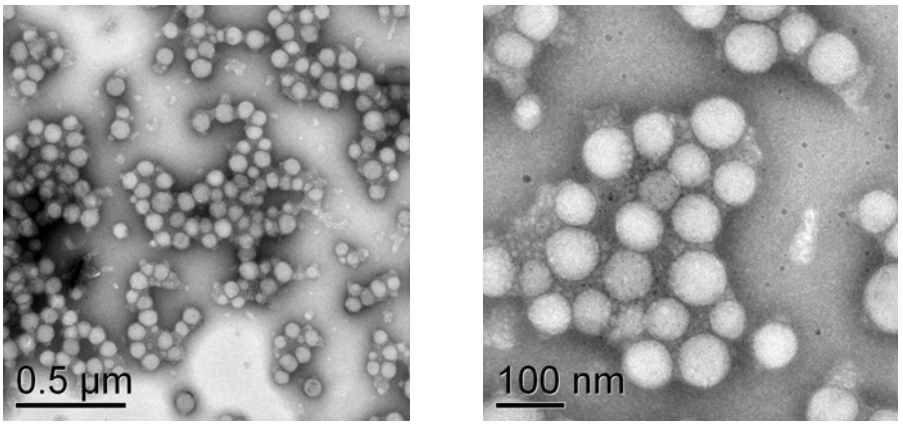

Figure 3.13. Stained TEM micrographs of **RFP** on 400-mesh carbon-coated copper grid at a concentration of 0.6 mg/mL.

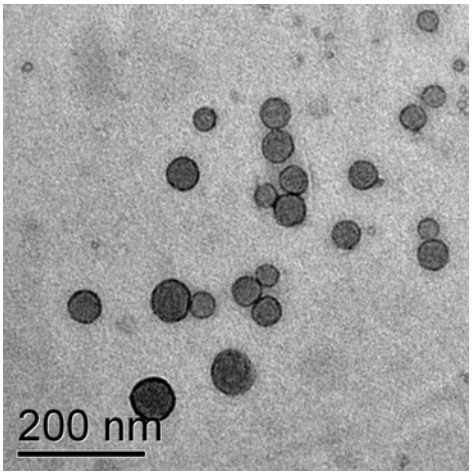

Figure 3.14. Stained TEM micrographs of **FFP3** on 400-mesh carbon-coated copper grid at the concentration of 0.01 mg/mL.

In contrast with **OFP1** and **OFP2** which formed elliptical micelles, **RFP** and **FFP3** self aggregated into hard spherical micelles. Due to their low PEG content, the color of micelle from the TEM images was lighter than the micelles formed from **OFP1** and **OFP2**. A thin shell (PEG) layer can be clearly seen from the TEM image of **FFP3**.

3.4 Optical property

Spectroscopic properties of conjugated molecules/polymers have varying degrees of sensitivity to backbone conformation. In order to investigate the conformation of molecules in micelles, their optical properties are studied by UV-vis absorption and fluorescence spectroscopy. The UV-vis absorption and photoluminescence (PL) spectra of the amphiphilic copolymers in DCM and aqueous solution were recorded on a Shimadzu UV 3101 spectrophotometer and Shimadzu RF-5301 PC spectrophotometer at room temperature, respectively. The effect of molecular packing on the fluorescence property of the micelles can be investigated by time resolved photoluminescent spectroscopy measurement.

3.4.1 Steady state fluorescence spectroscopy

For oligofluorenes and polyfluorenes, the alkyl substituents at C-9 on fluorene ring will not affect their optical properties. The structure of backbones is the main impact factor for their optical properties. The UV-vis absorption and PL spectra of copolymer **OFP1, OFP3**, rigid copolymer **RFP** and flexible copolymer **FFP3** are chosen as examples and shown in Figure 3.15.

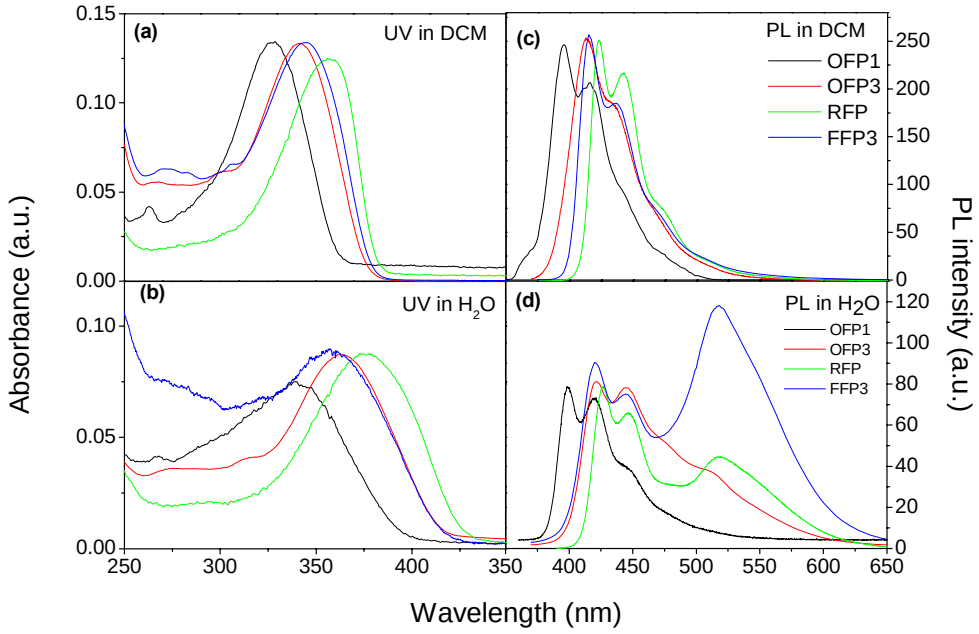

Figure 3.15. UV-vis absorption and PL emission spectra of **OFP1**, **OFP3**, **RFP** and **FFP3** in DCM and aqueous solution at room temperature.

For these amphiphiles, their absorption spectra in aqueous solution are quite similar as that in DCM and exhibit unstructured absorption bands. The absorption of copolymers displays a strong featureless π–π* transition that peaks at about 349 nm for **OFP1**, 362 nm for **OFP3**, 384 nm for **RFP**, and 369 for **FFP3** in DCM. The energy of π–π*

transition depends on the conjugation length. Thus the maximum absorption of amphiphiles shifts to longer wavelength with the increasing number of fluorene units. UV spectra of rigid copolymer **RFP** and flexible copolymer **FFP3** showed different maximum absorption peak wavelength, which is 384 nm for **RFP** and 369 nm for **FFP3**. The shorter absorption peak wavelength of **FFP3** indicated its shorter conjugation length because the interruption of conjugation of flexible copolymer by non-conjugated flexible units decreased its effective conjugation length. We can find that there is several nanometer differences of the absorption bands for the micelles in aqueous solution compared with that in organic solvent, which should be ascribed to the solvent effect. The similar UV-vis absorption spectra in DCM and water indicated that aggregation of the amphiphilic copolymers in micelles will not cause much difference in the conjugation length of the polymer backbone.

In contrast to the absorption spectra, the photoluminescence spectra of the micelle samples demonstrated dramatically different features from their PL spectra in DCM. In DCM solution, all the copolymers exhibited a well-resolved vibronic structure (Figure 3.15 (c)). The main peak, the side peak (or the shoulder), and the tailed emission band are assigned to $\pi^* \rightarrow \pi$ 0-0, 0-1 and 0-2 intrachain transition, respectively.[9] The energetic space for all the solution samples is about 150 to 170 meV, which is a typical vibrational energy of carbon-carbon bond stretching.[10,11] The PL spectra of the micelles in aqueous solution, shown in Figure 3.15 (c) and (d). Figure 3.15 (d) exhibited well resolved vibronic structure. For **OFP1**, three clear emission peaks at 400, 423, and 449 nm with medium intensity are observed, which are associated with the 0-0, 0-1 and 0-2 intrachain transition, respectively. The broad and dominant emission band for **RFP** peaks at 518 nm,

which is red-shifted by 96 nm compared to the main peak of the PL spectrum of **RFP** in DCM. The broad emissive band is most likely attributed to the excimer emission resulted from the close packed polymer chains in the micelles. Excimer emission has been observed in other polyfluorenes.[12-14] The high intensity of excimer emission than the single polymer chain emission indicated that more excimers were formed, suggesting a stronger aggregate state. The excimer emission of **RFP** is accompanied by two emission bands with similar intensity from single polymer chain, which peak at 415 nm and 437 nm, respectively. Similar to **RFP**, **FFP3** micelles also exhibit strong excimer emission with the maximum emissive wavelength of 518 nm. All the UV-vis and PL spectra in DCM and aqueous solution are summarized in Table 3.2.

Table 3.2. Summary of UV-vis absorption and PL spectra of amphiphilic graft copolymers in DCM and aqueous solutions at room temperature.

Samples	UV-vis absorption				PL emission	
	λ (in DCM)		λ (in H_2O)			
	λ_{max}(nm)	λ_{on}(nm)	λ_{max}(nm)	λ_{on}(nm)	λ_{max} (in DCM)	λ_{max} (in water)
OFP1	349	388	339.5	391.5	396.5 (418, 442)	417.5 (518.5)
OFP2	336	386	339.5	380	396 (419)	401.5 (476.5)
OFP3	361.5	407.5	363.5	413	412 (432)	420 (442)
RFP	381	413.5	377.5	424	422, 441, (474)	427, 447, 518
FFP1	355	410.5	362	404	417 (439)	420, 444, 518
FFP2	364.5	392	363	411	417 (437)	418, 442, 518
FFP3	369	406	364	425.5	415, 437 (471)	422, 441, 518

The fluorescence efficiencies of the polymeric micelles in aqueous solution have been measured with the quinine sulfate 0.1 M H_2SO_4 solution as standard. It was found that the efficiencies in aqueous solution decreased much compared with the efficiencies in DCM solution (shown in Table 3.3).

Table 3.3. Fluorescence quantum yields of polymeric micelles in aqueous solution at room temperature.

Samples	**OFP1**	**OFP2**	**RFP**
In DCM	82.9	72.4	55
In water	6.6	6.5	2.3

3.4.2 Time-resolved fluorescence spectroscopy

In order to investigate the emissive process of the micelles, time resolved fluorescence measurement was conducted. Fluorescence lifetimes were measured by time-correlated single-photon counting (TCSPC) technique (PicoQuant, PicoHarp 300). The frequency-doubled output of a mode-locked Ti:sapphire laser (Tsunami, Spectra-Physics) was used for excitation of the sample at 400 nm. The output pulses from Ti:sapphire centered at 800 nm had a duration of 40 femtosecond (fs) with a repetition rate of 80 MHz. The Ti:sapphire laser was pumped by 5 W output of a frequency doubled diode pumped Nd:YVO_4 laser (Millennia Pro, Spectra-Physics). For lifetime measurements the fluorescence was collected by an optical fiber which is directed to the detector. An avalanche photodiode (APD) was used as detector. The decay time profile was monitored at different wavelengths. Outputs of the APD (start pulse) and a fast

photodiode (stop pulse) were processed by the PicoHarp 300 module. The width of the instrument response function was 100 ps. All intensity decay fits were convoluted with the instrumental response function. The samples were exactly the same samples used for fluorescence spectroscopy.

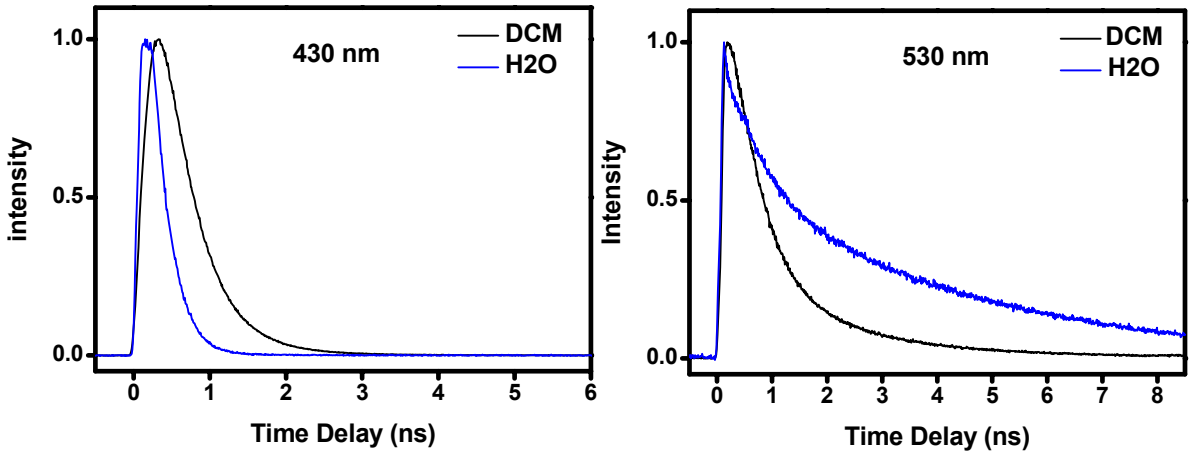

Figure 3.16. TCSPC decay profiles of **OFP1** in DCM and aqueous solution at the concentration of 1 mg/mL, observation wavelengths were 430 nm and 530 nm, respectively.

Analysis of PL spectrum of **OFP1** micelles suggested that the emission band between 370 nm to 450 nm is mainly contributed from the emission from single polymer chains; while the emission band beyond 450 nm is dominantly from excimer emission. Thus, to understand the detailed exciton decay process of the micelle sample, the fluorescence lifetimes were measured at the emission wavelength of 430 nm and 530 nm for **OFP1** micelles. Figure 3.16 shows the fluorescence decay profiles of **OFP1** in aqueous solution at the concentration of 1 mg/mL. For the fluorescence decay curve at emission wavelength of 430 nm, it fits nicely with a single exponential function:

$$I(t) = \alpha \exp(-t/\tau) \quad (1)$$

where τ is the lifetime and α is the corresponding amplitude.

The curve at emission wavelength of 530 nm was fitted well with a double exponential function:

$$I(t) = \alpha_1 \exp(-t/\tau_1) + \alpha_2 \exp(-t/\tau_2) \quad (2)$$

where τ_1 and τ_2 are the shorter and longer lifetime components, respectively, and α_1 and α_2 are the corresponding amplitudes.

The fit results showed that the fluorescence decay curve at 430 nm is monoexponential. The fluorescence lifetime was around 240 ps, shorter than the exciton lifetime of terfluorene in organic solvent (500 ps).The shorter lifetime might indicate that there are some trap sites in the micelles. For 530 nm emission, existence of two fluorescence lifetime components with τ_1 of 732 ps (α_1 = 0.46) and τ_2 of 4754 ps (α_2 = 0.54) was observed. This fit result implies that **OFP1** molecules are present in two different forms in the water solution. The two fluorescence lifetime components can be assigned to the emission from single polymer chains and excimers of **OFP1**, respectively,[15] which is in good agreement with the conclusion drawn earlier from the PL spectra measurements. In comparison of the values of α_1 and α_2, we can find that the contribution of single chain emission and excimer emission to the dominant emissive peak at 516 nm is roughly about the same. The similar results were also collected from **RFP** and **FFP3**. Their fits results are listed in Table 3.4.

Table 3.4. Fluorescence lifetime of **OFP1**, **RFP** and **FFP3** in aqueous solution at room temperature.

Sample and concentration (mg/mL)	430 nm		530 nm			
	α	τ	α_1	τ_1	α_2	τ_2

OFP1 (1 mg/mL)	1.0	297.5	0.58	630.9	0.42	5210.5
RFP (0.6 mg/mL)	1.0	243.8	0.46	732.1	0.54	4754.3
FFP3 (0.01 mg/mL)	1.0	298.5	0.45	815.0	0.55	4450.0

3.5 Cytotoxicity evaluation and biolabeling

The preliminary investigation of the fluorescent micelles for bio-imaging application has been performed with BV-2 microglial cells, the brain macrophages. **RFP** fluorescent micelle aqueous solution (0.3 mg/g) was added to the culture media with the concentration of 1%, 2%, 5%, and 10% (v/v). After cultured for 12, 24, 48, and 72 hours, the viability of BV-2 cells was measured. The number of the cells cultured with the fluorescent micelle solutions increased synchronously with the number of cells in pure culture media, indicating that the fluorescent micelles are non-cytotoxic (Figure 3.17).

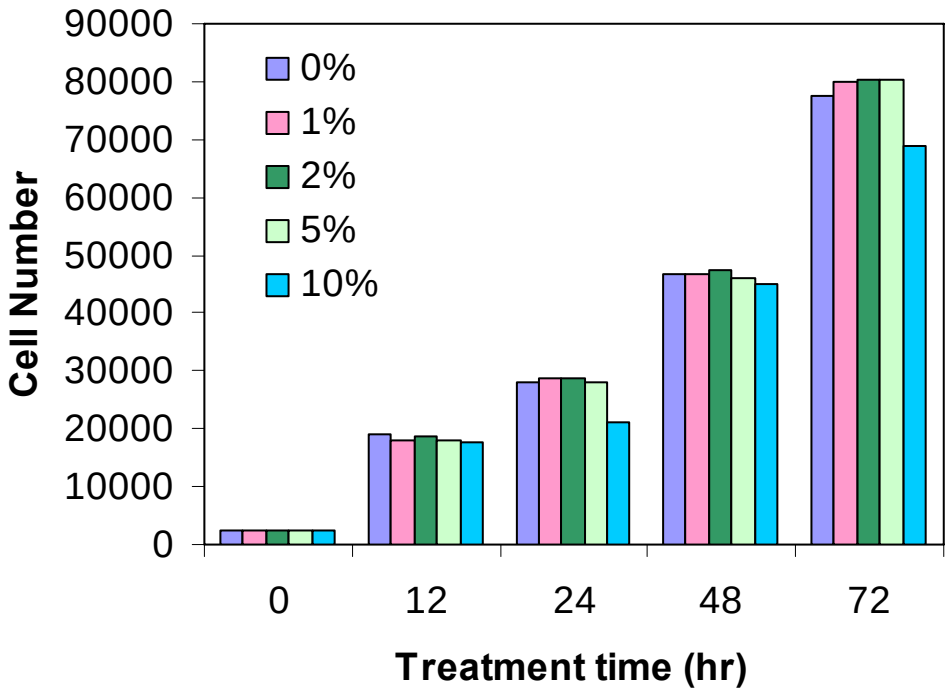

Figure 3.17. The effect of culture time and concentration of fluorescent micelles on the growth of BV-2 cells.

The uptake of the cells to the fluorescent micelles was recorded by confocal laser scanning microscope. The BV-2 cells were cultured for 2 days, and then fluorescent micelles solution (0.003 mg/g) was added and cultured for 2 hours. Figure 3.18 and 3.19 show the confocal image of BV-2 cells cultured for 2 hours in the presence of 0.003 mg/g of fluorescent micelles solution. The confocal microscopy indicated that the cells can be uniformly labeled by the micelles.

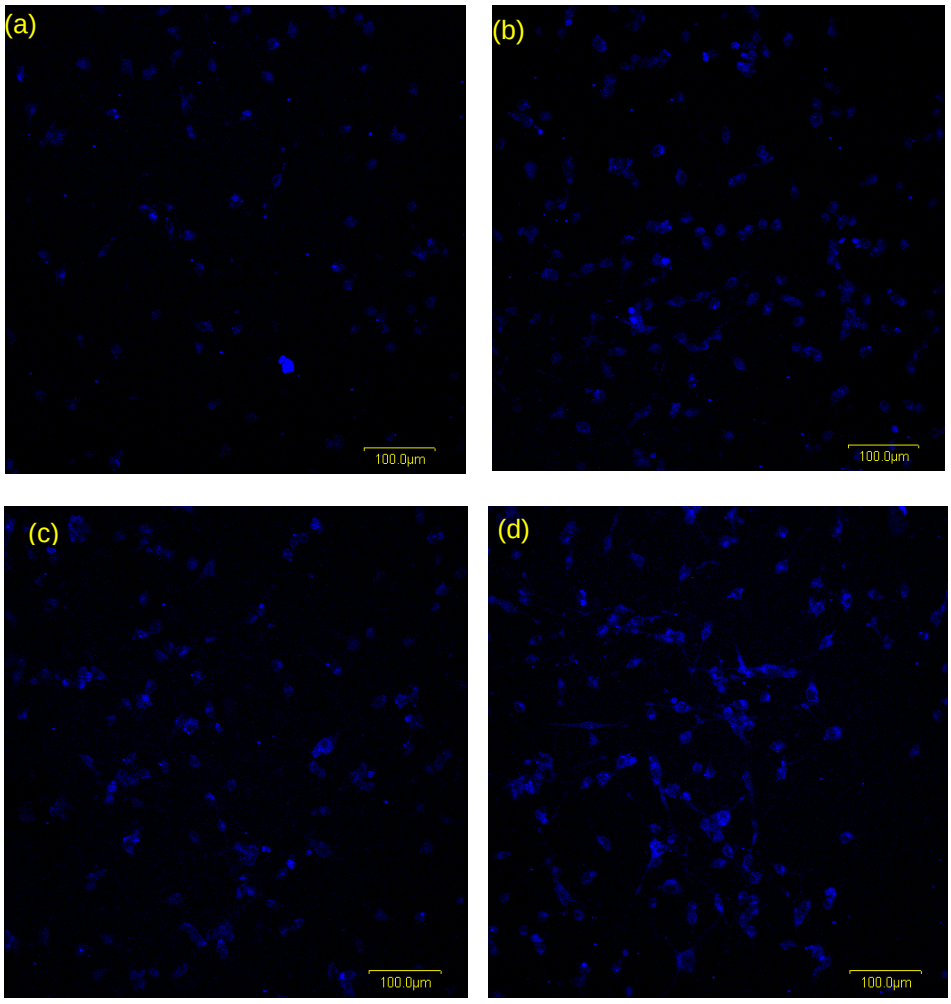

Figure 3.18. Confocal images of activated BV-2 cells cultured for 2 hours in the presence of fluorescent micelles solution (0.003 mg/g) after stimulated by stimulating agent (SA, lipopolyacchande) for 24 hours at different concentration: (a) without SA (b) 1 μL/mL of SA (c) 2 μL/mL of SA (d) 5 μL/mL of SA.

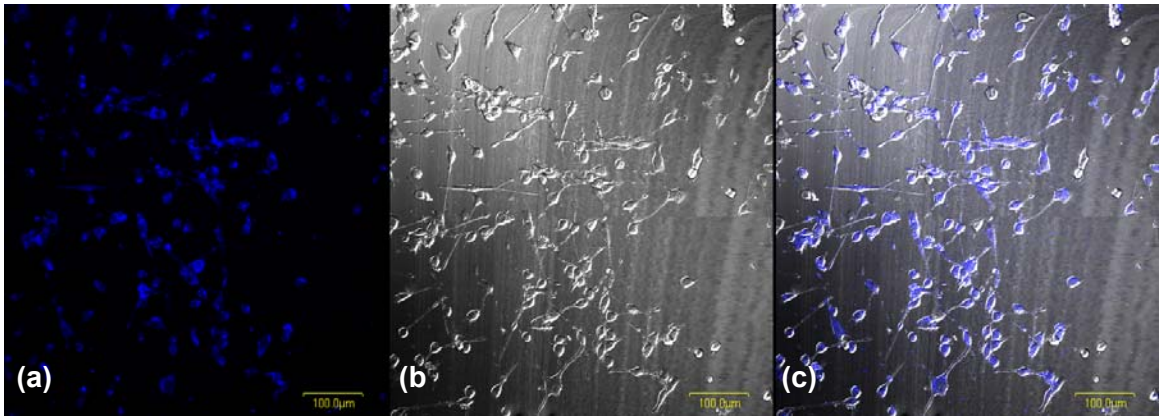

Figure 3.19. Confocal images f BV-2 cells cultured for 2 h in the presence of **RFP** fluorescent micelle solution (0.003 mg/g): (a) fluorescence view; (b) phase-contrast view, and (c) picture ovelaped from (a) and (b).

References

1. J. Jo, C. Chi, S. Hoger, G. Wenger, D. Y. Yoon, *Chem. Eur. J.* **2004**, *10*, 2681.
2. S. Rangelow, P. Petrov, I. Berlinova, C. Tsvetanov, *Polym. Bull.* **2004**, *52*, 155.
3. S. J. Yang, S. Zhang, *Supermolecular Chem.* **2006**, *18*, 389.
4. T. Nie, Y. Zhao, Z. Xie, C. Wu, *Macromolecules* **2003**, *36*, 8825.
5. E. R. Pike, J. B. Abbiss, *Light Scattering and Photon Correlation Spectroscopy*; Kluwer Academic Publishers: Netherlands, **1996**; p 178.
6. C. Wu, J. Fu, Y. Zhao, *Macromolecules* **2000**, *33,* 9040.
7. T. Song, S. Dai, K. C. Tam, S. Y. Lee, S. H. Goh, *Langmuir* **2003**, *19*, 4798.
8. X. Li, K. Y. Mya, X. Ni, C. He, K. W. Leong, J. Li, *J. Phys. Chem. B* **2006**, *110*, 5920.
9. S. Guha, Y. T. Rice, C. M. Martin, M. Chandrasekhar, R. Guentner, P. Scanduicci de Freitas, U. Scherf, *Phys. Rev*. **2003**, *67*, 125204.
10. H. Meng, Z.-K. Chen, W. Huang, *J. Phys. Chem. B.* **1999**, *103,* 6429.
11. J. L. Bredas, J. Cornil, A. J. Heeger, *Adv. Mater.* **1996**, *8*, 447.
12. G. Zeng, W. L. Yu, S. J. Chua, W. Huang, *Macromolecules* **2002**, *35*, 6907.
13. S. A. Jenekhe, *Adv. Mater*. **1995**, *7*, 309.
14. J. Kim, *Pure Appl. Chem.* **2002**, *74*, 2021.
15. C. Chi, C. Im, G. J. Wegner, *J. Chem. Phys*. **2006**, *124*, 024907.

4. Conclusions

4.1 Conclusions

A series of amphiphilic graft copolymers that based on oligofluorene/polyfluorene backbones and PEG side chains have been successfully synthesized by Suzuki coupling and polycondensation. In order to investigate the architecture effect on aggregation behavior, amphiphiles with different hydrophilic/hydrophobic ratio and molecular weights have been synthesized. The effect of flexibility of backbone on micellization was also investigated by synthesis of rigid backbone and flexible backbone polymers. Their chemical structures and molecular weights were characterized by NMR and GPC. All the amphiphiles can self-assemble into nanoscale polymeric micelles in aqueous solution and monodispersed copolymer micelles were obtained from most of them.

The *CAC*, particle size and size distribution in solution of micelles were measured by DLS. It was found that the *CAC* ranged from 10^{-4} to 10^{-1} mg/mL. The diameter of micelles in solution can be tuned in a wide range by structure modification, from 85 nm to 178 nm. The results also showed that the rigidity of polymer backbone affected the *CAC* values. It was found that the introduction of flexible units favored micellization at lower concentration, which indicated their better stability in the future dilution. Micelles from flexible polymer **FFP1**, **FFP2**, **FFP3** formed at very low CAC values, which is one order of magnitude lower than the rigid polymers. Although the hydrophilic/hydrophobic ratio was different for flexible polymers, their *CAC* did not change much, which means that the flexible units play an important role in *CAC*s of the flexible polymers. The apparent molecular weight $M_{w,\,agg}$, aggregation number N_{agg} and second virial coefficient

A_2 were characterized by SLS. The results indicated that the architecture of molecules play an important role in the intermolecular packing in micelles.

The solid state morphologies of micelles were characterized by AFM and TEM. The AFM and TEM results were in good agreement with the LS results, indicating that the particle size in solid state was smaller than their size in aqueous solution due to the shrinkage of shell, which was swollen in solution. Clear core-shell structure can be seen from TEM images. Soft micelles were formed from the oligomer **OFP1**, **OFP2** and **OFP3** due to their higher PEG content. **OFP1**, **OFP2** and **OFP3** demonstrated elliptical sphere particles. In addition, these soft micelles easily aggregate in solid state even at low concentration. Low PEG content polymeric amphiphiles, such as **RFP** and **FFP3** can form uniform and hard spherical micelles in large area. Clear micelle borders can be seen from AFM and TEM micrographies of them.

Optical properties of the amphiphilic copolymer micelles were studied by steady state fluorescence and time-resolved spectroscopy measurement. The intermolecular packing in micelle cores resembled the behaviors of conjugated molecules in thin film. Broad and red-shifted light emission peak at 518 nm in PL spectra was found from micelle aqueous solutions, which is assigned to be excimer emission due to the close packing among micellar conjugated cores. Longer-lived component (ns) existed in the PL decay profile is attributed to excimers.

Preliminary biocharacterization has proved the biocompatibility and non-cytotoxicity of polymeric micelles. It was also found that the luminescent micelles can be uniformly uptaken by BV-2 cells. The fluorescent property, good biocompatibility and excellent

long term stability of the micelles allow the stable fluorescent micelles wide applications in bio-labeling, drug delivery and tracing.

It can be concluded that these novel luminescent amphiphilic copolymers can form stable, biocompatible and monodispersed nanoparticles, which showed great potential in bioimaging.

4.2 Outlook

Amphiphilic block and graft copolymers have been widely used as drug delivery carriers. Easy control in particle size, good structural stability, and good water solubility are the consideration. For a drug delivery system, it is necessary to consider two factors: particle size and surface characteristics. The nanoscopic size of polymeric micelles may impart selectivity for tumor tissues, which may help minimize harmful side effects and toxicity. The size of particles should be small enough to avoid any mechanical clearance by filtration in the lungs or in the spleen. Usually, polymeric micelles with the size smaller than 100 nm in diameter are able to pass through microvasculature. Upon micellization, the hydrophobic core regions serve as reservoirs for hydrophobic drugs, which may be loaded by chemical, physical, or electrostatic means, depending on the specific functionalities of the core-forming block and the solubilizate. PEO is FDA-approved for parenteral administration and is widely used in a variety of biomedical and pharmaceutical applications. In addition, PEO has long been recognized for its ability to minimize protein adsorption to surfaces. Thus, the polymeric micelles in this project have the potential to be used as drug delivery carriers due to their hydrophilic segment PEG and the potential functionaliztion of the core structure. The particle size still can be

reduced further, for this purpose, different molecular weight PEGs and different backbone architectures can be adopted to tune the particle size and micelle properties. Further functionalization of the hydrophilic corona will allow them to perform as molecular recognition or anchors for specific surface.

The fluorescent property of the micelles could be useful to trace drug delivery process. The color tunability of polyfluorene backbone allows synthesis of nanoparticles with multicolor emission by minor modification of the polymer backbones. Copolymerization is one of the choices to tune the emission from blue to green and red conveniently.